AD

USAAVLABS TECHNICAL REPORT 68-18E

PREDICTION OF ROTOR INSTABILITY AT HIGH FORWARD SPEEDS

VOLUME V
FLAPPING AND FLAP-LAG INSTABILITY

By

N. L. Elman

Charles F. Niebanck

Lawrence J. Bain

February 1969

U. S. ARMY AVIATION MATERIEL LABORATORIES
FORT EUSTIS, VIRGINIA

CONTRACT DA 44-177-AMC-332(T)

UNITED AIRCRAFT CORPORATION
SIKORSKY AIRCRAFT DIVISION
STRATFORD, CONNECTICUT

Disclaimers

The findings in this report are not to be construed as an official Department of the Army position unless so designated by other authorized documents.

When Government drawings, specifications, or other data are used for any purpose other than in connection with a definitely related Government procurement operation, the United States Government thereby incurs no responsibility nor any obligation whatsoever; and the fact that the Government may have formulated, furnished, or in any way supplied the said drawings, specifications, or other data is not to be regarded by implication or otherwise as in any manner licensing the holder or any other person or corporation, or conveying any rights or permission, to manufacture, use, or sell any patented invention that may in any way be related thereto.

Disposition Instructions

Destroy this report when no longer needed. Do not return it to the originator.

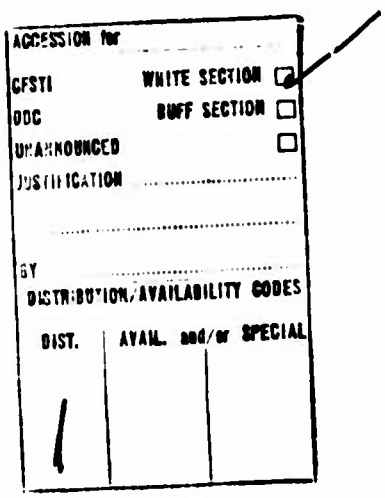

DEPARTMENT OF THE ARMY
U. S. ARMY AVIATION MATERIEL LABORATORIES
FORT EUSTIS, VIRGINIA 23604

This contract was initiated to determine the aeroelastic stability limits of articulated and unarticulated helicopter rotor systems at high forward speeds. The four primary modes of aeroelastic instability (classical flutter, stall flutter, torsional divergence, and flapping or flatwise bending instability) were investigated. The possibility of a flap-lag instability suggested by Dr. Maurice I. Young of the Vertol Division, The Boeing Company, was investigated as a special case of flapping instability.

The results are published as a five-volume set; the subject of each volume is as follows:

Volume I	Equations of Motion
Volume II	Classical Flutter
Volume III	Stall Flutter
Volume IV	Torsional Divergence
Volume V	Flapping Instability

These reports have been reviewed by the U. S. Army Aviation Materiel Laboratories. These reports, which are published for the exchange of information and the stimulation of ideas, are considered to be technically sound with regard to technical approach, results, conclusions, and amended parameter ranges for accurate usage.

Task 1F125901A13904
Contract DA 44-177-AMC-332(T)
USAAVLABS Technical Report 68-18E
February 1969

PREDICTION OF ROTOR INSTABILITY AT HIGH FORWARD SPEEDS

SER-50469

Volume V

Flapping and Flap-Lag Instability

By

H. L. Elman

Charles F. Niebanck

Lawrence J. Bain

Prepared by

United Aircraft Corporation
Sikorsky Aircraft Division
Stratford, Connecticut

for

U. S. ARMY AVIATION MATERIEL LABORATORIES
FORT EUSTIS, VIRGINIA

SUMMARY

The purposes of this research program were to extend or develop analytical methods for determining rotor blade aeroelastic stability limits and to perform stability calculations over a range of design and operating variables for articulated and nonarticulated configurations. The usefulness of simpler analytical methods is investigated by comparing results with operating boundaries from the more elaborate analysis.

Volume V deals with an investigation of the unstable flapping or flatwise bending tendency which arises during operation at high forward speeds and reduced rotational speeds. An explanation of flapping instability is given. This instability is basically due to negative aerodynamic spring forces on the upstream side of the rotor. The principal parameters influencing flapping or flatwise bending are enumerated and discussed. The simplified analysis used a single degree of freedom, rigid flapping for an articulated blade or the first flatwise bending mode for a nonarticulated blade. This analysis was used to calculate response to an instantaneous gust, and practical operating boundaries were defined in terms of maximum allowable flapping or bending excursions. The simple analysis was used to investigate a range of various parameters. These included mass ratio for both articulated and nonarticulated blades. Aerodynamic root cutout, pitch-flap coupling, pitch-flap velocity coupling, and mechanical flap damping were investigated for articulated blades. Nonarticulated rotor parameter variations included first mode bending frequency ratio, aspect ratio, and control gyroscope feedback. The simple analysis showed that the rotor flapping gust response was essentially proportional to gust amplitude and independent of advancing tip Mach number, if blade excursions were within the normally acceptable limits. The blade mass ratio and pitch-flap coupling were found to have the most important effects on flapping instability. The simple analysis was supplemented with similar calculations with the extended Normal Mode Transient Analysis. These results showed that the simpler analysis predicted all trends correctly and provided results which were somewhat conservative with respect to those of the Normal Mode Transient Analysis. This conservatism is appropriate to the use of the simpler analysis in preliminary design studies. Recommended preliminary design practices are stated, which are intended to prevent difficulties with flapping-type instabilities.

The existence of a flap-lag instability was investigated with the Normal Mode Transient Analysis, which included blade stall, compressibility, and reverse-flow effects. Three advance ratio conditions were chosen, with the rotor operating in high-speed flight under stalled conditions. While large control pulses were found to produce blade excursions which were unacceptably large from a practical standpoint, no tendency of the rotor to become catastrophically unstable was noted.

FOREWORD

The investigation presented in this volume is part of a general study of rotor blade aeroelastic instabilities, which is contained in five volumes. The work was performed under Contract DA 44-177-AMC-332(T) with the U. S. Army Aviation Materiel Laboratories, Fort Eustis, Virginia. The program was monitored for USAAVLABS by Mr. Joseph McGarvey.

The rotor blade flapping and flatwise bending instability analysis and calculations are the result of work done at the United Aircraft Research Laboratories by Mr. H. L. Elman, and at Sikorsky Aircraft by Mr. Charles F. Niebanck. The investigation of coupled flap-lag instability was performed at Sikorsky Aircraft by Mr. Lawrence J. Bain.

Volume I of this report contains the development of the differential equations of motion of an elastic rotor blade with chordwise mass unbalance.

Volume II presents a linearized discreet azimuth classical flutter analysis for rotor blades, with an appropriate parameter variation study, a comparison with test data, and a comparison with results calculated by using the method of Volume I.

Volume III describes a stall flutter analysis based on the calculation of aerodynamic work for a cycle of blade torsional vibration. Two-dimensional unsteady airfoil test data were used in the evaluation of the aerodynamic work. The analysis was used to generate stall flutter boundaries.

Volume IV contains the results of a study of static torsional divergence. A set of design charts and the effects of a range of parameter variations are presented. The results of the static divergence calculation are compared with results calculated by using the method of Volume I.

TABLE OF CONTENTS

LIST OF ILLUSTRATIONS

LIST OF TABLES

LIST OF SYMBOLS

A^*	speed of sound, ft/sec
AR	aspect ratio of blade
b	number of blades
B	tip loss factor
c	chord, ft
c_o	reference chord, ft
C_{FD}	flap damper coefficient, ft-lb-sec/rad
C_L/σ	rotor lift coefficient-solidity ratio, $C_L/\sigma = L_R/\rho b c_o \Omega^2 R^3$
D_F	ratio of flap damping to critical damping in hover
$\bar{e}$	flap-lag hinge offset
EI_E	edgewise bending stiffness, lb-ft^2
EI_F	flatwise stiffness, lb-ft^2
EI_O	reference value of blade bending stiffness, lb-ft^2
I_B	blade mass moment of inertia about flapping hinge, ft-lb-sec^2
k_z	mass radius of torsional gyration divided by rotor radius
K_{CF}	increment in square of nondimensional flapping frequency due to centrifugal effects
L_R	rotor lift, lb
m	blade mass per unit span, slugs/ft
$\bar{m}$	nondimensional local blade mass per unit span, m/m_0
m_0	reference blade mass per unit span, slugs/ft
$M_{1,90}$	advancing tip Mach number
q_{vi}	ith edgewise nondimensional modal amplitude, q_{vi}/R
q_{wi}	ith flatwise nondimensional modal amplitude, q_{wi}/R
$q_{\theta i}$	ith torsional modal amplitude, rad

r	nondimensional radius measured from flapping hinge
r_{OA}	aerodynamic root cutout
r_{cs}	nondimensional radius of a torsionally rigid inboard blade section
r_t	tip value of outermost aerodynamically effective radius
R	rotor radius, ft
V	forward velocity, ft/sec or kn
w_g	gust velocity, ft/sec
y_{cg}	chordwise center-of-gravity offset, positive forward of coincident elastic axis, and 25% chord, ft
y_{cg}/c	ratio of center-of-gravity offset to blade chord
z_t	vertical deflection of blade tip, ft
β	flapping mode amplitude for articulated blade, rad or deg
γ_{w_1}	local value of normalized first natural vibration mode shape
δ_3	pitch-flap coupling angle, deg; $\tan \delta_3 = \frac{\partial \theta_0}{\partial \beta}$
δ_4	ratio of blade pitch to blade flapping velocity; $\delta_4 = \frac{\partial \theta_0}{\partial(\partial\beta/\partial\psi)}$
$\bar{\delta}_T$	vertical tip deflection divided by rotor radius
$\theta_{0_{LO}}$	elastic blade twist measured at tip, deg
θ_0	blade pitch angle at the 75% radius due to control inputs and automatic coupling (δ_3 and δ_4) , rad or deg
ζ	leading-lagging mode amplitude for articulated blade, positive in lead direction, rad or deg
ζ_L	leading-lagging mode amplitude for articulated blade, positive in lag direction, deg
λ_g	gust velocity divided by rotor rotational tip speed
μ	advance ratio, $V/\Omega R$
M_R	mass parameter, defined in Eq. (1)
ρ	air density, slugs/ft^3

σ	rotor solidity, $bc/\pi R$
$\bar{\omega}_{v_i}$	ith edgewise bending natural frequency divided by rotor rotational frequency
$\bar{\omega}_{w_i}$	ith flatwise bending natural frequency divided by rotor rotational frequency
$\bar{\omega}_{\theta_i}$	ith torsional natural frequency divided by rotor rotational frequency
ω_F	flapping mode natural frequency
Ω	rotor rotational speed, rad/sec
ψ	rotor blade azimuth, measured in direction of rotation from downwind, deg
ψ_0	rotor blade azimuth for gust encounter

SUBSCRIPTS

MAX	refers to the maximum value
MIN	refers to the minimum value

INTRODUCTION

It is well known that the stability of the flapping motion of an articulated helicopter rotor blade decreases with increasing flight speed, as considered in References 1, 2, 3, 4, 5, and 6. Some of the results given in the earlier of these investigations are contradictory in nature because of simplifying assumptions made. For example, the results of Reference 1, which were obtained without including the effects of reverse flow, indicate that no flapping instability is possible. On the other hand, the limited results of References 2 and 3, which were obtained with the consideration of reverse-flow effects, indicate that instability can occur at high advance ratios. The results of the more recent analyses (References 4, 5, and 6) have generally been limited to the definition of stability characteristics of specific configurations. Reference 6 does present some generalized results showing that blade Lock number is an important parameter. In addition, all of the work of the above references is limited to articulated rotors. It can be shown that hingeless rotors are susceptible to a flatwise bending type of instability which is produced by the same fundamental mechanism as that which produces the flapping instability on articulated rotors. The investigation contained in this volume determines, for both articulated and hingeless rotors, the operating speed limitations imposed by the reduction in blade static stability at high speeds; also it assesses the effectiveness of various design parameter changes in alleviating these limitations. For this purpose, general parametric studies were made, with rapid, simplified analyses being used. Some of the more significant trends and results of the parametric studies were then supplemented and verified by means of the Extended Normal Mode Analysis, which is based on the equations given in Volume I, in order to determine the effects of additional blade degrees of freedom.

The existence of a basic type of articulated rotor instability, associated with heavy rotor loads, was predicted in Reference 7, where an approximate analysis was used. With this analysis, it was concluded that moderate impulsive disturbances could initiate coupled, unstable flap-lag motion in a heavily loaded rotor. The investigation in this section was intended to show if this type of instability would be predicted with the more elaborate Normal Mode Transient Analysis, in which blade stall, reverse-flow, and compressibility effects, as well as blade elastic deflections are considered. The investigation was limited to six sample cases falling within the scope of the analysis in Reference 7. These sample cases are at advance ratios of 0.3, 0.5, and 0.7. Various sudden collective pitch increments were applied, and the blade response was calculated for several subsequent revolutions to investigate basic instabilities involving coupled flapping and lead-lag motion.

DESCRIPTION OF FLAPPING OR FLATWISE BENDING INSTABILITY

The operation of rotary-wing aircraft at high forward speeds results in operation at high advance ratio μ, since rotational speed must be reduced to prevent excessively high advancing blade tip Mach numbers. Flapping or flatwise bending instability arises because of the changes in relative flow direction caused by a blade position out of the plane of rotation on the upstream half of the rotor disc. This is illustrated schematically in Figure 1, which shows side views of both articulated and hingeless rotors. Because of the blade deflection, there are components of the flight velocity normal to the local span axis of the blade. These components contribute to the local angle of attack and result in incremental lift forces on the blades as shown. These incremental lift forces are destabilizing, since they are proportional to the blade deflection and are in a direction to cause an increase in that deflection. These destabilizing forces increase with aircraft forward velocity. The centrifugal forces stabilizing an articulated blade and the centrifugal and structural forces stabilizing the hingeless blade at best remain constant. Therefore, an unstable tendency will develop as the rotor is operated at even higher forward velocities.

Note that in the above qualitative description of the flapping or bending instability all force increments considered were proportional to the displacement of the blade. Hence, the instability can be considered as arising from a reduction in the static stability of the blade as it traverses the upstream half of the rotor disc.

PRINCIPAL PARAMETERS INFLUENCING FLAPPING OR FLATWISE BENDING INSTABILITY

In this section a brief discussion of the principal blade parameters which influence flapping or bending instability is presented. Other parameters of interest can be deduced by examination of the flapping equation of motion (Eq. 91 of Volume I) for the articulated rotor or the flatwise bending equation (Eq. 80 of Volume I) for the hingeless rotor. The parameters considered are given below along with a brief explanation of the mechanism by which such parameters can influence the static stability of the blade.

ROTOR ADVANCE RATIO, μ

The destabilizing aerodynamic nondimensional spring forces acting on the upstream rotor blades increase with advance ratio. Certain components of these forces increase in a linear fashion with advance ratio, while others increase in quadratic fashion.

BLADE MASS PARAMETER, M_R

This parameter represents the ratio of blade aerodynamic forces to inertial forces. The lower the mass parameter, the more effective will be the centrifugal forces in stabilizing the rotor blade. A general expression for the mass parameter applicable to both hingeless and articulated rotors is

$$M_R = \frac{\rho c_0 R}{m_0 \int_0^{\bar{r}_1} \bar{m} \gamma_{w_1}^2 d\bar{r}} \qquad (1)$$

When the blade first bending mode shape γ_{w_1} is taken equal to $\bar{r}$ for the articulated rotor, the mass parameter for the articulated rotor is equal to the more familiar blade Lock number divided by the average value of blade lift curve slope.

PITCH-FLAP COUPLING

The destabilizing aerodynamic spring on the upstream blades of an articulated rotor can be reduced by introducing coupling between the flapping and pitching motions of the blade so that the blade pitch is reduced when the blade flaps upward. This is generally accomplished very simply by offsetting the pushrod radially from the flap-hinge axis. This coupling provides a large stabilizing aerodynamic spring force when the blade is operating in conventional flow. In reverse flow, however, such coupling is destabilizing. Unless the advance ratio is very high, the blade is operating in conventional flow for all except a small part of each revolution.

MECHANICAL FLAP DAMPING

Augmentation of the inherent aerodynamic flap damping of the blade with a mechanical device is another possible method for increasing the flapping stability. The flap damper is a device which produces a moment about the flapping hinge. The magnitude of this moment is proportional to the flapping velocity, and acts in opposition to that velocity. The stabilizing moment is, therefore, applied before large amplitudes are reached.

PITCH-FLAP VELOCITY COUPLING

Stabilization of the flapping motion of an articulated rotor blade can also be achieved by coupling the blade pitch to the blade's flapping velocity in such a manner that an upward flapping velocity causes an automatic reduction of blade pitch. This type of coupling introduces pitch changes before the undesirable flapping amplitudes occur, but it is also destabilizing in reverse flow.

NONARTICULATED BLADE BENDING STIFFNESS

The basic centrifugal forces stabilizing a rotor blade can be supplemented to some extent by elastic bending moments if the flapping hinges are eliminated, and the bending stiffness is increased well beyond present practice.

CONTROL GYRO STABILIZATION

The control gyro is basically employed as a device for aircraft stability augmentation. When it is used for stability augmentation, the gyro response to fuselage motions is employed to provide blade pitch control inputs which stabilize these fuselage motions. The gyro can also be used to change blade response characteristics as well, even in the absence of any fuselage motion. This particular function is provided by transmitting small components of the blade root flatwise bending moments to the gyro. The response of the gyro to the combined moments transmitted from the blades results in pitch control inputs to the blades. It is therefore of interest to assess the effect of such a control gyro on the flatwise bending instability at high advance ratios.

The scope of this work includes one typical gyroscope installation. No consideration is given to any fuselage motion except the steady forward velocity. In order to provide a component of pushrod force due to blade flatwise bending, the blade is swept forward slightly so that a small lead angle exists between the blade structural axis and the feathering axis. This causes the blade pushrod and horn to react a small component of the flatwise bending moment, as well as the usual blade root torsional moment. The total blade moment about the feathering axis, including the component of flatwise bending mentioned above, is reacted by the gyro through the blade pushrod. The gyro motion, and the resulting pitch input to the blades, depends on the pushrod loads applied to the gyro by all the blades.

PARAMETRIC STUDIES OF FLAPPING OR FLATWISE BENDING STABILITY WITH THE SIMPLIFIED ANALYSIS

PRELIMINARY DESIGN PROCEDURES FOR DEFINING PRACTICAL ROTOR LIMITS

The objectives of the parametric study phase of the investigation were (1) to determine practical operating limits imposed on rotor systems by the reduction in blade static stability at high advance ratio and (2) to assess the effects of important design parameters on such operating limits. As used here, the phrase "practical operating limit" is taken to mean that advance ratio for which the reduction in blade static stability becomes so severe as to cause an unacceptably large response to a representative instantaneous gust. It was concluded that practical operating limits should be considered rather than absolute stability limits because the latter is of little use to the designer. This is so because unacceptably large blade motions occur for quite moderate disturbances before the absolute stability boundary is reached. If very large out-of-plane blade motions occur, nonlinear effects due to the coupling of out-of-plane and lead-lag motions of the blade, and due to the reduction in stabilizing centrifugal forces with blade deflection amplitude must be considered. When out-of-plane blade deflections are limited to practical values compatible with fuselage clearance requirements (10 to 15 degrees of flapping on articulated rotors), such nonlinear effects are of secondary importance. This conclusion is supported by the results shown in Figures 2 and 3. Figure 2 shows the maximum nondimensional tip deflection obtained after the articulated blade encounters an instantaneously applied gust at an azimuth angle of 0 degrees. The response is shown with and without lag freedom, and it can be seen that lag effects are not of primary importance. Figure 3 shows the response of an articulated blade which is displaced in the flapping degree of freedom at two initial azimuth angles. The resulting time histories of blade flapping motion are shown for no additional disturbances and for no collective and cyclic pitch inputs. It should be noted that Figure 3 shows much larger excursions in flapping for an initial disturbance at an azimuth angle of 90 degrees than for the same initial flapping displacement at an azimuth angle of 0 degrees. In the work to follow, the response of the blade without initial flapping or bending to an instantaneous gust is studied. It was found that the largest blade excursions for a gust of a given size occurred if the gust was applied near an azimuth angle of 0 degrees.

Practical operating limits of the various rotor configurations analyzed were therefore determined by neglecting blade lag motion and by representing the out-of-plane motion of the blade by the rigid-body flapping mode for the articulated blade and by the first elastic flatwise mode for the hingeless blade. Blade responses in either case were determined by numerical integration of the appropriate equations of motion. Numerical integration was required because of the periodic coefficients in the equations of motion and the inclusion of nonlinear compressibility and stall effects in the representation of the blade aerodynamics. A more complete description of the general type of analysis used is given in Reference 8. The airfoil data used in Reference 8 was also used in this study. In computing rotor blade response to gusts, it was assumed that fuselage motions and rotor rpm

changes were negligible within the time period required for the blade responses to reach their maximum values (generally ½ to 1 revolution of the rotor) for these simple analyses. An instantaneously applied gust was assumed, and unsteady aerodynamic effects were neglected. These assumptions are conservative, and refinements are beyond the scope of the current analysis. The magnitude of the gust assumed in the bulk of the calculations was 30 fps; similarly, an advancing blade tip Mach number of 0.85 was also assumed. It will be shown, however, that these assumptions are not critical, inasmuch as the results obtained are approximately proportional to gust amplitude and almost independent of the advancing tip Mach number. Thus, normalized results can be obtained which can be applied to any practical combination of gust magnitude and advancing tip Mach number. Such normalized results are obtained by evaluating the derivative $d\bar{\delta}_T/d\lambda_G$.

where

$\bar{\delta}_T$ is the maximum tip deflection at any azimuth angle divided by rotor radius

λ_G is the ratio of gust velocity to rotor rotational tip speed

The quantity λ_G can be expressed in terms of advance ratio and advancing tip Mach number as

$$\lambda_G = \frac{w_G(1+\mu)}{M_{1,90}A^*} \qquad (2)$$

The blade was assumed to be initially trimmed to zero flapping or bending and to be at an azimuth angle of zero degrees when it encountered the gust. This initial azimuth angle generally resulted in the maximum tip deflection of the blade during the gust-induced transient.

The degree of linearity of the blade gust response with respect to λ_G and its independence of advancing tip Mach number are shown by the results presented in Figures 4 and 5. Although a small amount of scatter is present due to nonlinear stall and compressibility effects, the advantages of generality permitted by the linearizing assumption far outweigh the small errors introduced, which are generally less than 10% in maximum μ .

Once values of $d\bar{\delta}_T/d\lambda_G$ for several advance ratios have been determined for a particular rotor configuration, a comparison with maximum allowable values, as determined by maximum permissible blade tip excursions from the trim condition and maximum anticipated gust size, can be made to determine maximum operating advance ratios. The maximum allowable value of the derivative is approximately

$$\left(\frac{d\bar{\delta}_T}{d\lambda_G}\right)_{MAX} \cong \left(\frac{\bar{\delta}_T}{\lambda_G}\right)_{MAX} \qquad (3)$$

$$\left(\frac{\bar{\delta}_T}{\lambda_G}\right)_{MAX} = \left(\frac{\bar{\delta}_T \Omega R}{W_G}\right)_{MAX} = \left[\frac{\bar{\delta}_T A^* M_{1,90}}{(1+\mu) W_G}\right]_{MAX} \qquad (4)$$

The above general approach was used to investigate the independent effects of each of the parameters influencing flapping or bending stability which were described.

In order to assess the effect of the control gyroscope, blade response calculations were first performed with the gyroscope assumed fixed to the shaft. The loads on the gyroscope were calculated, and then the gyroscope's response to these loads. Finally, the gyro response was used to define new cyclic pitch control positions for another blade response calculation. The change in blade response due to the new control position was then noted. One such cycle of calculations was judged to be sufficient for this study. The single-degree-of-freedom analysis considered gyro loads due to blade flatwise moments only.

BLADE CONFIGURATIONS STUDIED

The rotor system configurations studied have a radius of 31 feet, with a flap-lag hinge offset of 3.4% of the rotor radius. All blades have uniform cross section and mass properties, except for aerodynamic root cutout. The specific rotor configurations which were analyzed are given in Table I.

As indicated in the listing in Table I, the investigation generally considered independent effects of the various design parameters. The only exception to this was the investigation of aspect ratio effects for the hingeless rotor. This parameter was varied by changing the number of blades of the rotor, keeping a constant rotor radius and solidity. By assuming all blade sections to be geometrically similar to those of the basic rotor blades, a specific simultaneous variation of mass parameter and frequency ratio resulted.

Control gyro parameters of interest are a lead angle of 1.5 degrees between blade axis and feathering axis and a gyro polar moment of inertia .01 times that of the rotor. The pushrod azimuth location leads the blade feathering axis by 45 degrees. No mechanical damping is applied to gyro motion.

GENERAL DISCUSSION OF RESULTS FROM THE SIMPLIFIED ANALYSIS

Tip deflection derivatives are presented for the articulated and nonarticulated rotors in Figures 6 through 10 and 11 through 13 respectively. In each of these figures, the derivative $d\bar{\delta}_T / d\lambda_G$ is plotted as a function of rotor advance ratio. The results were determined by using a 30-fps gust and an advancing blade tip Mach number of 0.85. However, as discussed previously, the results can be applied with confidence to situations involving other values of gust amplitude and advancing tip Mach number. Presented in

each figure are curves showing the characteristics of the basic rotor systems as well as those of rotor systems incorporating a specific design parameter change. Also shown on each of these figures is a curve representing a locus of maximum allowable derivative values as determined by Eqs. (3) and (4), based on the assumptions of a 30-fps gust, an advancing tip Mach number of .85, and a maximum allowable tip deflection of .26 times rotor radius. When the actual derivative for a given rotor is equal to the maximum allowable value, a rotor operating limit is defined. It should be noted that this is appropriate only to the assumed advancing blade tip Mach number and the assumed maximum gust velocity.

The tip deflection value (.26R) used in determining the maximum allowable derivative values in Figures 6 through 13 was selected principally from typical fuselage clearance requirements. For an articulated rotor with small flap hinge offset, such a deflection corresponds to a flap angle of about 15 degrees. For hingeless rotors, other factors, such as stress at the root of the blade, must be considered in selecting a maximum allowable tip deflection. For consistency, however, the same criterion was used for both rotor systems. It is evident that blade stresses are highly dependent on the detail design of the blade; as such, their determination for all hingeless rotors studied was beyond the scope of these parametric studies. The maximum operating advance ratios determined for the hingeless rotor on the basis of fuselage clearance considerations may therefore be optimistic. The attainment of such advance ratios in practice will be contingent upon acceptable blade stress amplitudes over the tip deflection range considered.

MAJOR EFFECTS OF PARAMETER VARIATIONS ON THE ARTICULATED ROTOR

Cross plots of the results of Figure 6 through 13 showing typical effects of various design parameters on maximum operating advance ratio, are presented in Figures 14 through 21. It is emphasized that these are typical results based on the assumption that fuselage clearance requirements will be the determining factor in defining allowable blade tip deflections and that the gust size and advancing tip Mach number are 30 fps and 0.85 respectively. Results for other combination of these quantities can readily be generated by using Eq. (4) and the more general derivative results of Figures 6 through 13.

Figure 14 shows that decreasing blade mass parameter by increasing blade flapping inertia or decreasing air density permits operation of the rotor at higher maximum advance ratios. This results from the fact that at low mass parameters, the stabilizing centrifugal forces acting on the blade are larger in relation to the destabilizing aerodynamic forces. The mass parameter of the basic blade is based on a sea level density. Operation at an altitude of 10,000 feet would reduce the mass parameter by about 25%.

The effect of pitch-flap coupling δ_3 on maximum advance ratio is shown in Figure 15, where it is evident that the addition of such coupling is beneficial. It is interesting to note, however, that a point of diminishing returns is reached where further increases in δ_3 produce little further imporvement in advance ratio capability. This is the result of the destabilizing effect of such coupling in reverse flow. Thus, it is to be

expected that δ_3 would be most effective at moderate advance ratios, where reverse-flow effects are not too pronounced.

Figure 16 shows the effect of increasing the aerodynamic root cutout of the blade. As might be expected, because of the relatively small contributions of the inboard portions of the blade to the destabilizing aerodynamic moments, little benefit from cutout results until unrealistically large cutouts are employed.

Figure 17 shows that the addition of mechanical flap damping is beneficial. However, dampers of impractically large size are required to achieve improvements of the same order of magnitude as those produced by pitch-flap coupling. To achieve critical damping, a flap damper is required which produces much greater damping than present lag dampers.

The effects of pitch-flap velocity coupling (shown in Figure 18) are qualitatively quite similar to those of pitch-flap coupling with high effectiveness at low advance ratios. This is as expected, inasmuch as both types of coupling are destabilizing in reverse flow.

MAJOR EFFECTS OF PARAMETER VARIATIONS ON THE NONARTICULATED ROTOR

The effect of mass parameter on maximum operating advance ratio for the nonarticulated rotor is shown in Figure 19. As with the articulated rotor, the effect of decreasing mass parameter is beneficial. For comparison, the articulated rotor results of Figure 14 have also been included in Figure 19, and it is evident that at equal mass parameters, the two types of rotors have essentially the same maximum advance ratio. This is not surprising in view of the fact that the basic hingeless rotor has structural stiffness small enough so that the stabilizing moments acting on the blade are still largely centrifugal, similar to the case with the articulated rotor. This is evidenced by the fact that the ratio of blade first mode natural frequency to rotor rotational frequency was 1.12 for the hingeless rotor, compared to 1.03 for the articulated rotor. Since the nonarticulated blade flapping stiffness is almost entirely the result of centrifugal force, the ratio of first mode flapping frequency to rotor rotational frequency can be assumed constant over the range of rotor rotational frequencies included in this study. Further, any benefits occurring from this small increase in total stiffness for the hingeless rotor are, to a large extent, compensated for by the fact that, for the same tip deflections, the higher slopes of the outboard portion of the bent nonarticulated blade aggravate the destabilizing aerodynamic forces at a given advance ratio.

The effect of frequency ratio on maximum advance ratio is shown in Figure 20. A dashed line is drawn connecting the points, since resonance effects can cause local irregularities in the shape of the curve.

In determining the results of Figure 20, all parameters but frequency ratio have been held constant, and no attempt has been made to relate the variations in frequency ratio to practical blade design changes. Most design changes which would be made to increase blade natural frequency to the levels shown in Figure 20 would probably involve changes in the mass pa-

rameter, spar taper, and thickness-to-chord ratio. In view of the potential difficulties associated with independent changes of blade frequency ratio, it was worthwhile to examine the effect of simultaneous variations in both frequency ratio and mass parameter associated with a specific type of blade modification. The particular modification considered was an independent change in blade cross section, expressed as a change in aspect ratio. In order to keep rotor solidity and radius constant, the aspect ratio and the number of blades were changed simultaneously. The chord and thickness of the blade cross section were changed in inverse proportion to the number of blades. The blade cross section was geometrically similar for all aspect ratios. The basic hingeless rotor had 5 blades of aspect ratio 20.4. The number of blades on the rotor was varied from 7 to 2 while maintaining constant rotor solidity and radius. Since blade characteristics alone were being studied, the poor vibration and ground resonance characteristics of the hypothetical 2-bladed nonarticulated rotor were ignored. By assuming all blades to have cross sections geometrically similar to that of the basic rotor blade, it was possible to obtain the following expressions which relate the frequency ratio and mass parameter of the modified blades to those of the basic blade:

$$\bar{\omega}_{W_1}^2 = \left[(\omega_{W_1}^2)_{BASIC} - K_{CF} \right] \left(\frac{AR_{BASIC}}{AR} \right)^2 + K_{CF} \qquad (5)$$

$$M_R = M_{R_{BASIC}} \left(\frac{AR}{AR_{BASIC}} \right) \qquad (6)$$

The effects of varying blade aspect ratio in this manner are shown in Figure 21, where frequency ratio, mass parameter, and maximum advance ratio are plotted as functions of aspect ratio. Low aspect ratios are seen to be beneficial, with the benefits produced almost entirely by mass parameter effects for the aspect ratio range considered.

The response of each of the five blades to the idealized instantaneous gust with and without cyclic pitch inputs due to control gyroscope feedback is shown in Figure 22. Each blade is identified by its azimuth angle at the onset of the idealized gust. As mentioned previously, cyclic pitch inputs are based on gyroscope response to pushrod loads determined with the gyroscope held fixed. In this single-degree-of-freedom analysis, the pushrod loads were the result of flapping moment components only, which are applied to the pushrods because of the 1.5-degree angular difference between the blade axes and the feathering bearing axis.

It is apparent from Figure 22 that the particular control gyroscope installation chosen has no significant effect on maximum blade response after the idealized gust.

FLAPPING OR FLATWISE BENDING INSTABILITY CALCULATIONS WITH THE EXTENDED NORMAL MODE TRANSIENT ANALYSIS

PURPOSES AND METHODS

A number of blade configuration and flight condition combinations were studied with respect to flapping or bending stability. These were carried out with the extended Normal Mode Transient Analysis to determine the effects on stability of higher flatwise bending modes, lag freedom, edgewise bending modes, and torsion. This was done for articulated rotors with and without chordwise center of gravity to 25% chord offset and with and without pitch-flap coupling. It was also done for nonarticulated rotors with and without chordwise center of gravity to 25% chord offset and with and without control gyroscope feedback effects. The blade elastic axis was at the 25% chord for all rotors considered.

The basic method of determining a practical stability boundary was essentially the same as for the similar work with the simplified analysis. In general, the blade was assumed to be at the zero azimuth position, with flapping, lagging, and higher modal displacements and velocities all starting from zero. For the gyro feedback studies, the individual blades were started in a similar manner at their azimuth positions when the first blade was at zero azimuth. The blade was then assumed to be instantaneously enveloped in an upward flow that represented an idealized gust, which then remained constant for the time period of interest. One essential difference between the simplified analysis and the Normal Mode Transient Analysis studies is the length of solution required to demonstrate that the system being studied has achieved a representative amplitude response. The simplified system, which considers only one flapping or flatwise bending degree of freedom, reaches essentially its maximum amplitude during the first rotor revolution after the onset of the instantaneous gust. Thus, no benefit would be obtained for simplified solutions of more than one rotor revolution in length. The extended Normal Mode Transient Analysis, however, considered lagging and edgewise bending motions, whose natural periods were considerably more than one revolution in length. It was thus expected that more revolutions of the rotor might elapse before the maximum flapping amplitude would be attained. On the other hand, a practical rotor installed on an aircraft would not be carried inexorably into a gust approximating the type being studied. Aircraft motions and control corrections would become significant after a certain period of time, and consideration of these effects is beyond the scope of this investigation. In order to provide a conservative compromise, the blade motion solution was allowed to run for 10 rotor revolutions. This is a time period of the order of 3 to 5 seconds. If the response of the rotor to the idealized gust were desired over a longer period, a study similar to Reference 9, would be needed for meaningful results. Thus, the information obtained by allowing the blade motion solution to run past 10 revolutions would have little practical value, since significant control correction and fuselage motions would be taking place.

ROTOR CONFIGURATIONS AND FLIGHT CONDITIONS STUDIED

The pertinent characteristics of the basic rotor system used for the flapping or bending stability studies with the extended Normal Mode Transient Analysis are given in Table II. The rotor configurations and flight conditions investigated are listed in Tables III and IV, respectively. The modal frequencies for the articulated and nonarticulated configurations are given in Tables V and VI.

It should be noted that the extended Normal Mode Transient Analysis employs blade rigid flapping and lagging modes for the articulated blades, in addition to the elastic modes listed in Table V.

Note that configurations 1 and 2 in Table II are similar to configurations 1 and 16 studied with the simplified analysis, which are given in Table I.

RESULTS OF FLAPPING OR BENDING INSTABILITY CALCULATIONS WITH THE NORMAL MODE TRANSIENT ANALYSIS

The basic results of the procedure described previously are given in Table VII for the various configuration and flight condition combinations studied. More detailed results are presented graphically, to permit further understanding of the effects of higher flatwise bending modes, lag freedom, edgewise bending modes, and torsion.

It should be noted that the results contained in Table VII refer to the maximum excursions experienced after the onset of the instantaneous gust. Much of the discussion to follow is based on excursions during a typical rotor revolution a few seconds after the gust has been applied. It is felt that these results may be more representative of response to a gust with a more gradual onset.

DISCUSSIONS OF FLAPPING OR FLATWISE BENDING INSTABILITY RESULTS

The single-degree-of-freedom analysis results have been discussed earlier under the appropriate subsections. Practical rotor operating limits and preliminary design procedures were described in conjunction with the single-degree-of-freedom analysis. In this subsection, these limits and procedures will be discussed in relation to the Normal Mode Transient Analysis results. Where deviations appear between the results of the single-degree-of-freedom analysis and the Normal Mode Transient Analysis, possible reasons for the deviation, and the range of usefulness of the single-degree-of-freedom analysis, are discussed.

The first type of graphical presentation of the Normal Mode Transient Analysis results appears in Figures 23 through 29, as time histories of flapping and leading for the articulated blade, and as modal amplitudes for the nonarticulated blade. All 10 revolutions included in the solution are generally presented. It will be noted that not every configuration and flight condition combination listed in Table VII is included in these plots. Inclusion of these other combinations in this set of graphs would offer no additional information of particular interest. These will, however, be mentioned and described during the discussions to follow.

Figure 23 shows flap and lead time histories for the articulated blade, with no pitch-flap coupling and the center of gravity at the 25% chord position (configuration 1 in Table II). Results are shown for μ = .5, 1.0, and 1.25, with ΩR adjusted to keep the advancing blade tip Mach number at .85. The articulated blade time history for μ = .60 is not shown, since it was similar to that for μ = .50, except for a larger amplitude. Note that the low-frequency transient lead motion decays in each case. Ultimately, the one-per-revolution lead motion visible would remain.

The blade is seen to lag during the first half revolution in each case. When the retreating side is reached, the blade is forced to lead to a much greater extent. The results for advance ratio μ = 1.5 were qualitatively similar, but with somewhat larger flapping amplitudes, and with lead transient amplitudes more than twice as large. Even for this case, the lead transient decayed. This case for μ = 1.5 was not plotted, since the motions were well beyond the range of practical interest. It should be particularly noted that for advance ratio μ = 1.25, the maximum flapping amplitude was reached in two rotor revolutions or less, and that once it was reached, variations were relatively minor.

Figure 24 shows first flatwise and edgewise modal time histories for the nonarticulated blade, tabulated as configuration 2 in Table III. These modal amplitudes for the nonarticulated blade are the corresponding tip deflections divided by rotor radius. The similar quantities for the articulated rotor are the tangents of the flapping and leading angles. Since these angles remain relatively small, they can be compared directly to the nonarticulated blade first bending modes, at least from a fuselage clearance standpoint. Note that the flatwise response for the nonarticulated

blade is generally larger than for the articulated blade. For advance ratio μ = 1.25, large edgewise motions develop in addition to the flatwise motions, and survival of the blade would be very doubtful. Since the time history response for advance ratio μ = .50 is similar to that shown for μ = .60, with smaller amplitudes, only the μ = .60 case is presented in Figure 24.

Figure 25 shows a sample flapping and lagging response for the articulated blade with pitch-flap coupling, listed as configuration 3 in Table III. Response of the same configuration was about two-thirds as large for an advance ratio μ of 1.25 and was qualitatively similar. Response for an advance ratio of 1.0 was very small. The response at an advance ratio of 1.8 was impractically large, with an apparently divergent lead motion.

Figure 26 shows the flapping and leading time history for the articulated blade with the center of gravity located 6% of the chord aft of the elastic axis and 25% chord. This is listed as configuration 5 in Table III. This result is similar to the corresponding part of Figure 23, for an advance ratio μ of 1.25, with a more abrupt buildup of flapping amplitude and with a noticeable tendency of blade motion towards the lagging direction. These general tendencies were less apparent in the similar results for advance ratio μ = .5, .6, and 1.0. In these cases, the flapping and leading motions were substantially identical to the corresponding cases with the blade balanced on the 25% chord.

Figure 27 shows modal time histories for the nonarticulated blade with the center of gravity 6% of the chord aft of the elastic axis and 25% chord. This is configuration 6 in Table III. The motions are similar to the corresponding part of Figure 24 with an advance ratio of 1. A more abrupt onset of flatwise motions is evident, together with a somewhat smaller edgewise motion. The corresponding results for advance ratios of .5 and .6 were generally similar to those for the balanced blade. However, the response of the balanced blade at an advance ratio of .5 was about 25% greater. Note that for these 6% aft center-of-gravity cases at μ = .5 and .6, the maximum flapping amplitudes were reached during the first revolution, rather than later, as for the balanced blade cases. Figure 28 was made more detailed to present the second, third, and fourth revolution modal time history for the same blade configuration at an advance ratio of 1.25. In this case, the motions grew catastrophically large for this nonarticulated blade during the fifth rotor revolution, causing the computer program to terminate the solution automatically. The gust amplitude used causes immediate flapping amplitudes beyond the practical limits, but it could be expected that the same instability would be triggered by a smaller disturbance. Inspection of Figure 28 shows that torsion, first edgewise, and first flatwise modes are involved in the instability.

Figure 29 presents the flapping and leading time histories for the articulated blade with center of gravity 10% of the chord aft of the elastic axis and 25% chord, listed as configuration 7 in Table III. An apparent instability was manifested by slowly growing lead-lag motion. The advance ratio is 1.25 for this figure. A similar case was computed for μ = 1.50. Very large motions occurred, as high as β = .54 and ζ = - .28. In

this last case, however, the motions appeared to diminish toward the end of the 10-revolution interval.

Inspection of the set of figures described in the preceding discussion shows that the blade flapping motion generally became essentially cyclic within three rotor revolutions after the idealized gust onset. This was true even though the articulated lead-lag motion and the nonarticulated edgewise motion had not yet reached their corresponding cyclic motions. More detailed inspection of the computer output showed that torsion and flatwise bending modal amplitudes also generally became nearly cyclic after a few rotor revolutions. These observations permitted the use of the tenth revolution as a sample representing any of the others after maximum flapping amplitude had been reached. The computer program automatically provided detailed information about total blade deflections during this revolution. Since blade flapping, flatwise bending, and torsion mode time histories were virtually identical for any of the revolutions, it was valid to consider blade vertical and torsional deflections as cyclic. Detailed information about any particular revolution could be obtained, if necessary, by running separate Normal Mode Transient Analysis cases. However, the tenth revolution information was adequate for the purposes of this portion of the investigation.

The next set of Figures, 30 through 34, were prepared to aid in the comparison of different configurations, and also to present total blade deflections due to flapping, flatwise bending, and torsion.

Figure 30 shows articulated and nonarticulated blade tip vertical deflection nondimensionalized by rotor radius, together with blade tip elastic twist. These data were plotted as time histories against blade azimuth angle. Note that articulated and nonarticulated flapping response is almost identical for the advance ratios μ = .5 and μ = .60. The nonarticulated blade exhibits a larger amount of torsional motion for these advance ratios. When advance ratio is unity, both blade types undergo substantial torsional deflection, but the tip deflection increases considerably more for the nonarticulated than for the articulated blade. Figure 31 shows similar results for the articulated blade at advance ratio μ = 1.25. The nonarticulated blade results for this advance ratio are not presented here, since impractically large flatwise and edgewise bending deflections resulted, as shown previously in Figure 24.

Figure 32 (a) shows articulated blade results with and without pitch-flap coupling, at an advance ratio μ of 1.0. This type of coupling causes flapping response to be very small, and a pronounced beneficial effect on torsion response is evident. Apparently, the beneficial effects of pitch-flap coupling prevail on the retreating blade at this advance ratio. Figure 32 (b) and (c) show the similar results for advance ratios μ of 1.25 and 1.50. The maximum flapping response with this amount of coupling occurs when the blade is close to the 360-degree azimuth position. It occurs soon after the 180-degree azimuth position with no pitch-flap coupling. As mentioned previously, the similar results for advance ratio μ = 1.8 showed impractically large response.

Figure 33 shows articulated blade results with and without center-of-gravity offset. The 6% aft center-of-gravity offset causes some increase in flapping response at the lowest advance ratio $\mu = .5$ and a comparatively pronounced increase in torsional response, as shown in Figure 33(a). A similar result is obtained at advance ratio $\mu = .60$, shown in Figure 33(b). At the higher advance ratios, $\mu = 1.0$ and $\mu = 1.25$, shown on Figure 33(c) and (d), the 6% center-of-gravity offset has very little effect on flapping response during a typical revolution. A moderate increase in peak-to-peak torsion response occurs at the higher advance ratios. It should be remembered that the response with the center-of-gravity offset is somewhat larger during the first revolution after an instantaneous gust. The tenth revolution blade deflections for the 10% aft center-of-gravity offset configuration at $\mu = 1.25$ are shown in Figure 33(e). The flapping deflections are seen to be smaller with this center-of-gravity offset, but it should be remembered from Figure 29 that in this case, completely cyclic variations in flapping were not yet reached by the tenth revolution. A peak flapping response approximately 38% higher occurs in the eighth revolution. The torsion response contains high-frequency excursions of rather large amplitude, and it can be seen that these torsional deflections are not cyclic. It also can be seen that these oscillations appear on the advancing blade and tend to quench on the retreating blade.

Figure 34 contains corresponding results with and without 6% aft center-of-gravity offset for the nonarticulated rotor. These results are qualitatively similar to those for the articulated blade. As mentioned earlier, the instantaneous gust encounter for this nonarticulated configuration at $\mu = 1.25$ resulted in a rapidly diverging instability.

The aft center-of-gravity location would be expected to increase nose-up blade torsion with positive flapping in conventional flow and thus would increase blade flapping amplitude. In regions of reverse flow, the torsion-flapping coupling is made less destabilizing by moving the center of gravity aft on the blade. The area of reverse flow increases with advance ratio and accounts at least partially for the center-of-gravity effects shown in Figures 33 and 34. Note that advancing blade tip speed remains constant for these plots, so that retreating blade reverse-flow velocities increase with advance ratio. This would tend to magnify retreating blade effects as forward speed increases.

The effect of a control gyro is presented next, in Figures 35 through 39. The calculations were carried out using the method and configuration described previously for the single-degree-of-freedom analysis. In this case, however, the blade root bending moment and feathering couple were obtained from the Normal Mode Transient Analysis and were used in the calculation of gyro response. The effect of the gyro control inputs was determined for each of the five blades for a full revolution at an advance ratio $\mu = .60$. The total tip vertical deflection and torsional deflection are shown. One revolution was sufficient to show that the control gyro had at best an insignificant effect on flatwise response. It may, in fact, increase response on subsequent rotor revolutions. These results cannot be considered to be general, however, since other control gyro installations may behave differently. The entire character of the gyro response will

probably change as aircraft speed increases at constant advancing tip Mach number. The higher advance ratios would result in higher blade loads and therefore higher loads on the gyroscope. The slowing of the rotor and gyro rotational speed will also radically increase the response of the gyroscope to a given load. Thus, the gyroscope action would tend toward the response of a swashplate of high inertia.

The final set of figures for this investigation summarizes and compares the various results. Figure 40 shows the maximum and minimum values reached by flapping angle β and nondimensional tip deflection $\bar{\delta}_T$ during a typical revolution of the articulated blade after the gust onset, as calculated by the Normal Mode Transient Analysis. The maximum nondimensional tip deflections as calculated by the single-degree-of-freedom analysis are shown for comparison. Figure 41, which is similar to Figure 40, shows the corresponding results for the nonarticulated blade.

Figures 40 and 41 demonstrate that the single-degree-of-freedom analysis provides a conservative estimate of flapping response up to and well beyond the practical limits. It can also be seen that the single-degree-of-freedom analysis prediction for the articulated rotor is much more conservative than the corresponding prediction for the nonarticulated rotor. The data given in Figure 2 show that lead-lag motion alone cannot account for the discrepancy. From Figures 30 and 31, it can be seen that torsional motion of the blade also has an appreciable effect on the blade angle of attack distribution, thereby influencing blade loadings and flapping response. Apparently, the combined effects of blade torsional deflection and lead-lag cause the fairly important mitigation in flapping response for the articulated blade. It should be noted from Figures 23 and 24 that the first harmonic edgewise response of the nonarticulated blade is much larger than the corresponding first harmonic lead-lag motion of the articulated blade. Note, however, that the nonarticulated first edgewise modal amplitude peaks at approximately ψ = 90 degrees, while the articulated blade lead-lag motion peaks at about ψ = 270 degrees. It appears that torsional deflection leads to a beneficial lead-lag motion for the articulated blade. This is not present in the case of the nonarticulated blade, so the solution remains close to the single-degree-of-freedom result. Figures 40 and 41 also show that the blade tip deflection in both the articulated and nonarticulated cases is essentially composed of rigid flapping or first mode bending, respectively, as expected.

Figure 42 shows similar nondimensional vertical deflection envelopes for the articulated blade with and without pitch-flap coupling, as determined by the Normal Mode Transient Analysis and by the single-degree-of-freedom analysis. Note that only upward deflections are presented for the single-degree-of-freedom analysis. It can be seen that the single-degree-of-freedom analysis predicts the effect of pitch-flap coupling conservatively.

Figures 43 and 44 show the effects of aft center-of-gravity position on the articulated and nonarticulated blades respectively, as predicted by the Normal Mode Transient Analysis. These figures show that an aft center-of-gravity offset of 6% has little effect on flapping response, except at the lower advance ratios, where aft center of gravity causes an increase in

flapping. It should be remembered that these envelopes are for a typical revolution and that aft center of gravity would increase flapping somewhat during the first revolution after the instantaneous gust, as shown in Table VII and Figures 26 and 27.

Flight condition 7 of Table IV gave results for β_{MAX}/λ_G which were similar to corresponding results for condition 3, as shown in Table VII. Thus, the linearity of the flapping response with respect to gust amplitude is also present in the solutions of the extended Normal Mode Transient Analysis. This permits the calculation of response to more elaborate gust representations through use of the principle of superposition, and the various statistical methods that may be employed. Because of the basic rotor symmetry, upward or downward gusts would have similar responses of opposite sense on a lightly loaded rotor.

The use of the single-degree-of-freedom analysis and the preliminary design methods presented earlier seems to be well justified for blades similar to those treated here, if it is recognized that the results for articulated blades may be rather conservative. It appears that articulated blade torsion and lagging may exert an important effect, especially for advance ratios near unity and greater. In order to show the effect on permissible flight conditions of gust velocity, Figure 45 has been prepared by using Eq. 4, data from Figure 5, and Table VII. The powerful effect of pitch flap coupling shown in Figure 42 is clearly demonstrated here. It can be seen that the discrepancy between the single-degree-of-freedom solution and the Normal Mode Transient Analysis solution is of less practical importance than would be inferred from Figures 40 and 42. Extrapolation on Figure 45 indicates that a speed exists for which any indefinitely small disturbance will cause the blades to reach their flapping limits, but this speed is very high, on the order of 400 knots. This result is, of course, applicable only to the specific blade configuration considered.

FLAP-LAG INSTABILITY

The existence of a basic type of articulated rotor instability under heavy loads was predicted in Reference 7, where an approximate analysis was used. With this simple analysis, it was concluded that a heavily loaded rotor could develop catastrophically large flapping motions due to coupling with lead-lag deflections, as a result of quite moderate initial disturbances. The investigation in this section was intended to determine if this type of instability would be predicted with the quite elaborate Normal Mode Transient Analysis, in which blade stall, reverse-flow, and compressibility effects, as well as elastic deflections, are considered. The investigation was limited to a few sample cases for which flap-lag instability could be anticipated using the analysis of Reference 7. These sample cases are at advance ratios, μ , of 0.3, 0.5, and 0.7. Various sudden collective pitch increments were applied, and the blade response was calculated for several subsequent revolutions to investigate basic instabilities involving coupled flapping and lead-lag motion.

The Normal Mode Transient Analysis was used to investigate the possibility of unstable flapping motion of an articulated rotor due to nonlinear coupling with lead-lag motion. The existence of such behavior is discussed in Reference 7, where it is theorized that an impulsive disturbance of the rotor could initiate coupled, unstable motion. Whether or not the motion becomes completely unstable is determined by the amount of viscous damping in the system; since the flap damping is primarily aerodynamic in nature, the significant parameter becomes the mechanical viscous lag damping. In this investigation, the S-58 (CH-34) rotor parameters were used to define the dynamic system, and the transient response to a disturbance was determined as follows. At each of three forward speeds, a high rotor loading condition was established with the Normal Mode Transient Analysis, and the steady-state flapping and lagging motions were determined. With these motions utilized as initial conditions, an increment of collective pitch was introduced and the resultant transient blade motion was calculated. This procedure was duplicated with and without normal mechanical lag damping. The results obtained are presented in Figures 46 through 51.

In Figure 46, the steady-state blade motions at $\mu = 0.5$ and $C_L/\sigma = 0.06$ are shown, followed by the response of the blade to an instantaneous 2-degree increase in collective pitch (8 degrees to 10 degrees). Normal lag damping is in effect. After three revolutions of the rotor, an additional 2 degrees of collective pitch is applied (10 degrees to 12 degrees), and two more rotor revolutions are shown. In Figure 47, the transient response to the same inputs of collective pitch and steady-state condition are shown, the difference in this case being the absence of mechanical lag damping. Comparison of the fifth transient revolution from each of these figures reveals no significant difference in blade motions and no indication of catastrophic flapping instability. Figure 48 shows the transient response without lag damping to an instantaneous 4-degree increase in collective pitch (8 degrees to 12 degrees) for the same initial conditions as Figure 47. After five revolutions, there is still no significant difference in the flapping motion from that shown in Figure 46. An increase

of 14% in the maximum lag angle has taken place after the single large pitch change, compared with that for the two smaller changes. The lagging amplitude is, nevertheless, decreasing in the fourth and fifth revolutions after the disturbance. The transient response to a 2-degree increase in collective pitch (0 degrees to 2 degrees) at $\mu = 0.7$ was calculated in a similar manner, starting from a steady-state rotor lift condition of $C_L/\sigma = 0.057$. The results obtained without lag damping are shown in Figure 49. After five revolutions, the flapping amplitude has steadied out. The lag motion, however, has assumed a high-frequency character with small amplitude. This response is a result of the excitation of the second edgewise bending mode which has a frequency of 9.13 cycles per revolution. The final condition investigated was at $\mu = 0.3$ with a collective pitch of $\Theta.75R = 11.75$ degrees and a steady-state rotor lift coefficient-solidity ratio of 0.10. At this steady condition, a 4-deg collective pitch increment was added and subtracted, and the resulting transient responses were calculated in each case. The results are shown in Figures 50 and 51. In the first case, the flapping and lagging amplitudes steady out quickly, and their harmonic content remains essentially one per revolution. In the second case, the motions steady out with amplitudes of only 2.5 degrees in flapping and 1.0 degree in lagging. Neither of these cases exhibits any instability in blade motion.

For reference, the nominal rotor lift coefficient-solidity ratios were computed for the final revolutions shown in Figures 46 through 51. In Figures 46, 47, and 49, the final values obtained were $C_L/\sigma = 0.10$; in Figures 48 and 50, the final values were $C_L/\sigma = 0.11$. In Figure 51, decreasing collective pitch resulted in a final $C_L/\sigma = 0.03$. These values are in good agreement with the steady-state lift values that would be expected if the collective pitch increments were applied slowly rather than instantaneously.

In Reference 10, a method incorporating only flap and lead-lag degrees of freedom is used to calculate the blade response to a disturbance. The predicted blade behavior discussed above is in general qualitative agreement with the results shown in Reference 10. The results of Reference 10 include slowly diverging or converging blade motions following the initial disturbance. In the present investigation fewer rotor revolutions were considered than in Reference 10, because of the greater complexity of the method. Therefore a very slow noncatastrophic divergence or convergence cannot be definitely detected as such. The results shown in Figure 48 may fall into this category. Disregarding such tendencies toward gradual amplitude changes, the present analysis indicates that although rotor disturbances in the form of sudden changes in collective pitch may cause flapping and lagging motions that are unacceptable practically, such changes do not induce catastrophic instability. The mechanical viscous restraint of the lag motion tends to moderate the transient blade response, but its absence or presence does not affect the conclusion just stated.

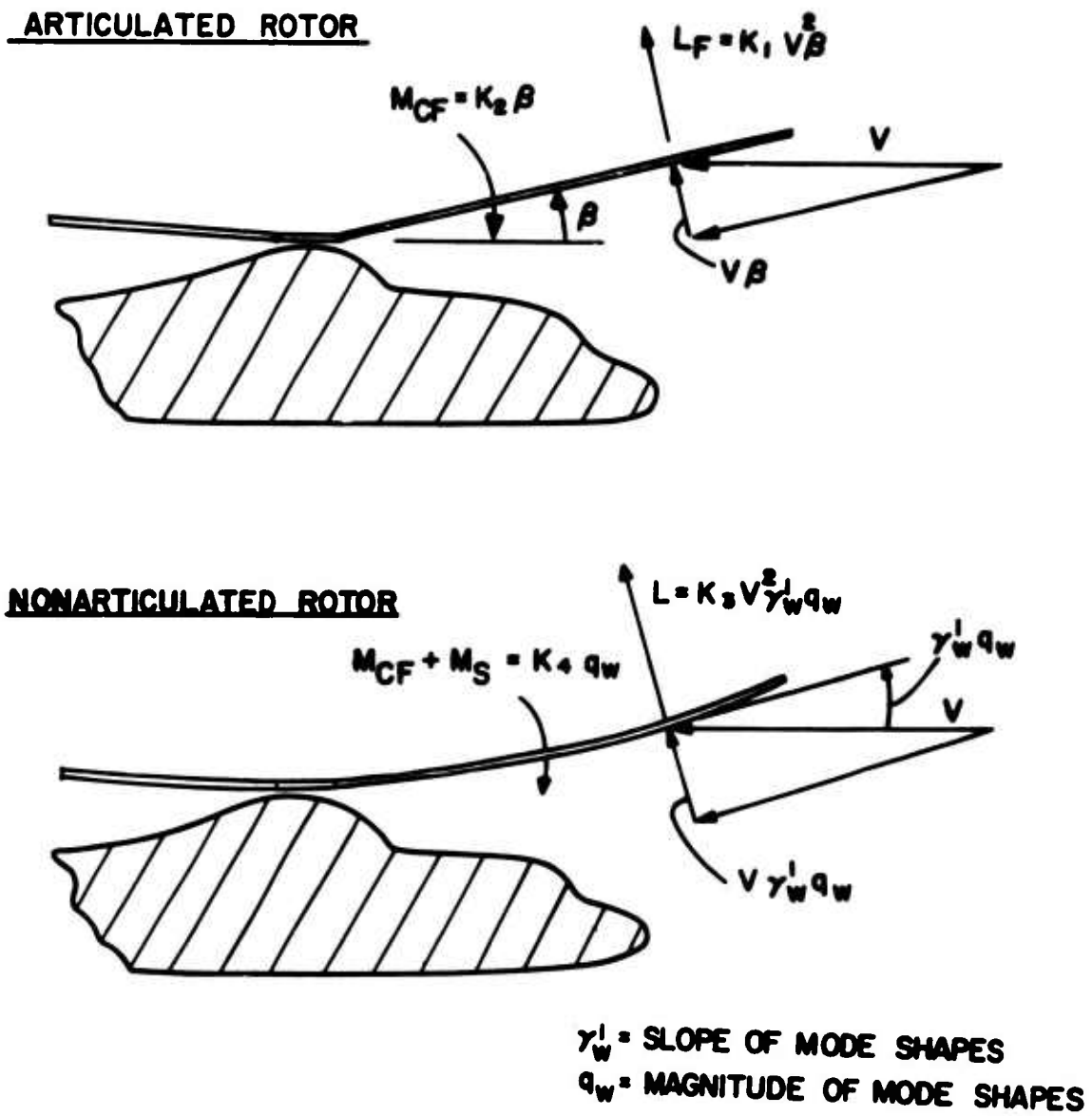

Figure 1. Mechanism of Flapping or Flatwise Bending Instability.

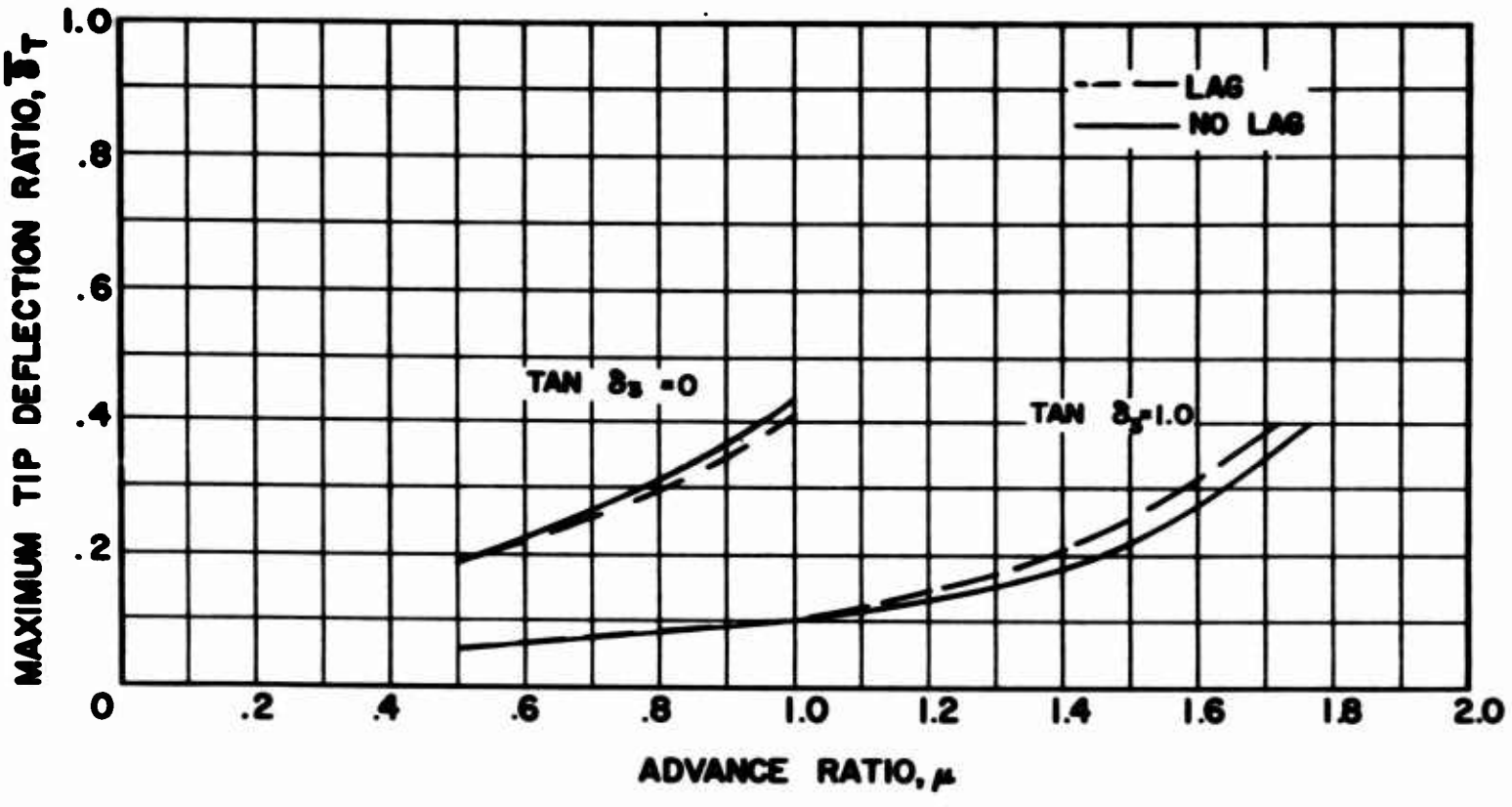

Figure 2. Effect of Lag Coupling on Flapping Amplitude for Articulated Rotor; M_R =1.85, C_{FD} = 0, $M_{1,90}$ = .85, W_G =30 FT/SEC, $\bar{r}_{OA}$ = .12, ψ_0 = 0°, δ_4 = 0.

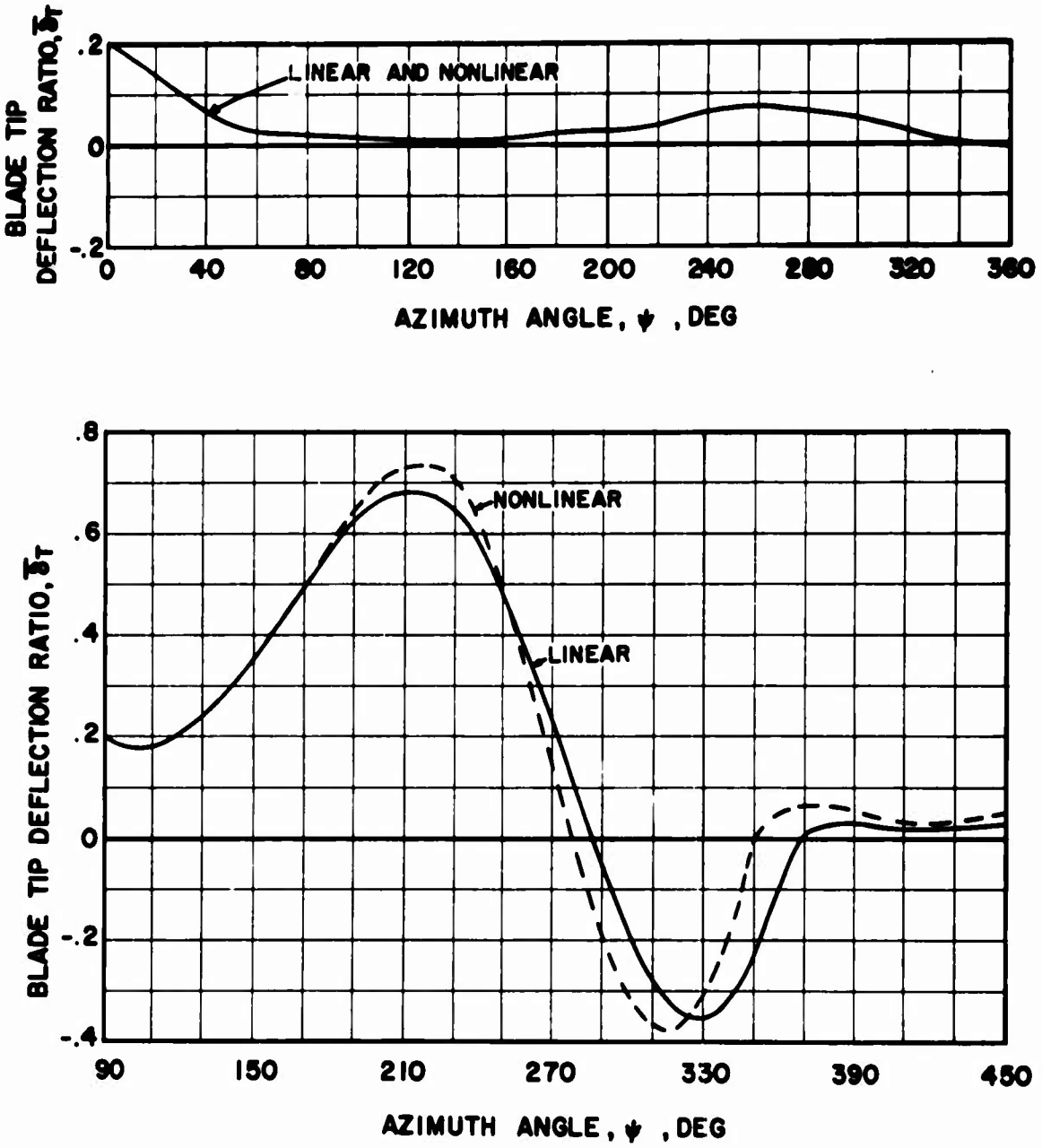

Figure 3. Typical Effect of Centrifugal Spring Force Nonlinearity on Articulated Rotor Blade Transient Response; $\mu = 1.5$, $M_R = 1.85$, $C_{FD} = 0$, $M_{1,90} = .85$, $W_G = 30$ FT/SEC, $\bar{r}_{OA} = .12$, $\psi_O = 0°$, $\delta_4 = 0$

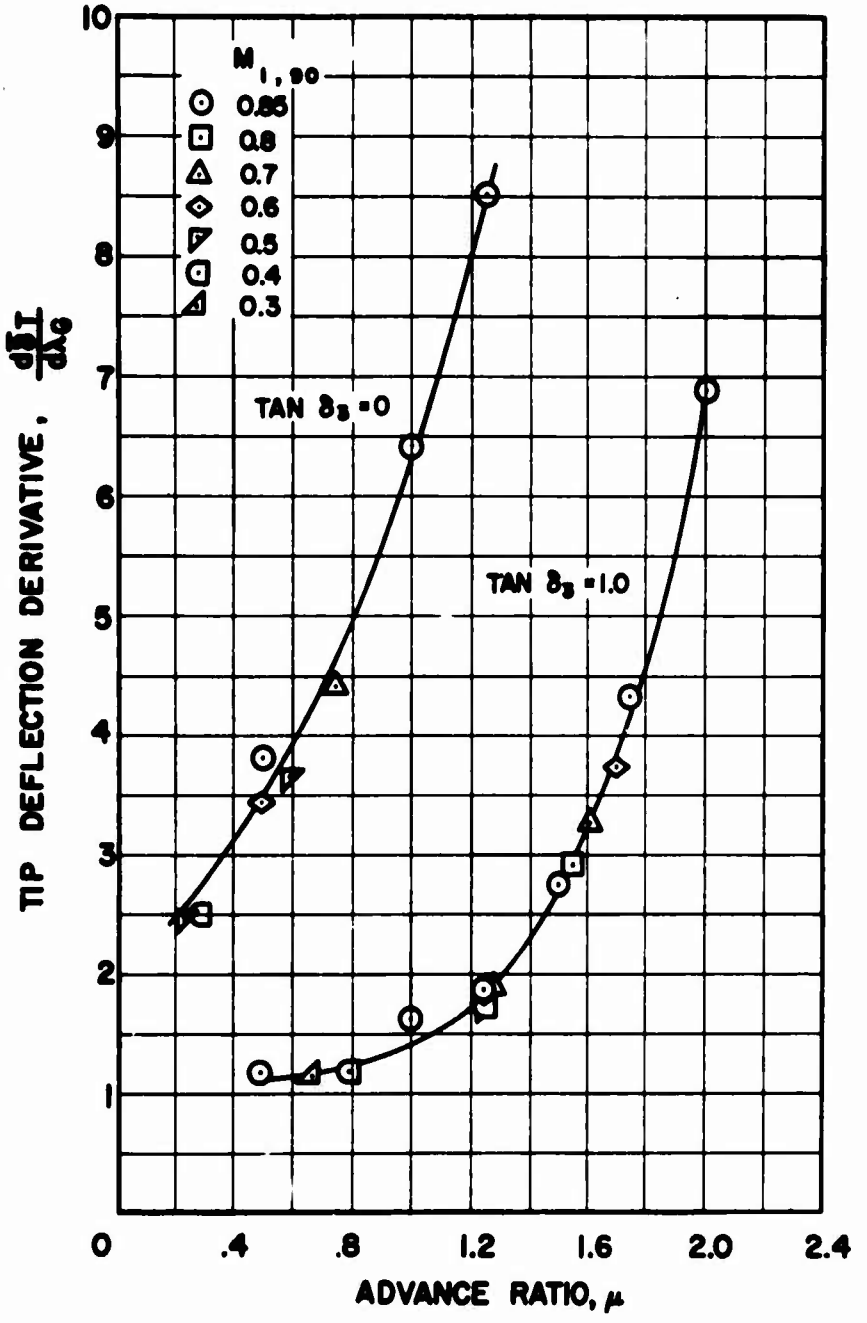

Figure 4. Effect of Advancing Blade Tip Mach Number on Tip Deflection Derivative; $M_R = 1.85, C_{FD} = 0$, $W_G = 30$ FT/SEC, $\bar{r}_{OA} = .12$, $\psi_0 = 0°$, $\delta_4 = 0$.

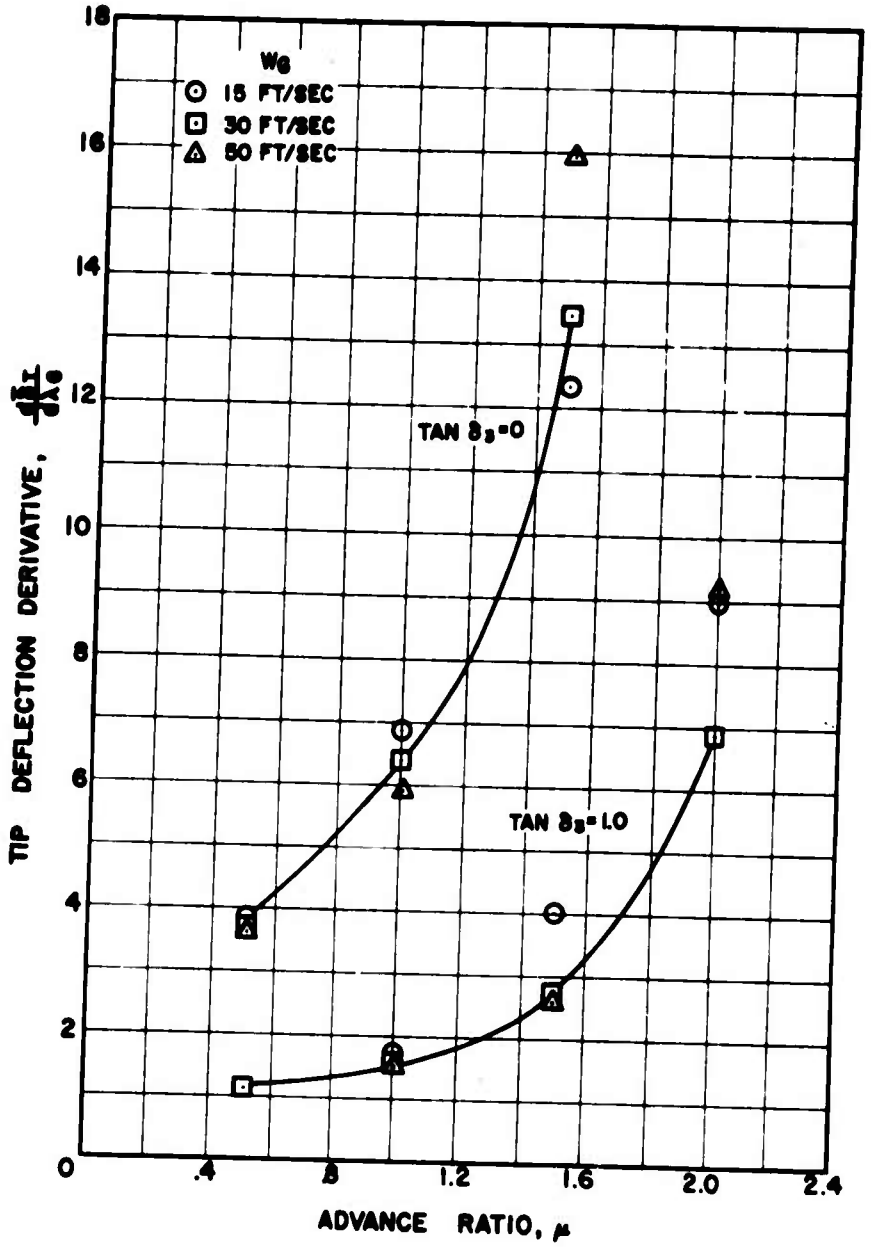

Figure 5. Effect of Gust Size on Tip Deflection Derivative for Articulated Rotor; M_R=1.85, C_{FD} =0, $M_{1,90}$=.85, $\bar{r}_{0A}$ =.12, ψ_0 =0°, δ_4 =0.

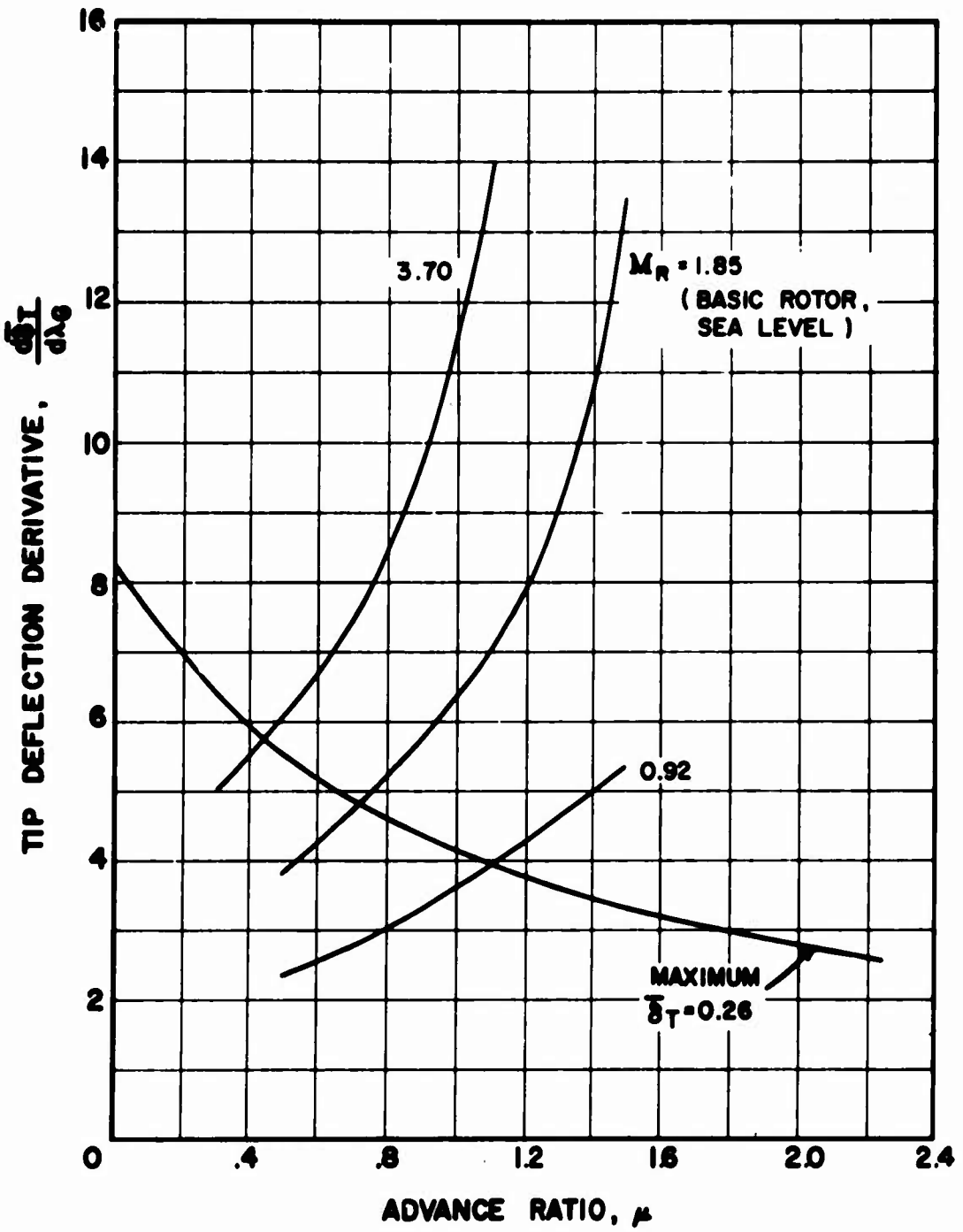

Figure 6. Effect of Mass Parameter on Tip Deflection Derivative for Articulated Rotor; $\delta_3 = 0°, C_{FD} = 0, M_{1,90} = .85, W_G = 30$ FT/SEC, $\bar{r}_{OA} = .12, \psi_0 = 0°, \delta_4 = 0$.

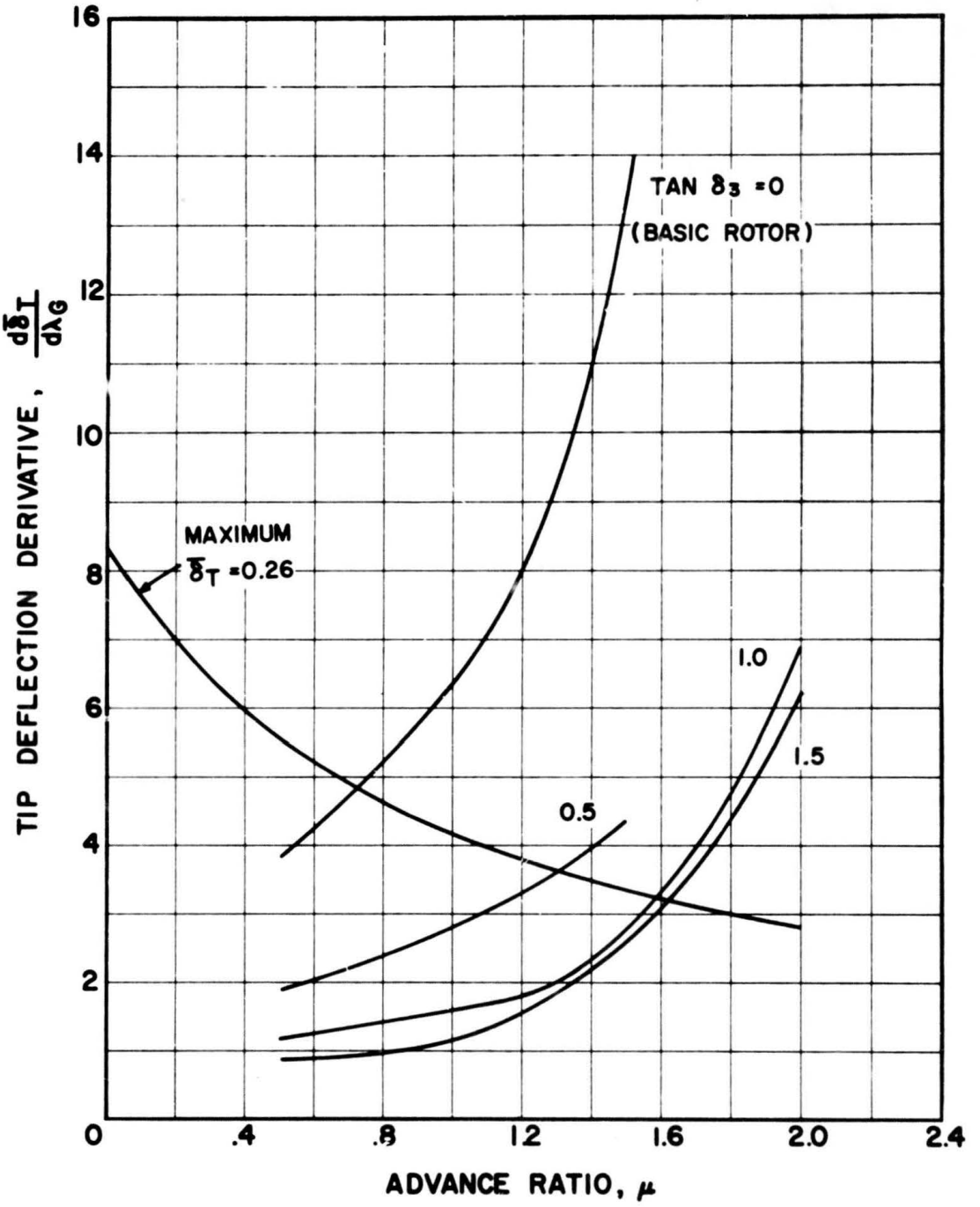

Figure 7. Effect of Pitch-Flap Coupling on Tip Deflection Derivative for Articulated Rotor; $M_R = 1.85$, $C_{FD} = 0$, $M_{1,90} = .85$, $W_G = 30$ FT/SEC, $\bar{r}_{OA} = .12$, $\psi_0 = 0°$, $\delta_4 = 0$.

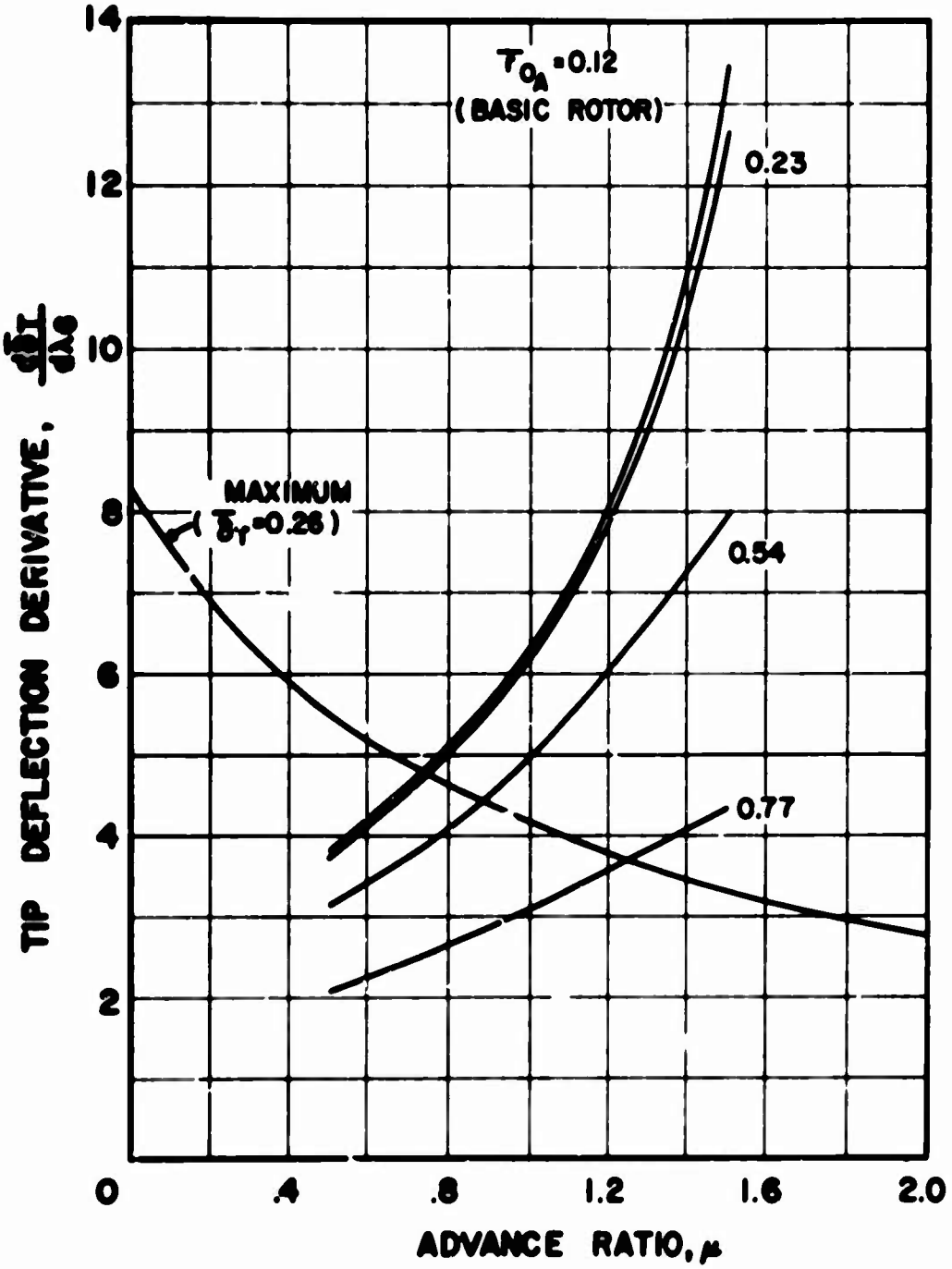

Figure 8. Effect of Aerodynamic Root Cutout on Tip Deflection Derivative for Articulated Rotor; $M_R = 1.85$, $\delta_3 = 0°$, $C_{FD} = 0$, $M_{1,90} = .85$, $W_G = 30$ FT/SEC, $\psi_0 = 0°$, $\delta_4 = 0$.

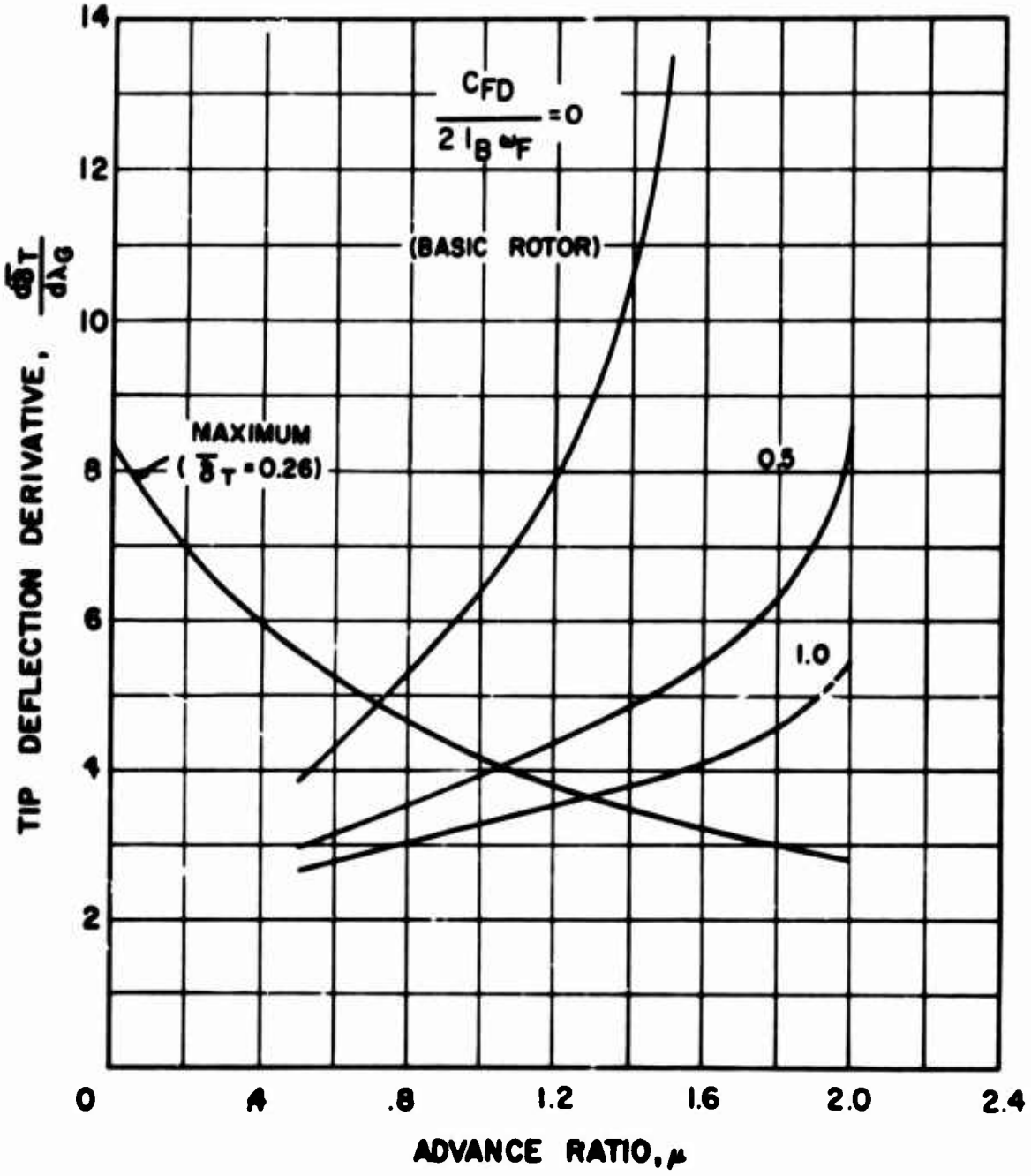

Figure 9. Effect of Flap Damper on Tip Deflection Derivative for Articulated Rotor; $M_\beta = 1.85$, $\delta_3 = 0°$, $M_{1.90} = .85$, $W_G = 30$ FT/SEC, $\bar{T}_{OA} = .12$, $\psi_0 = 0°$, $\delta_4 = 0$.

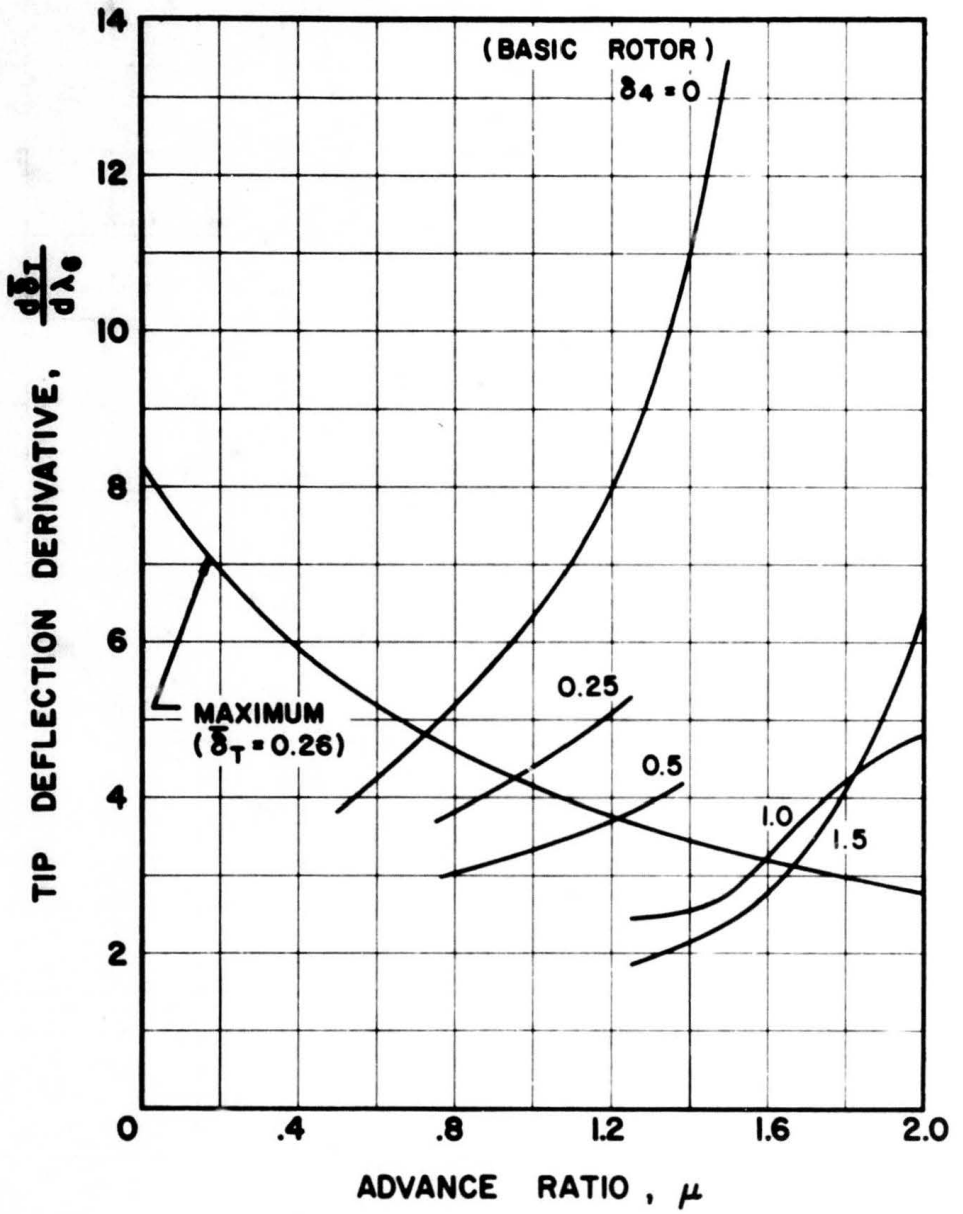

Figure 10. Effect of Pitch-Flap Velocity Coupling on Tip Deflection Derivative for Articulated Rotor; $M_R = 1.85$, $\delta_3 = 0°$, $C_{FD} = 0$, $M_{1,90} = .85$, $W_G = 30$ FT/SEC, $\bar{r}_{OA} = .12$, $\psi_0 = 0°$.

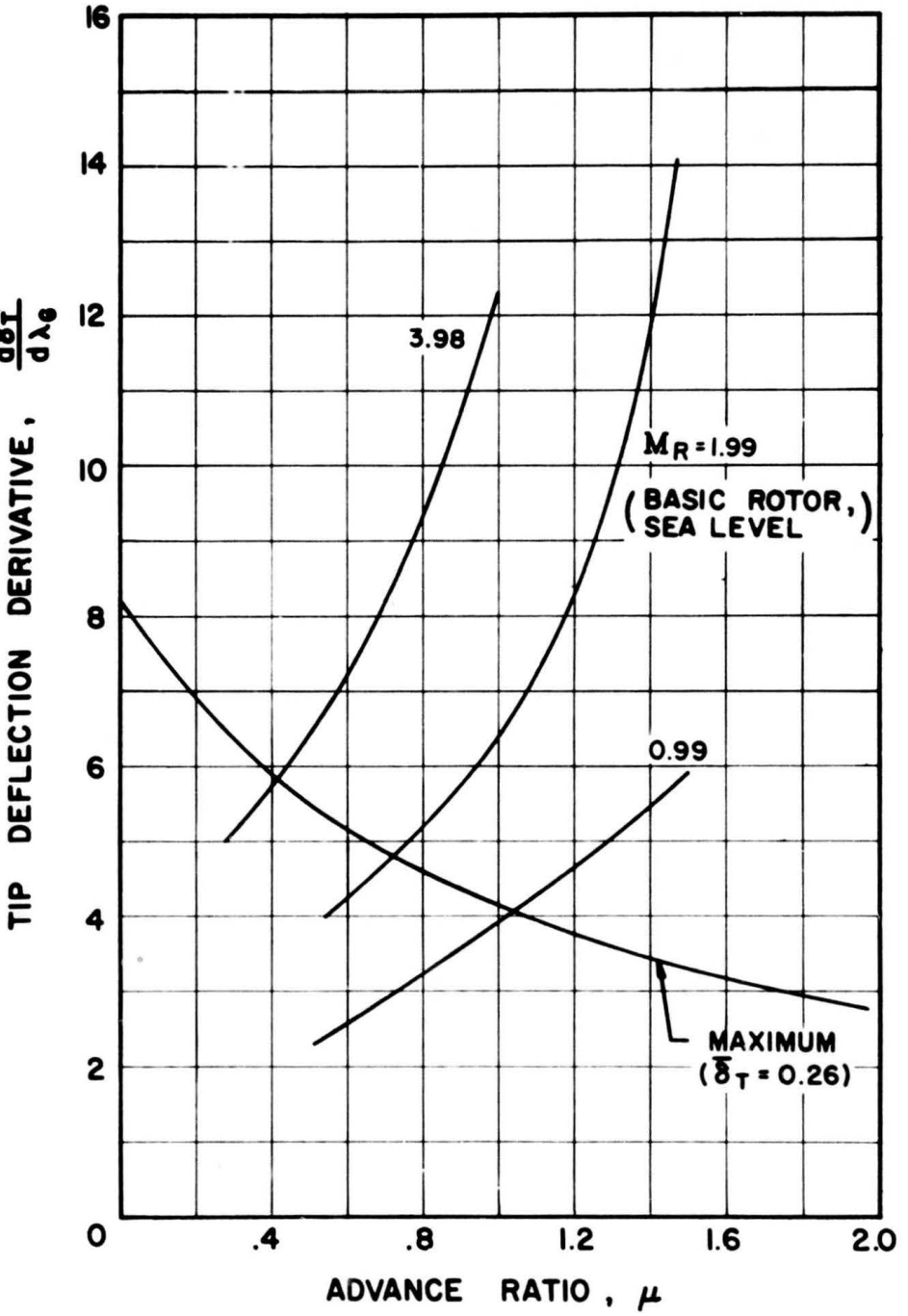

Figure 11. Effect of Mass Parameter on Tip Deflection Derivative for Nonarticulated Rotor; $\bar{\omega}_{W_I} = 1.12$, $M_{1,90} = .85$, $W_G = 30$ FT/SEC, $\bar{r}_{OA} = .12$, $\Psi_0 = 0°$.

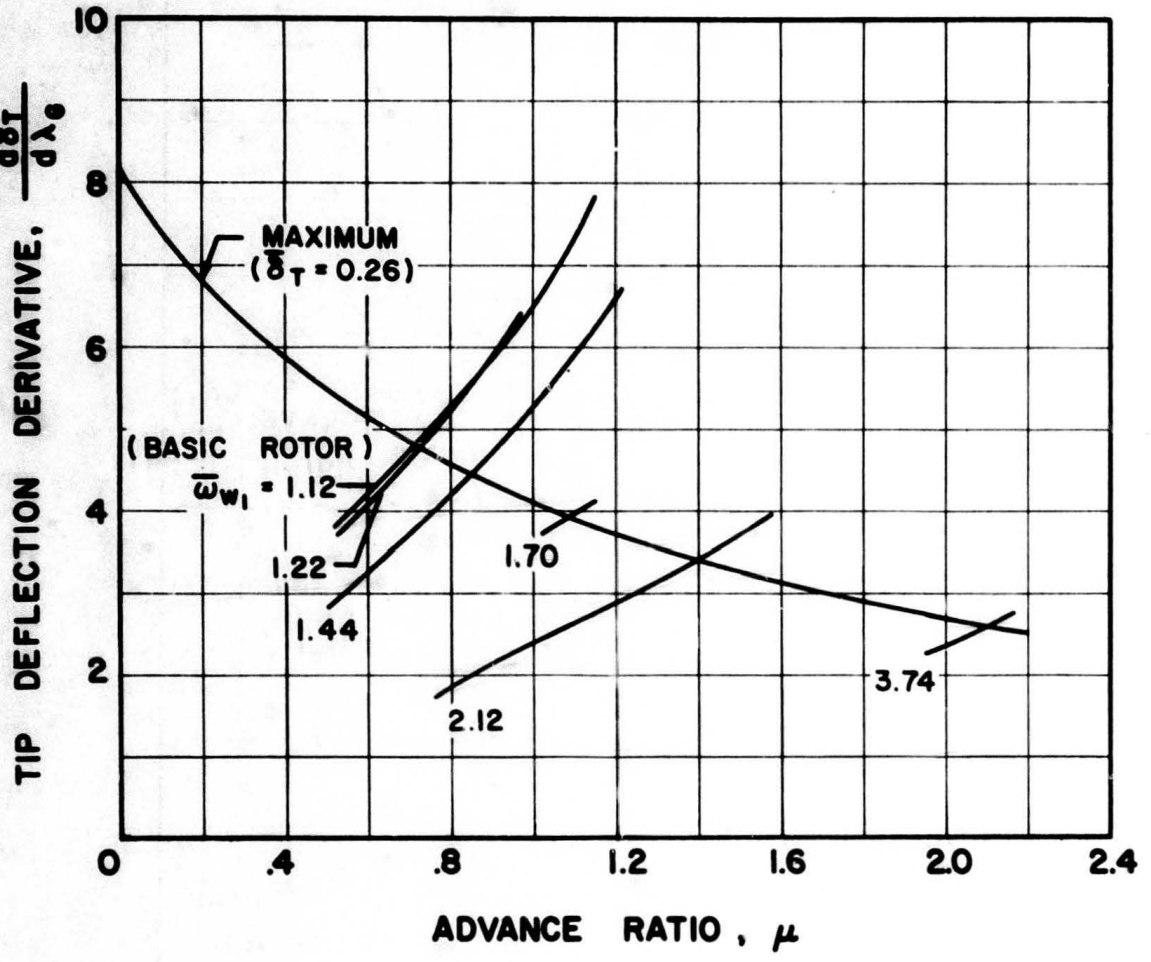

Figure 12. Effect of Frequency Ratio on Tip Deflection Derivative for Non-articulated Rotor; $M_R = 1.99$, $M_{1,90} = .85$, $W_G = 30$ FT/SEC, $\bar{r}_{OA} = .12$, $\psi_0 = 0°$.

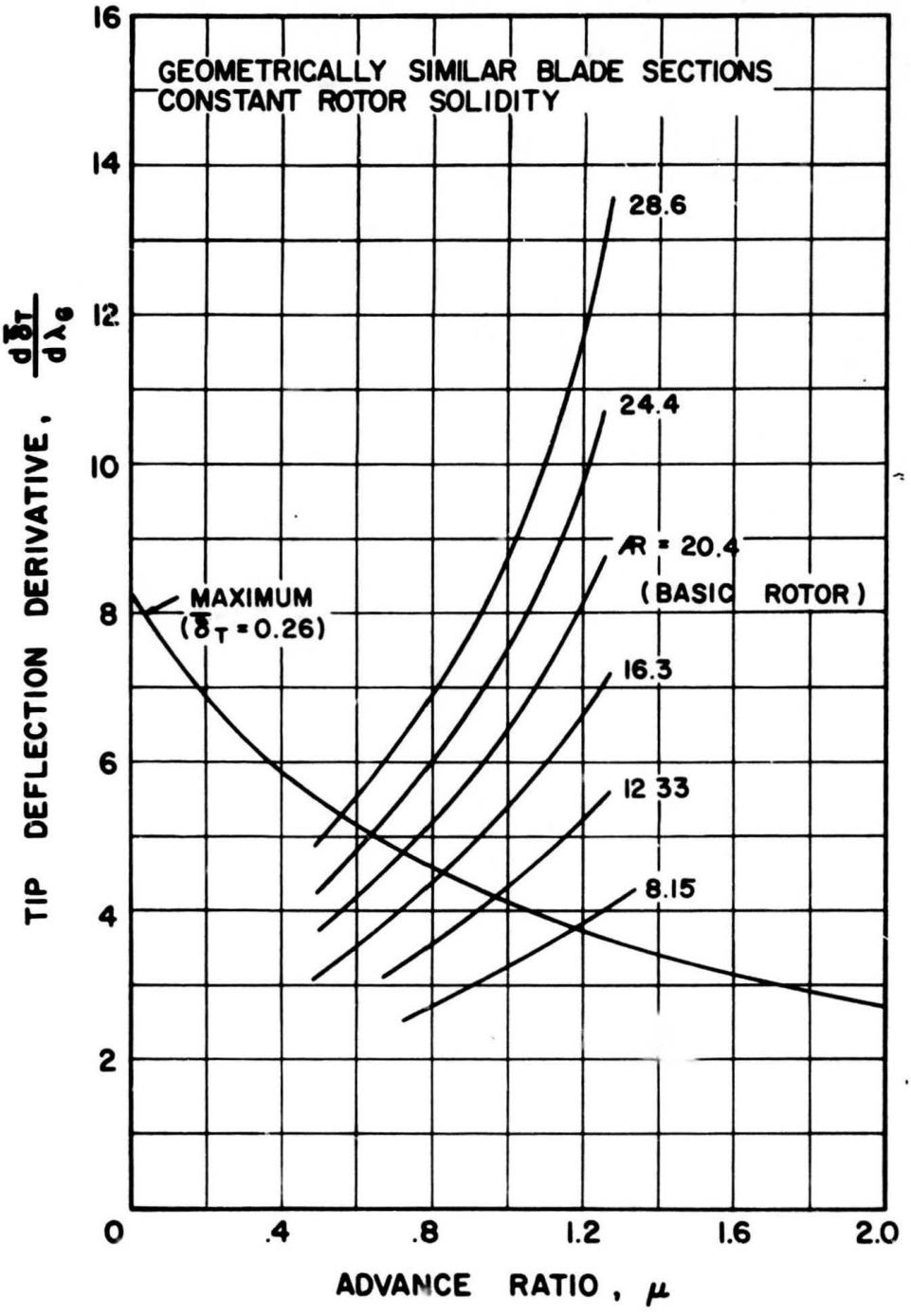

Figure 13. Effect of Aspect Ratio on Tip Deflection Derivative for Nonarticulated Rotor; $M_{1,90}$ = .85, W_G = 30 FT/SEC, $\bar{r}_{OA}$ = .12, ψ_0 = 0°, σ = .078.

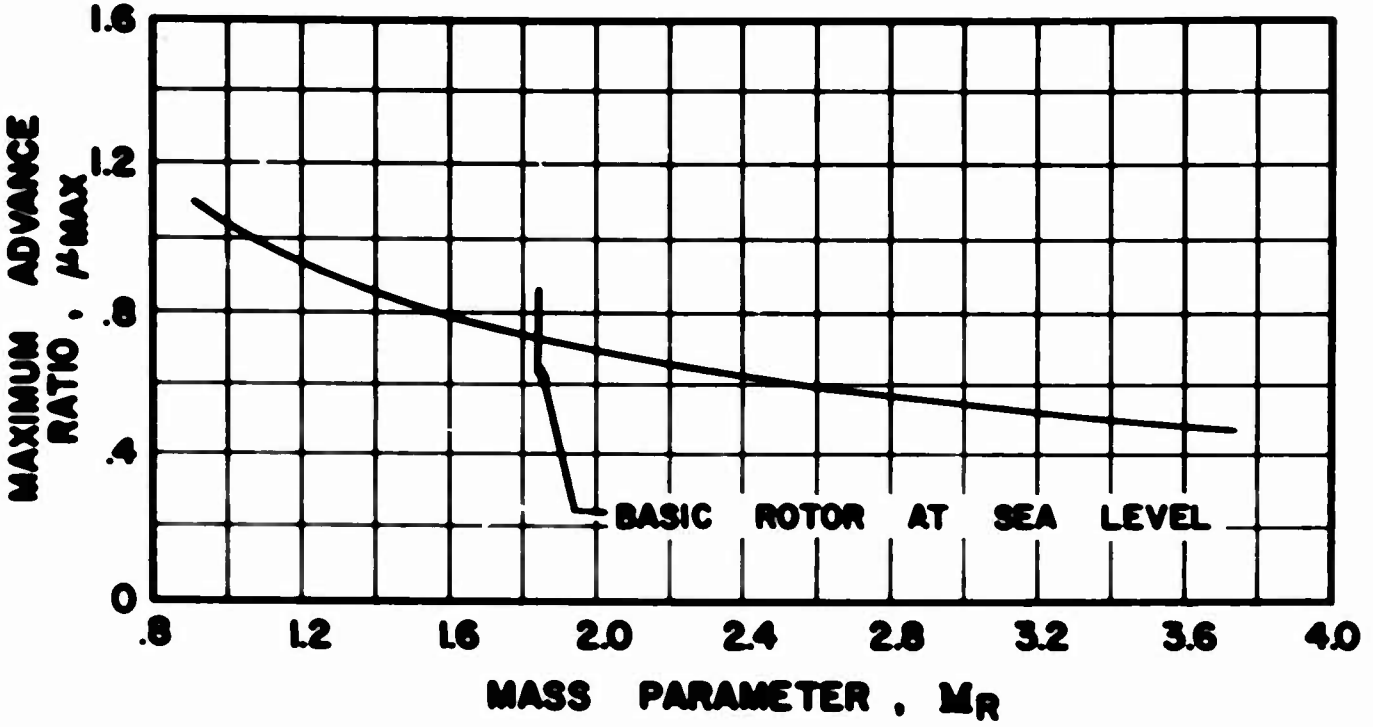

Figure 14. Effect of Mass Parameter on Maximum Advance Ratio for Articulated Rotor; $\delta_3 = 0°, C_{FD} = 0, M_{1,90} = .85, W_G = 30$ FT/SEC, $\bar{r}_{OA} = .12, \psi_O = 0°, \delta_4 = 0, \bar{\delta}_T = .26$.

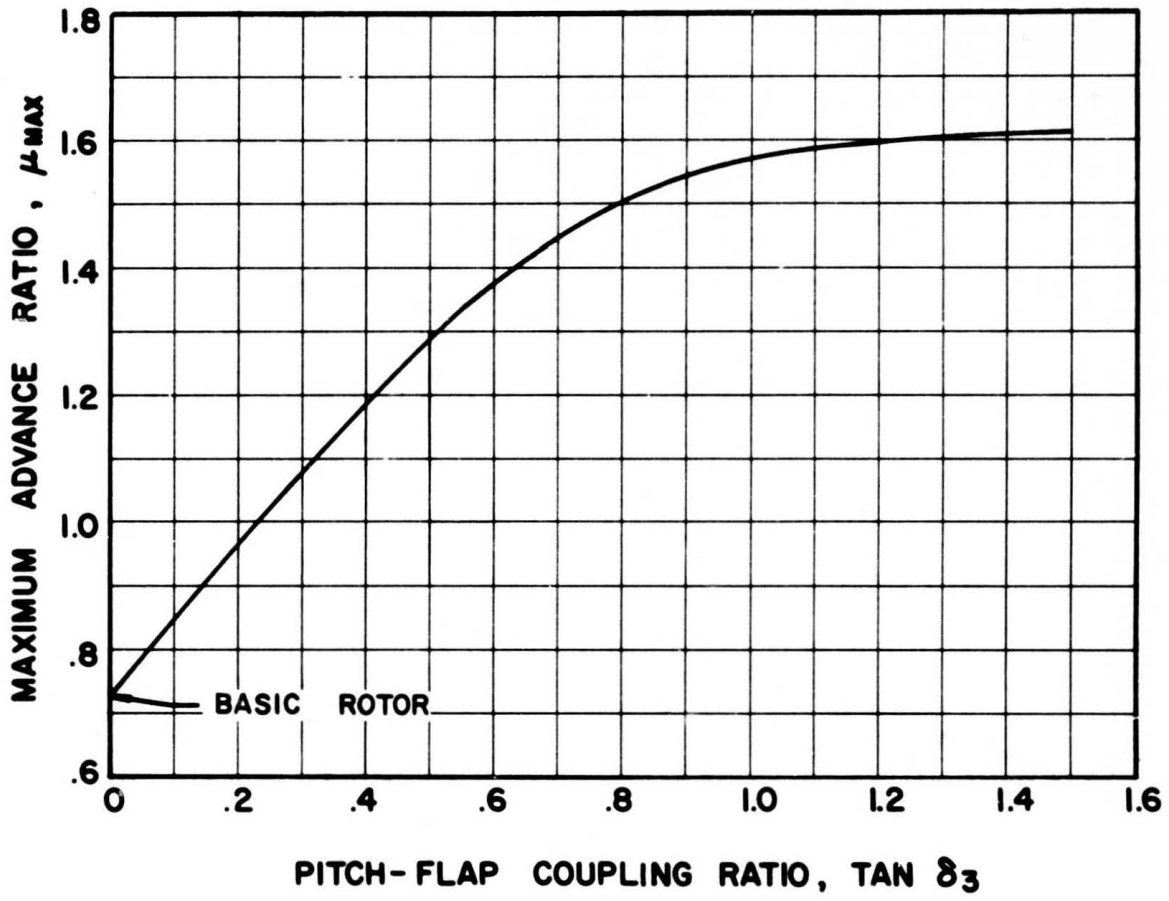

Figure 15. Effect of Pitch-Flap Coupling on Maximum Advance Ratio for Articulated Rotor; $M_R = 1.85$, $C_{FD} = 0$, $M_{1,90} = .85$, $W_G = 30$ FT/SEC, $\bar{r}_{OA} = .12$, $\psi_0 = 0°$, $\delta_4 = 0$, $\bar{\delta}_T = .26$.

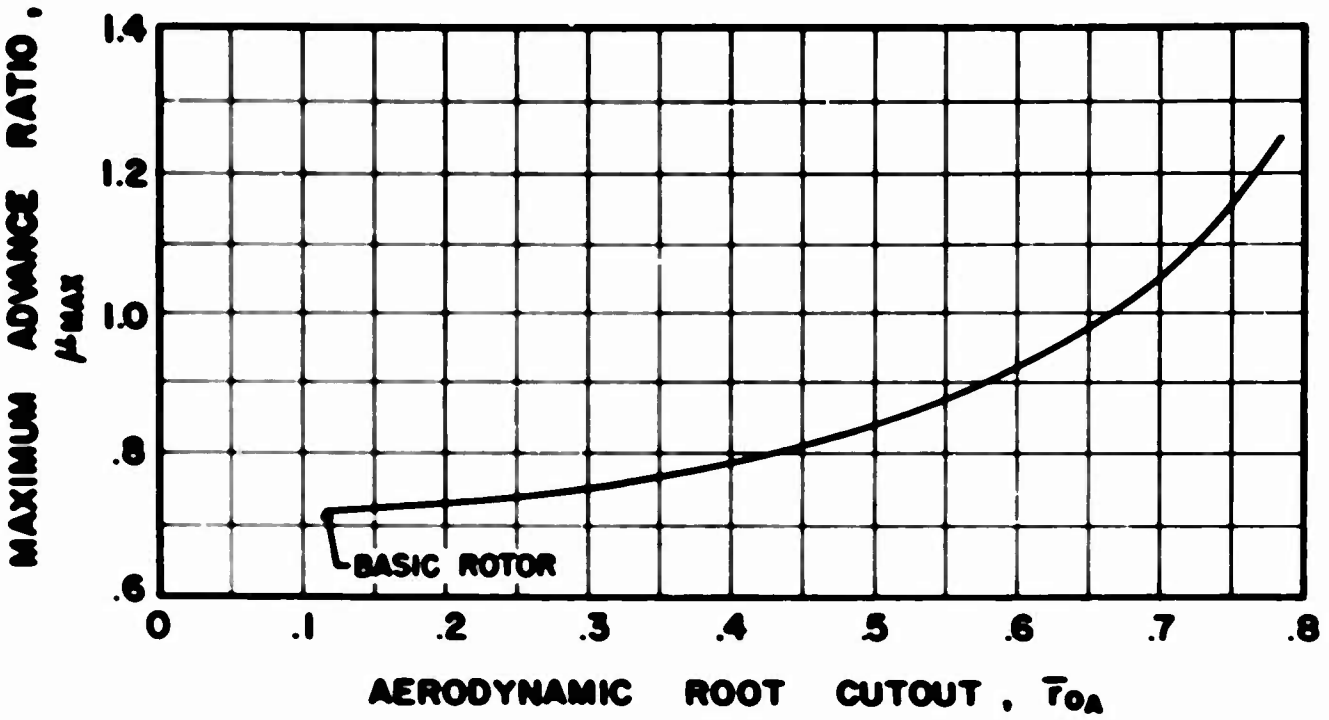

Figure 16. Effect of Aerodynamic Root Cutout on Maximum Advance Ratio for Articulated Rotor; $M_R = 1.85$, $\delta_3 = 0°$, $C_{FD} = 0$, $M_{1,90} = .85$, $W_G = 30$ FT/SEC, $\psi_0 = 0°$, $\delta_4 = 0$, $\bar{\sigma}_T = .26$.

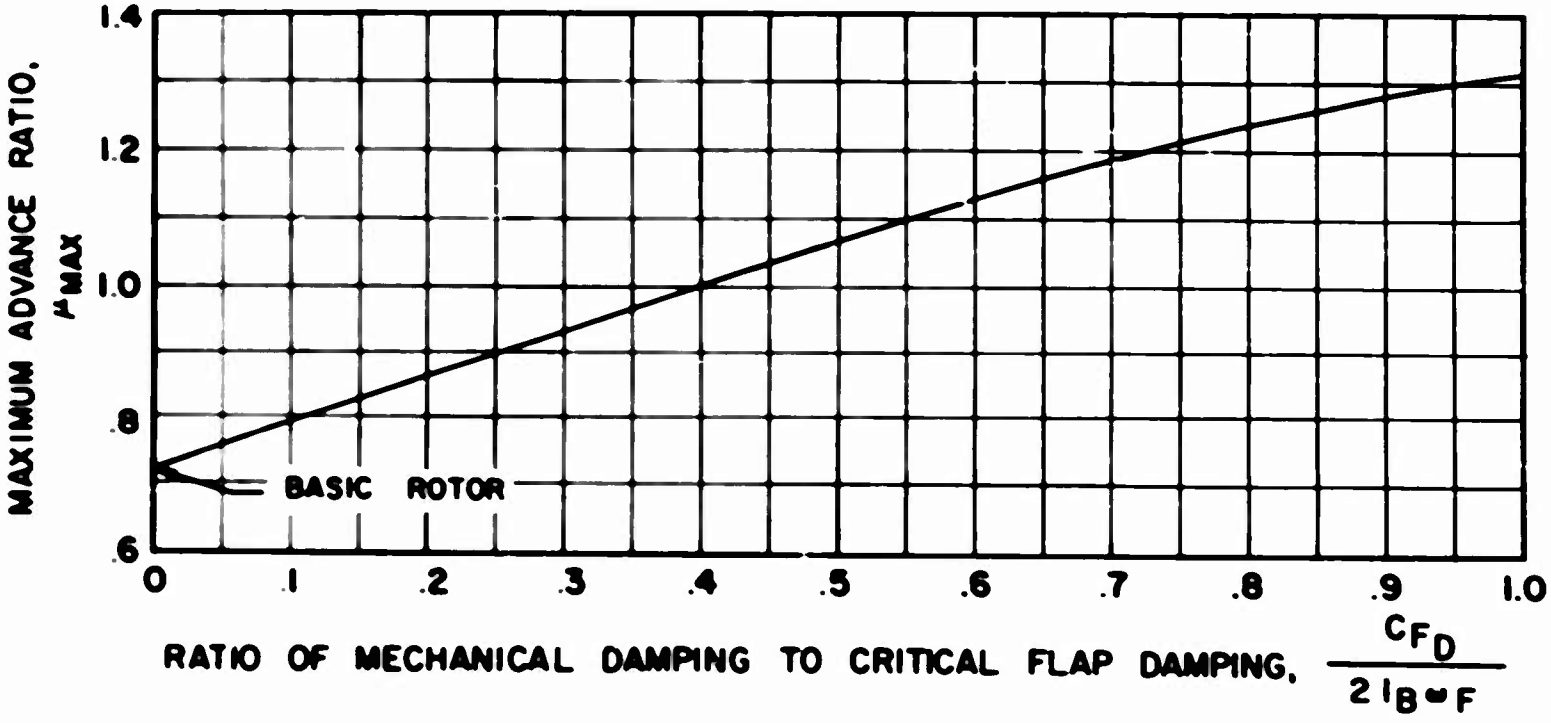

Figure 17. Effect of Mechanical Flap Damping on Maximum Advance Ratio for Articulated Rotor; $M_R = 1.85$, $\delta_3 = 0°$, $M_{1,90} = .85$, $W_G = 30$ FT/SEC, $T_{OA} = 12$, $\psi_0 = 0°$, $\delta_4 = 0$, $\delta_T = 26$

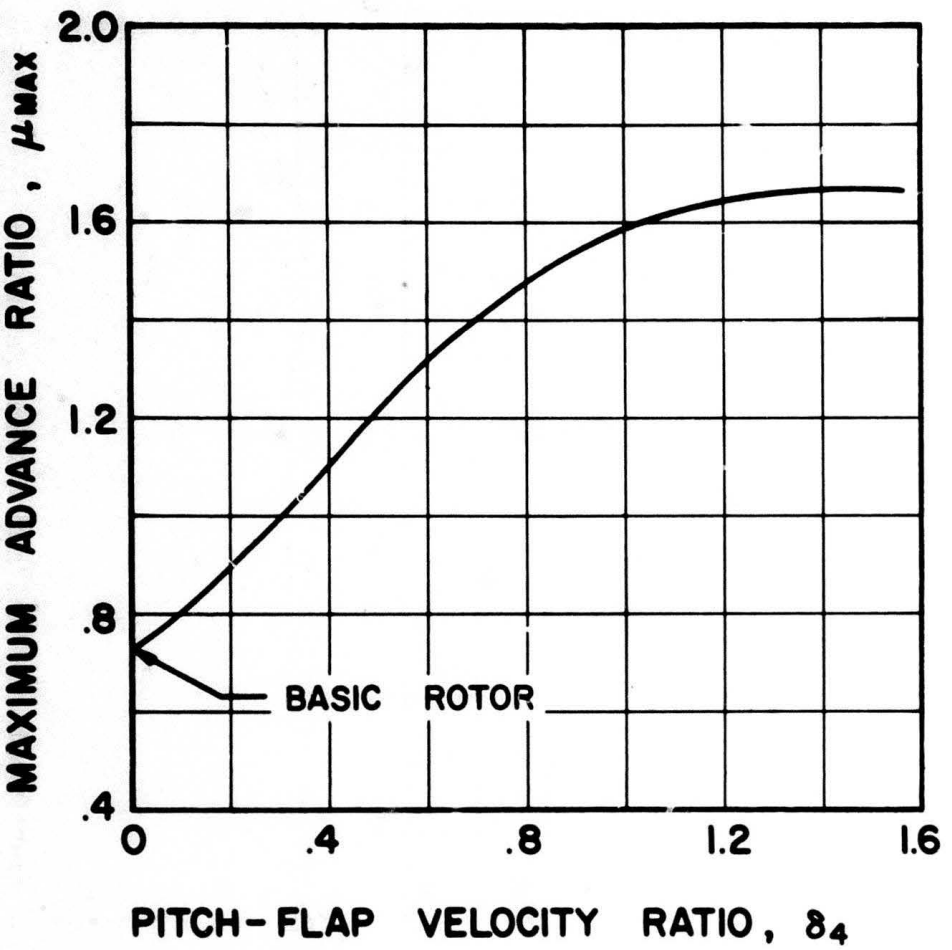

Figure 18. Effect of Pitch-Flap Velocity Coupling on Maximum Advance Ratio for Articulated Rotor; $M_R = 1.85, \delta_3 = 0°, C_{FD} = 0, M_{1,90} = .85, W_G = 30$ FT/SEC, $\bar{r}_{OA} = .12, \psi_0 = 0°, \bar{\delta}_T = .26$.

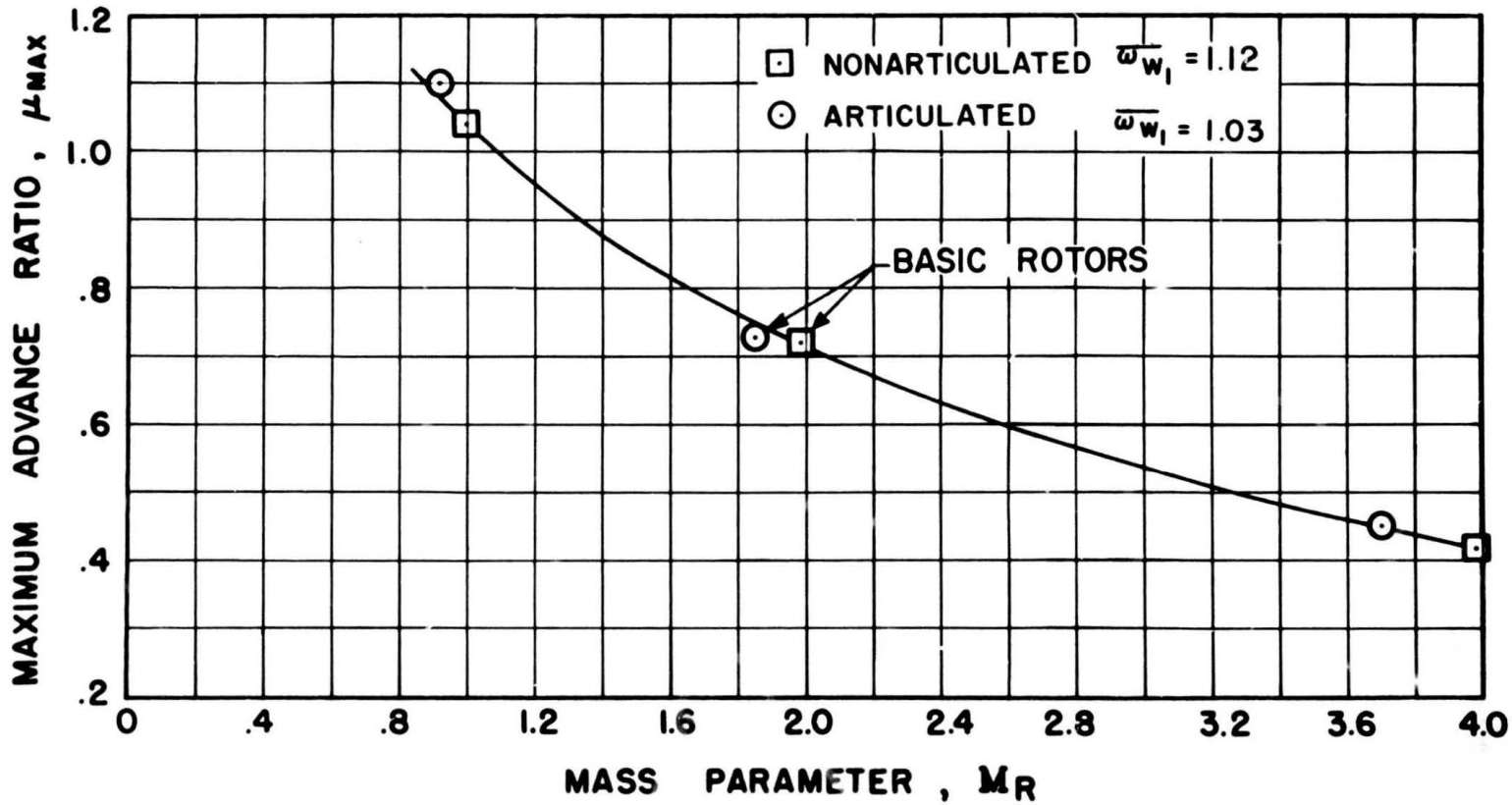

Figure 19. Effect of Mass Parameter on Maximum Advance Ratio; $\delta_3 = 0°, C_{FD} = 0$, $M_{1,90} = .85$, $W_G = 30$ FT/SEC, $\bar{r}_{OA} = .12$, $\psi_0 = 0°$, $\delta_4 = 0$, $\bar{\delta}_T = .26$.

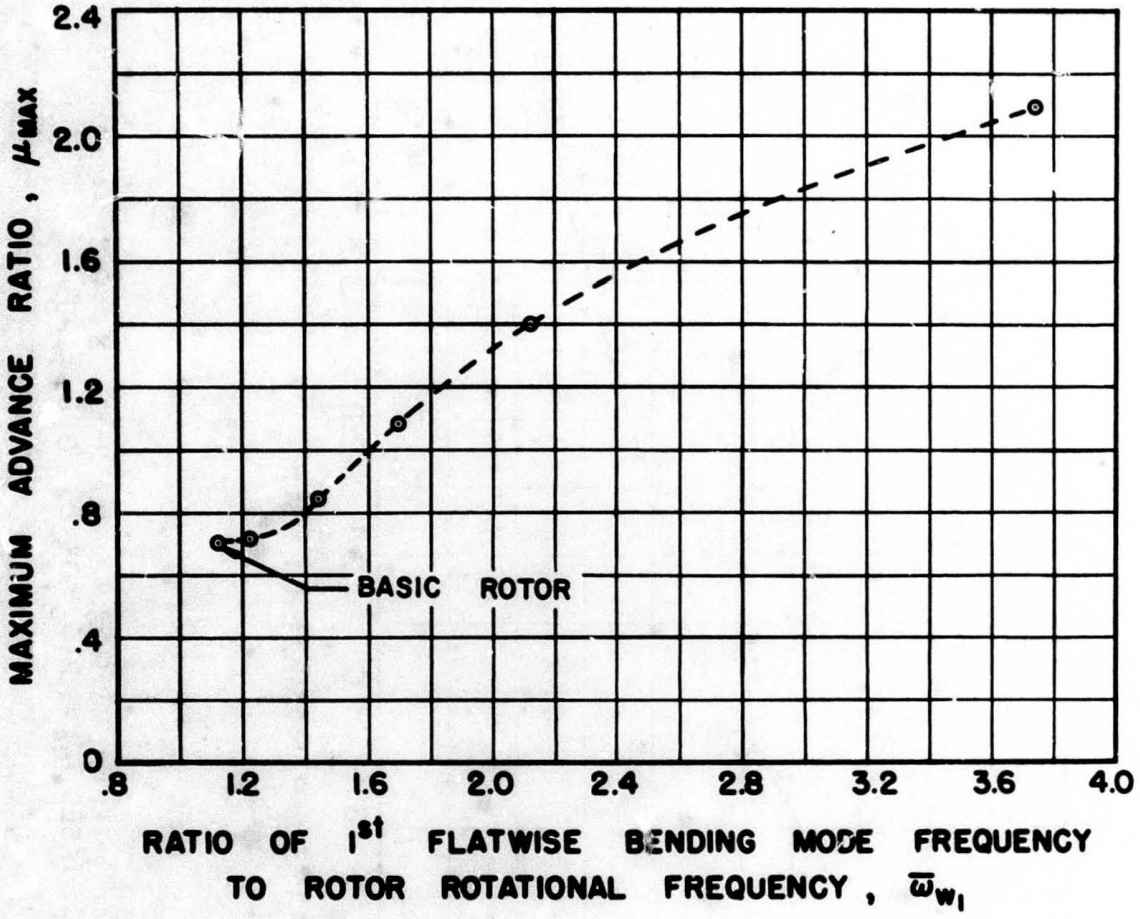

Figure 20. Effect of Frequency Ratio on Maximum Advance Ratio for Nonarticulated Rotor; $M_R = 1.99$, $M_{1,90} = .85$, $W_G = 30$ FT/SEC, $\bar{r}_{OA} = .12$, $\psi_0 = 0°$, $\delta_T = .26$.

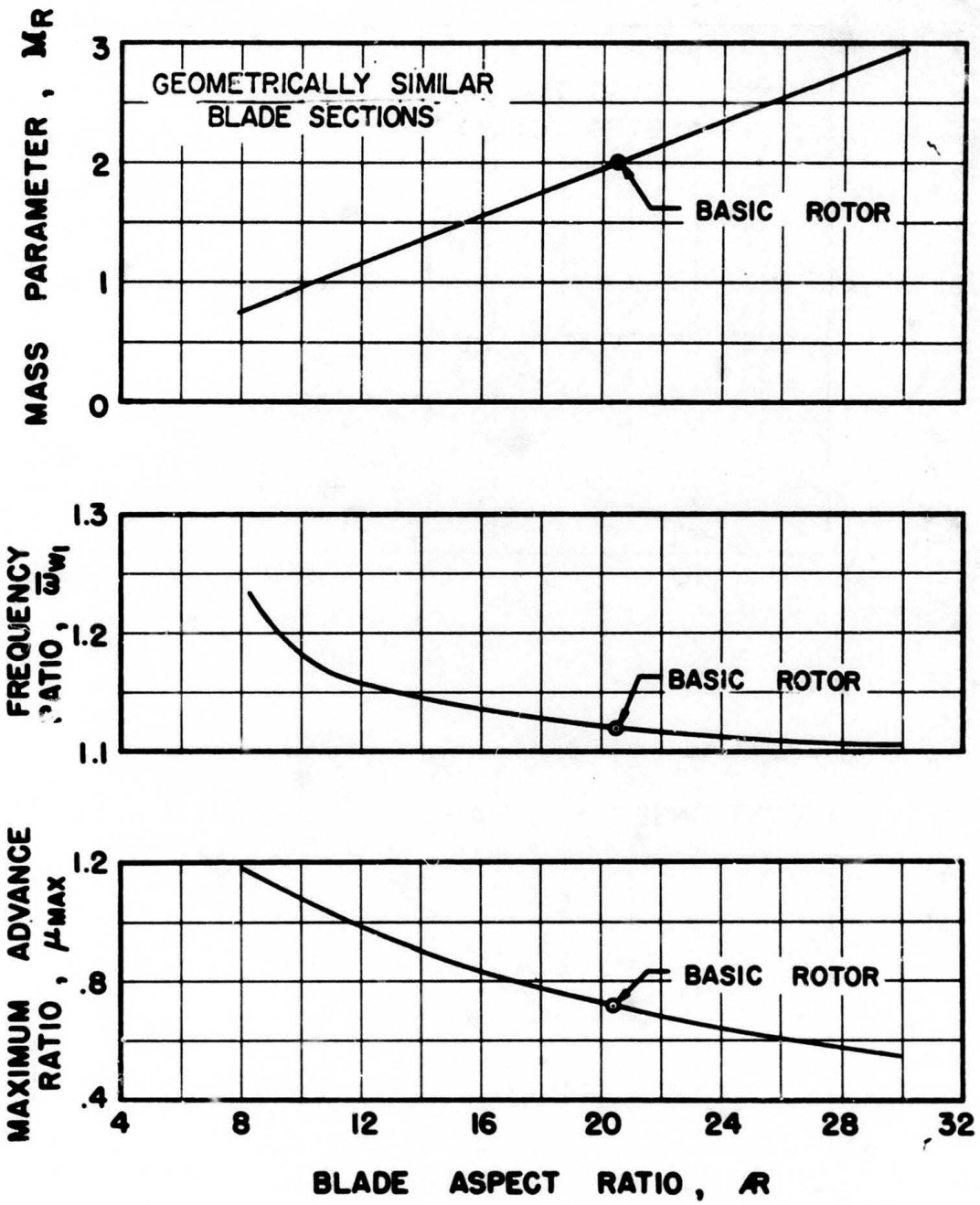

Figure 21. Effect of Blade Aspect Ratio for Nonarticulated Rotor; $M_{1,90} = .85$, $W_G = 30$ FT/SEC, $\bar{r}_{OA} = .12$, $\psi_0 = 0°$, $\bar{\delta}_T = .26$, $\sigma = .078$.

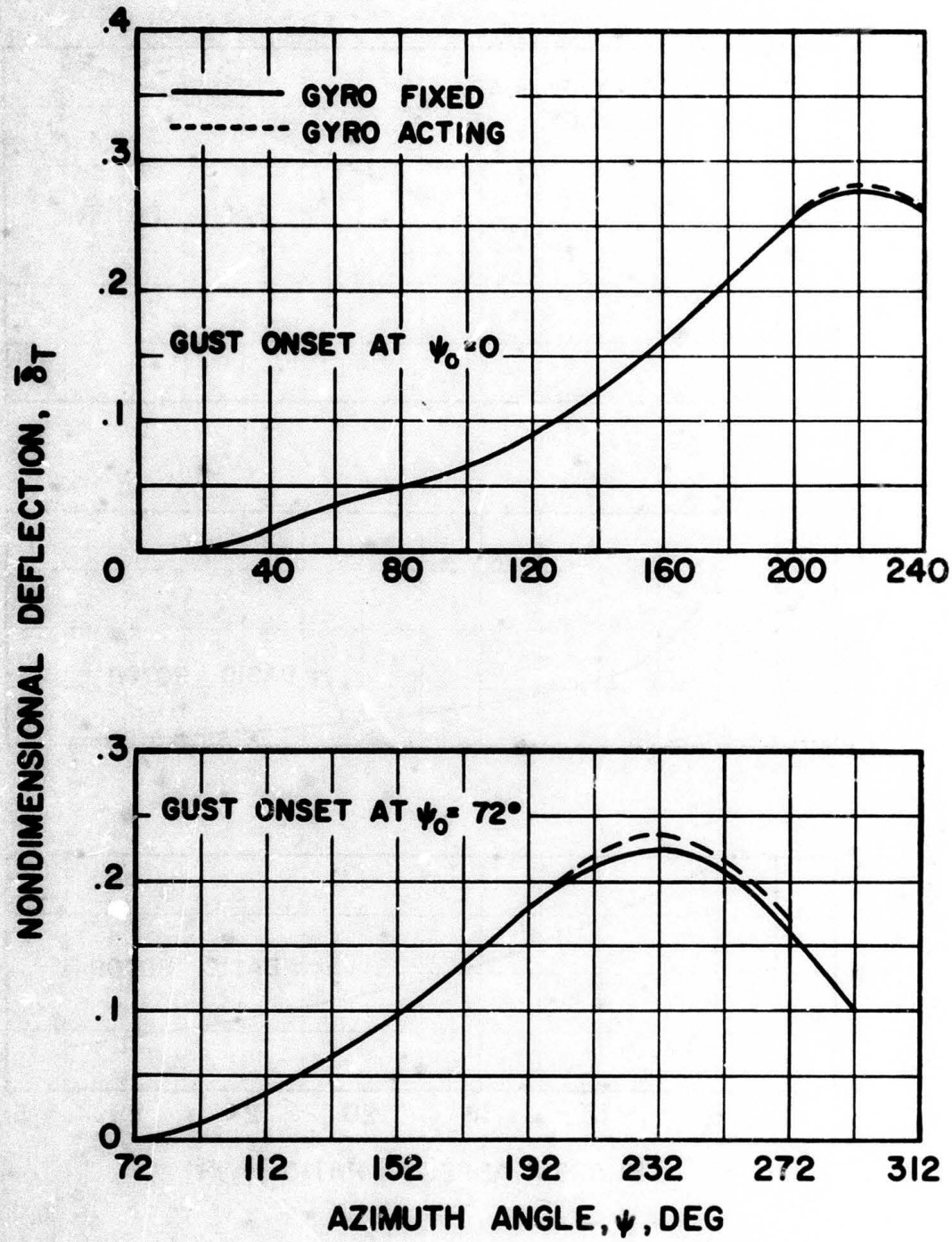

Figure 22. Effect of Gyro Feedback on Non-articulated Blade First Bending Mode Response During the First Revolution After an Idealized Gust; $\mu = .75, M_R = 1.99, \bar{\omega}_{W_1} = 1.12, M_{1,90} = .85, W_G = 30$ FT/SEC, $\bar{r}_{OA} = .12$.

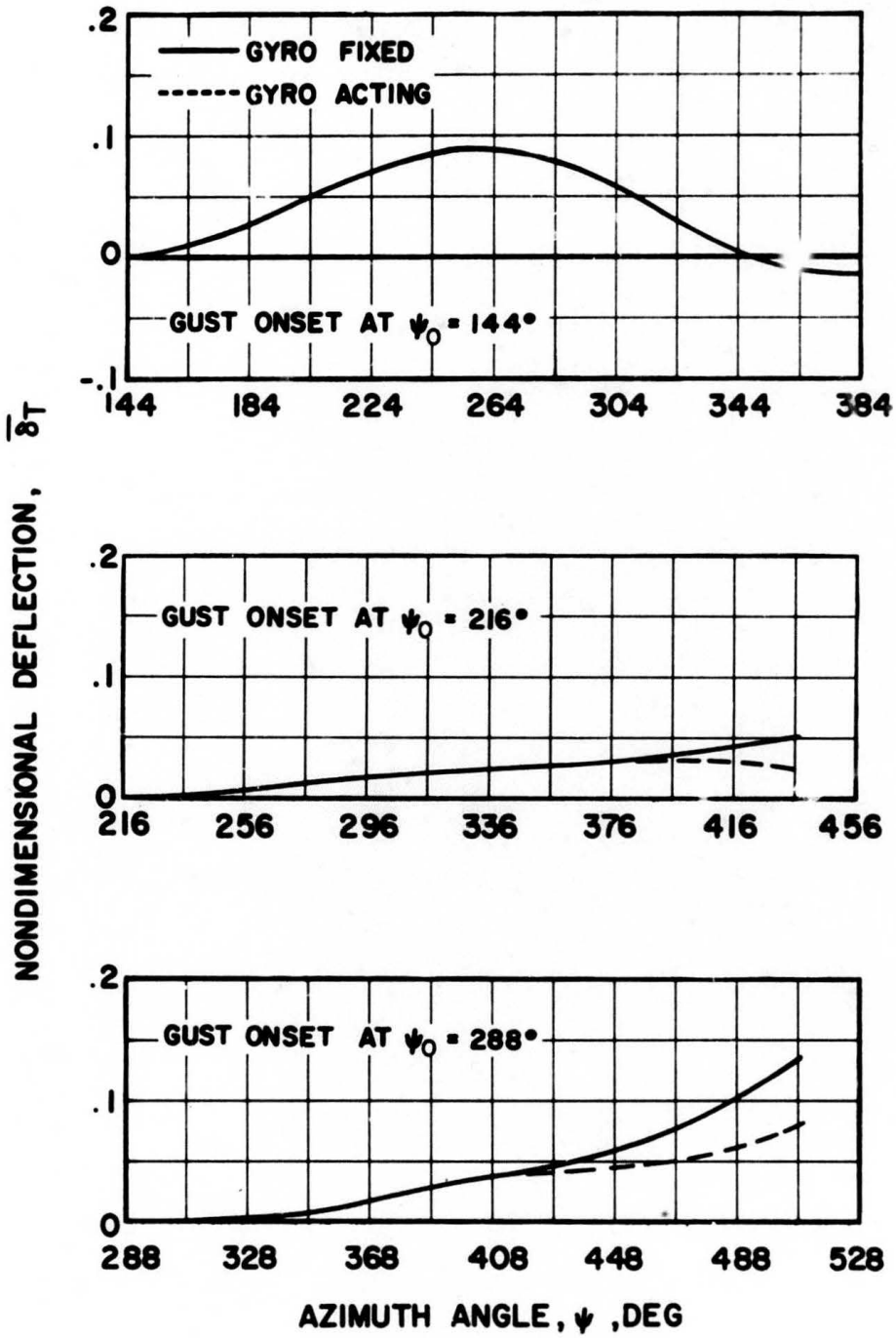

Figure 22. Concluded.

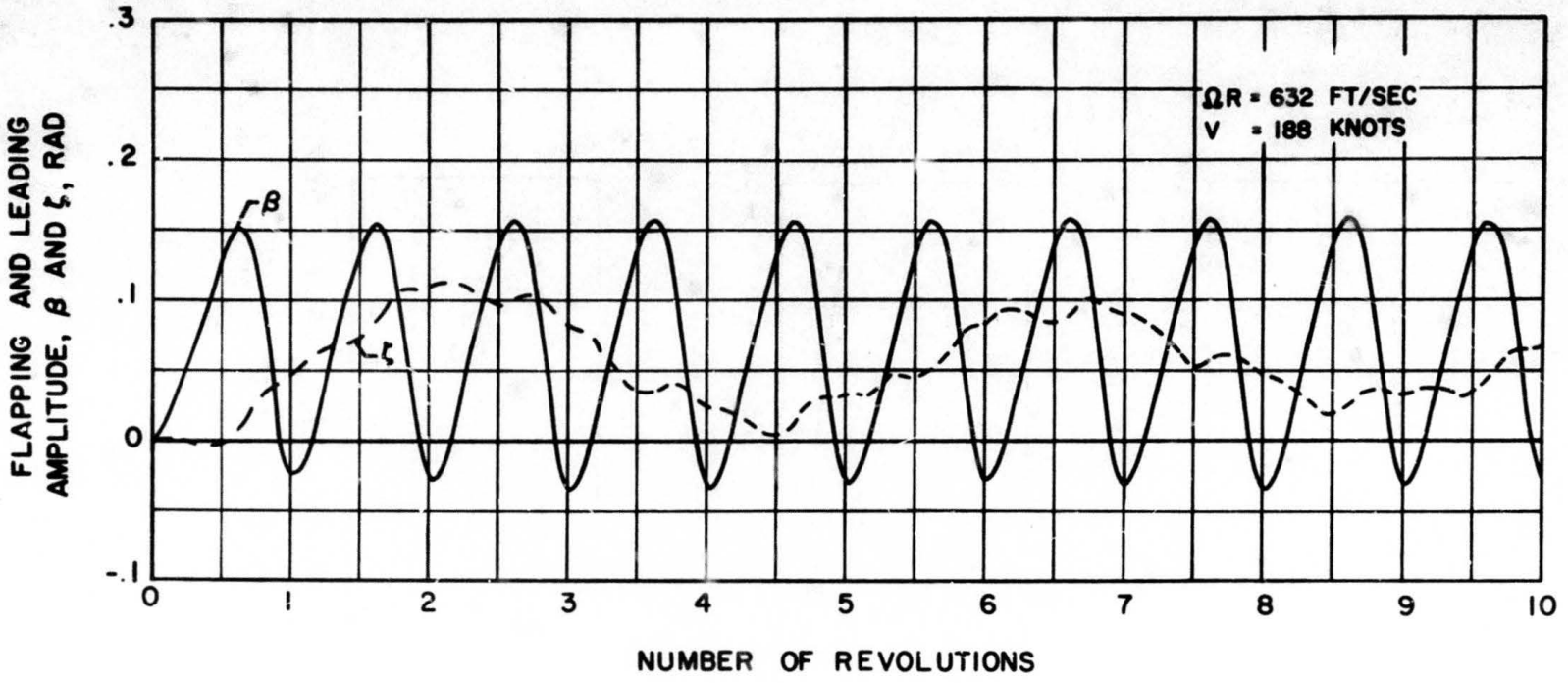

(a) $\mu = .50$

Figure 23. Flapping and Leading Time History After an Instantaneous Gust for the Articulated Blade; $M_R = 1.85$, $\delta_3 = 0°$, $C_{FD} = 0$, $M_{1,90} = .85$, $W_G = 30$ FT/SEC, $\bar{r}_{OA} = .12$, $\psi_0 = 0°$, $\delta_4 = 0$.

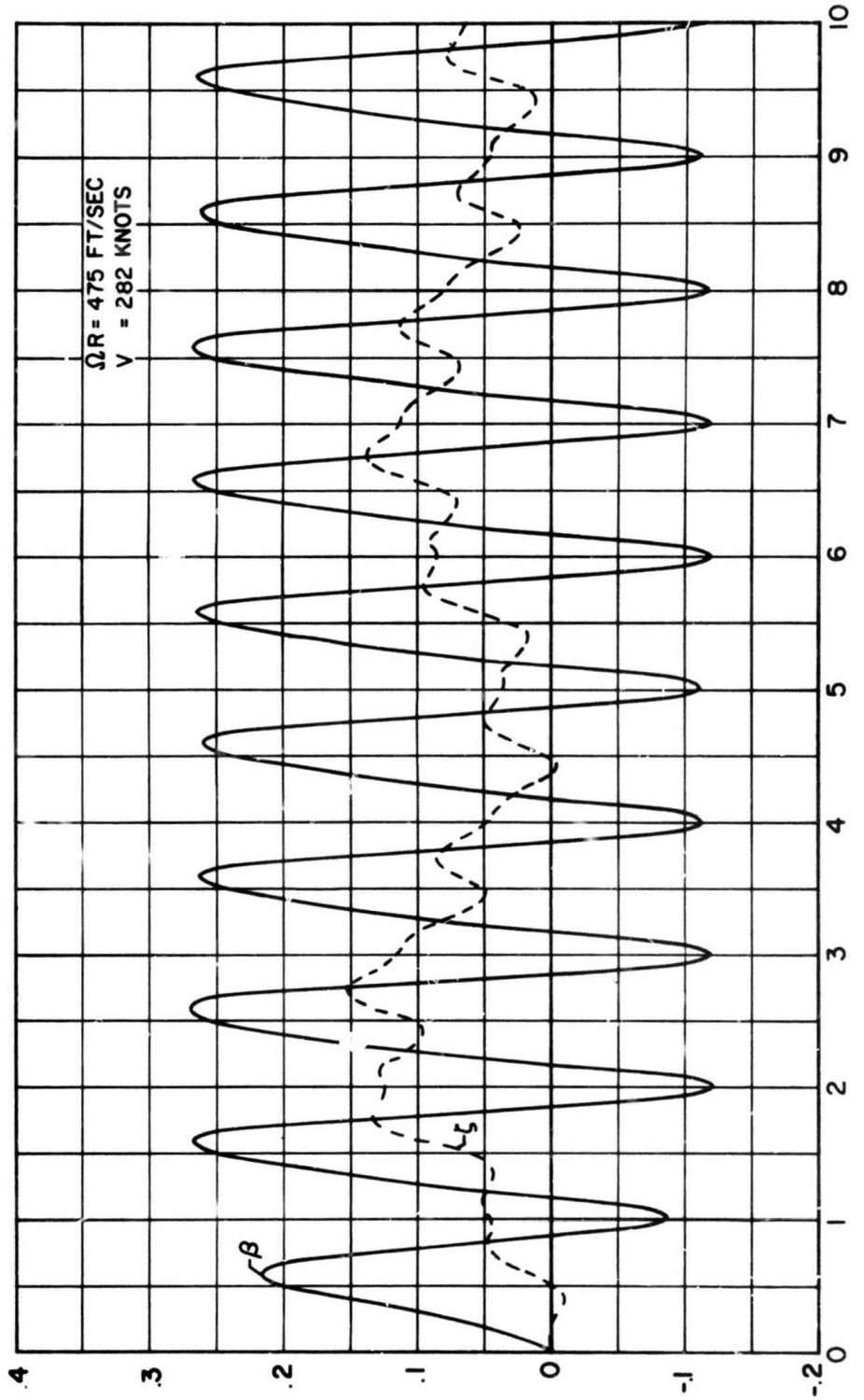

(b) $\mu = 1.0$

Figure 23. Continued.

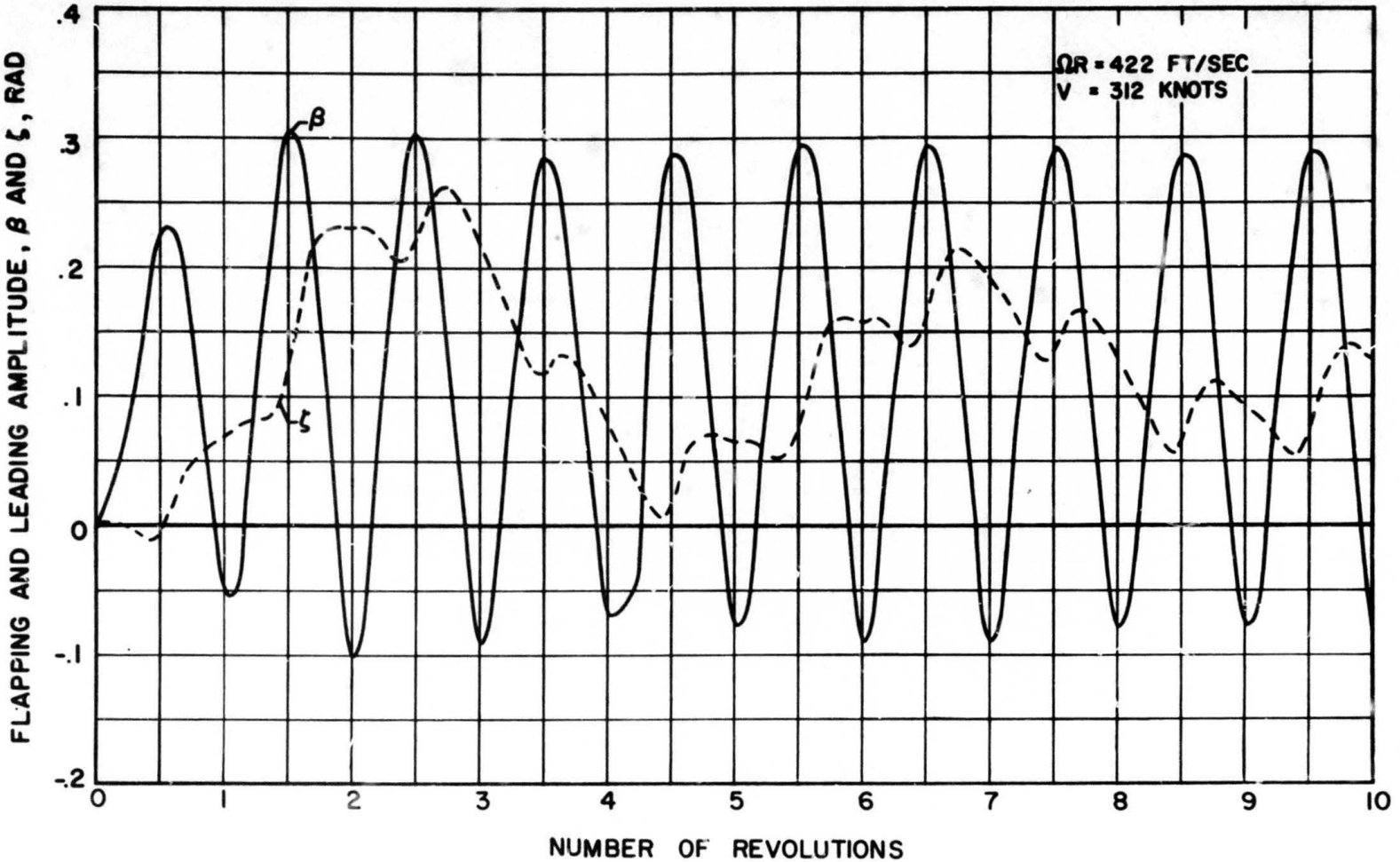

(c) $\mu = 1.25$

Figure 23. Concluded.

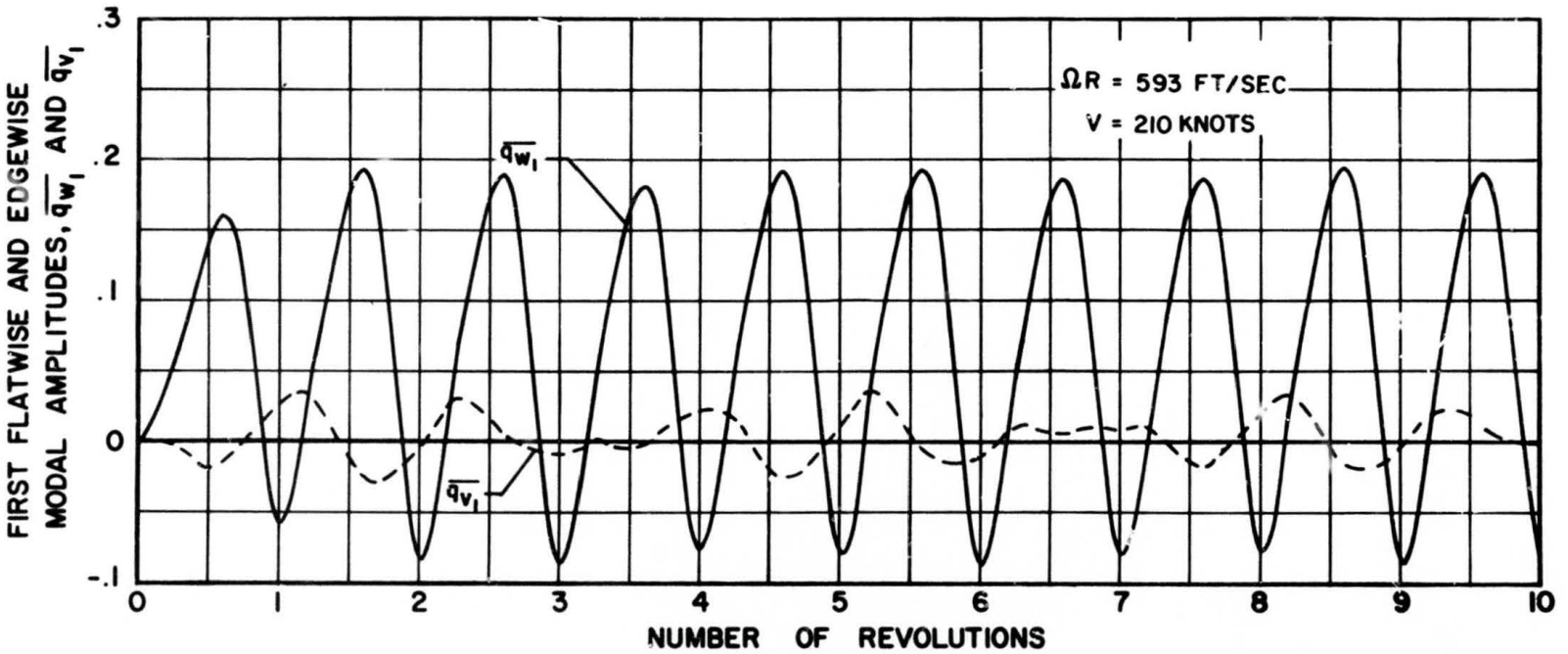

(a) $\mu = .6$

Figure 24. First Flatwise and Edgewise Modal Time History After an Instantaneous Gust for the Nonarticulated Blade; $M_R = 1.99$, $\overline{\omega}_{w_1} = 1.12$, $M_{1,90} = .85$, $W_G = 30$ FT/SEC, $\bar{r}_{OA} = .12$, $\psi_0 = 0°$.

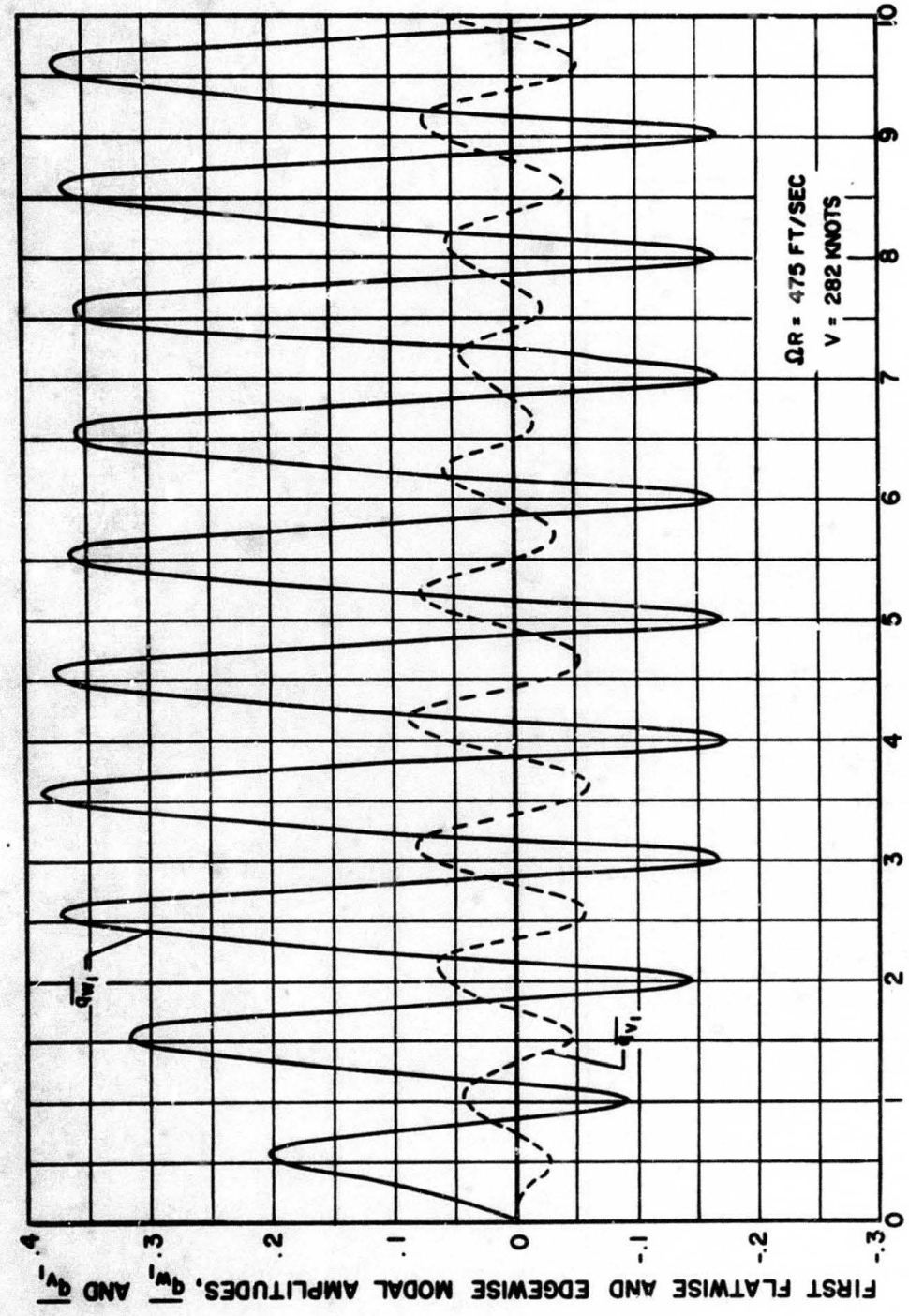

(b) $\mu = 1.0$

Figure 24. Continued.

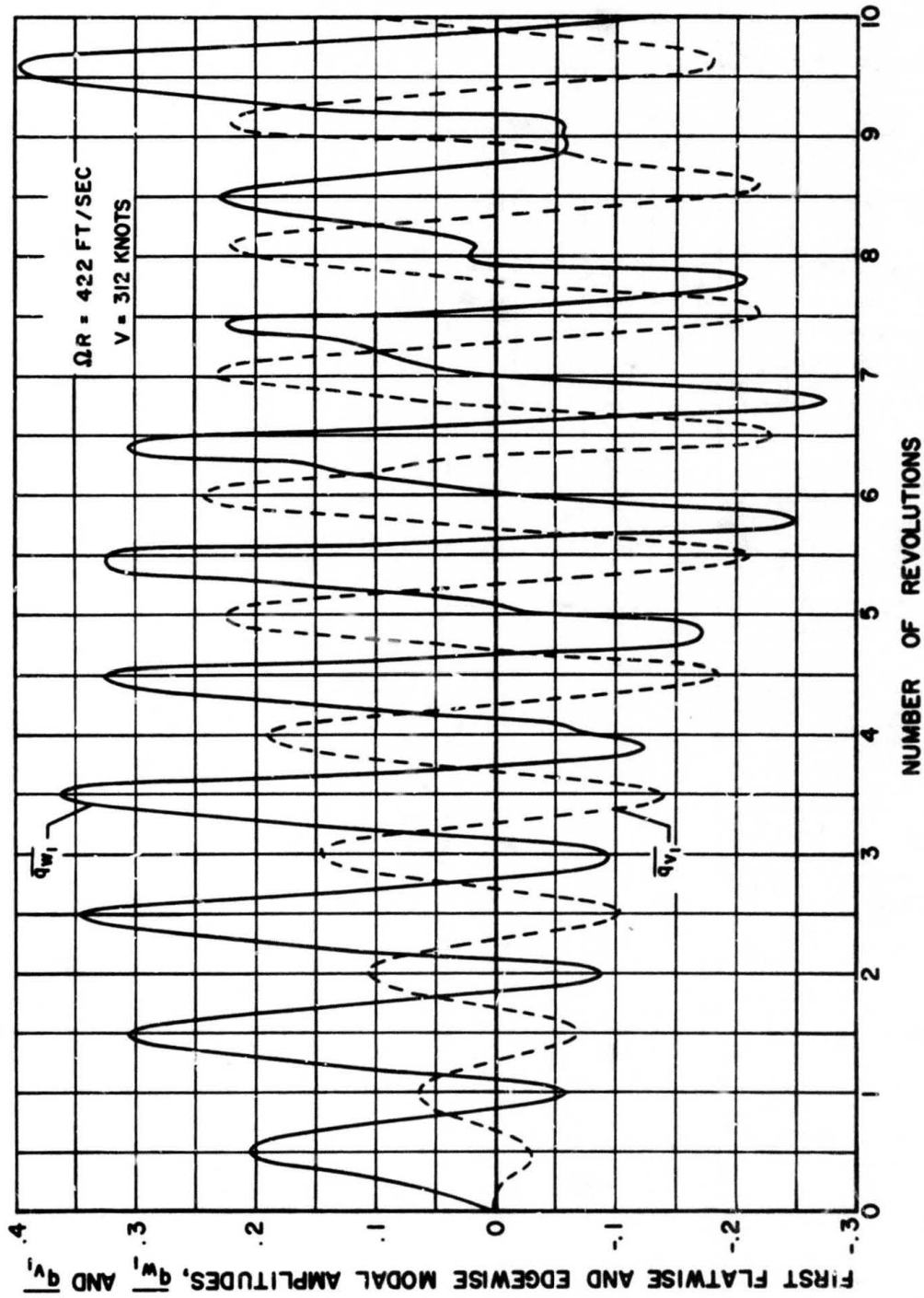

(c) $\mu = 1.25$

Figure 24. Concluded.

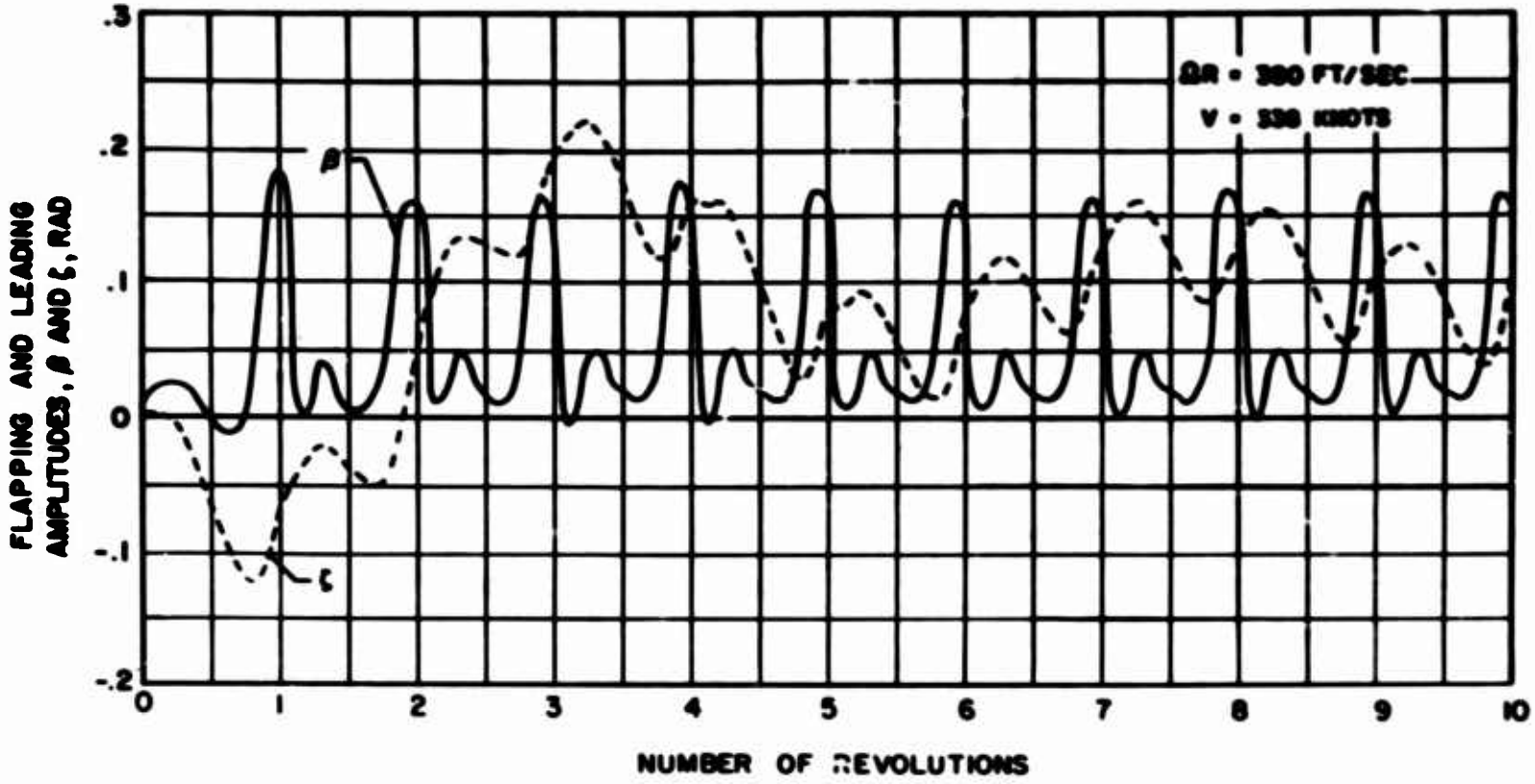

Figure 25. Flapping and Leading Time History After an Instantaneous Gust for the Articulated Blade With Pitch-Flap Coupling; $\mu = 1.5$, $M_R = 1.85$, $\delta_3 = 45°$, $C_{FD} = 0$, $M_{1,90} = .85$, $W_g = 30$ FT/SEC, $\gamma_{OA} = .12$, $\psi_0 = 0°$, $\delta_4 = 0$.

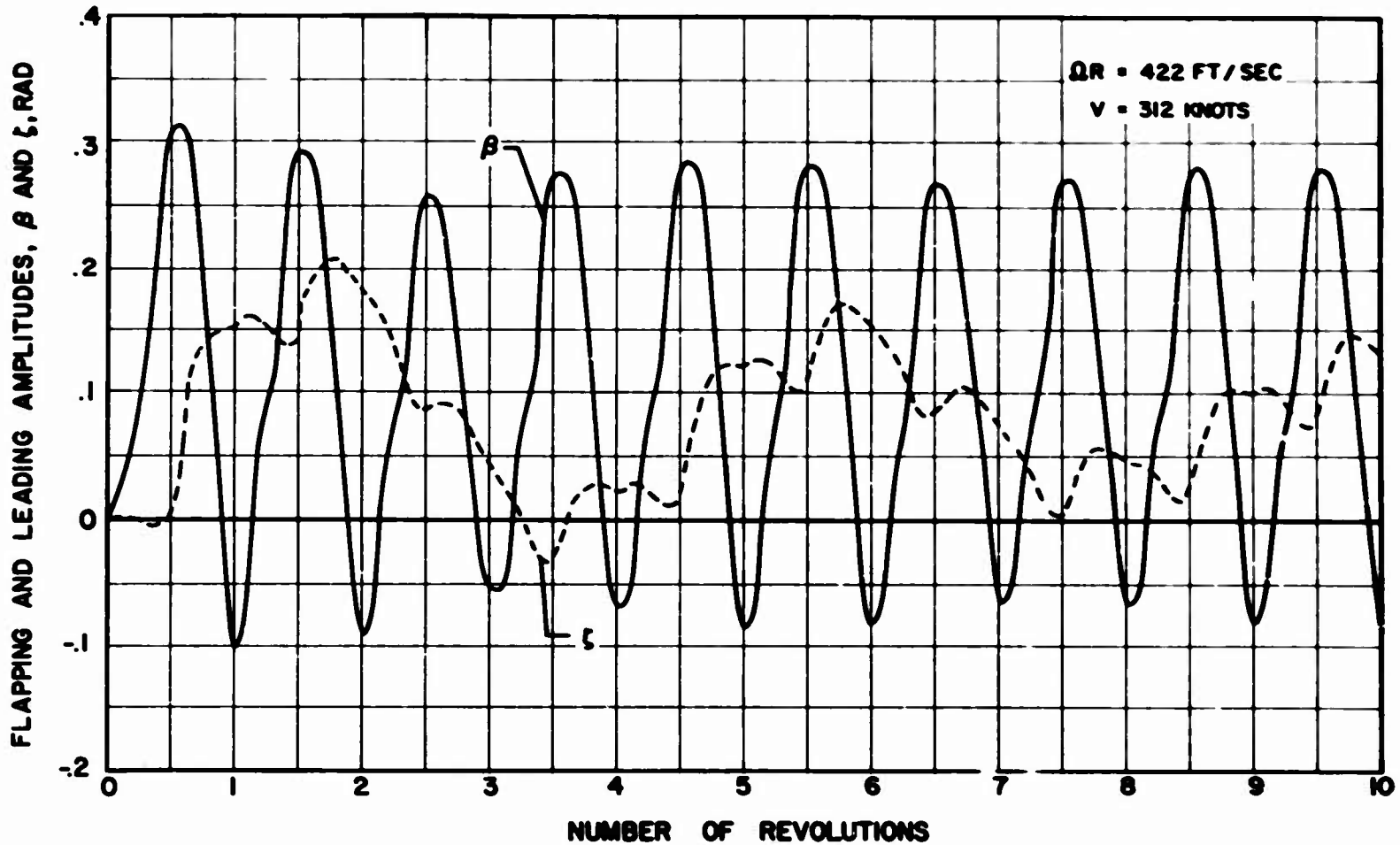

Figure 26. Flapping and Leading Time History After an Instantaneous Gust for the Articulated Blade With Center of Gravity 6% Aft of the 25% Chord; μ =1.25, M_R=1.85, δ_3=0°, C_{FD}=0, $M_{1,s0}$=.85, W_G=30 FT/SEC, $\bar{r}_{OA}$=.12, ψ_0=0°, δ_4=0.

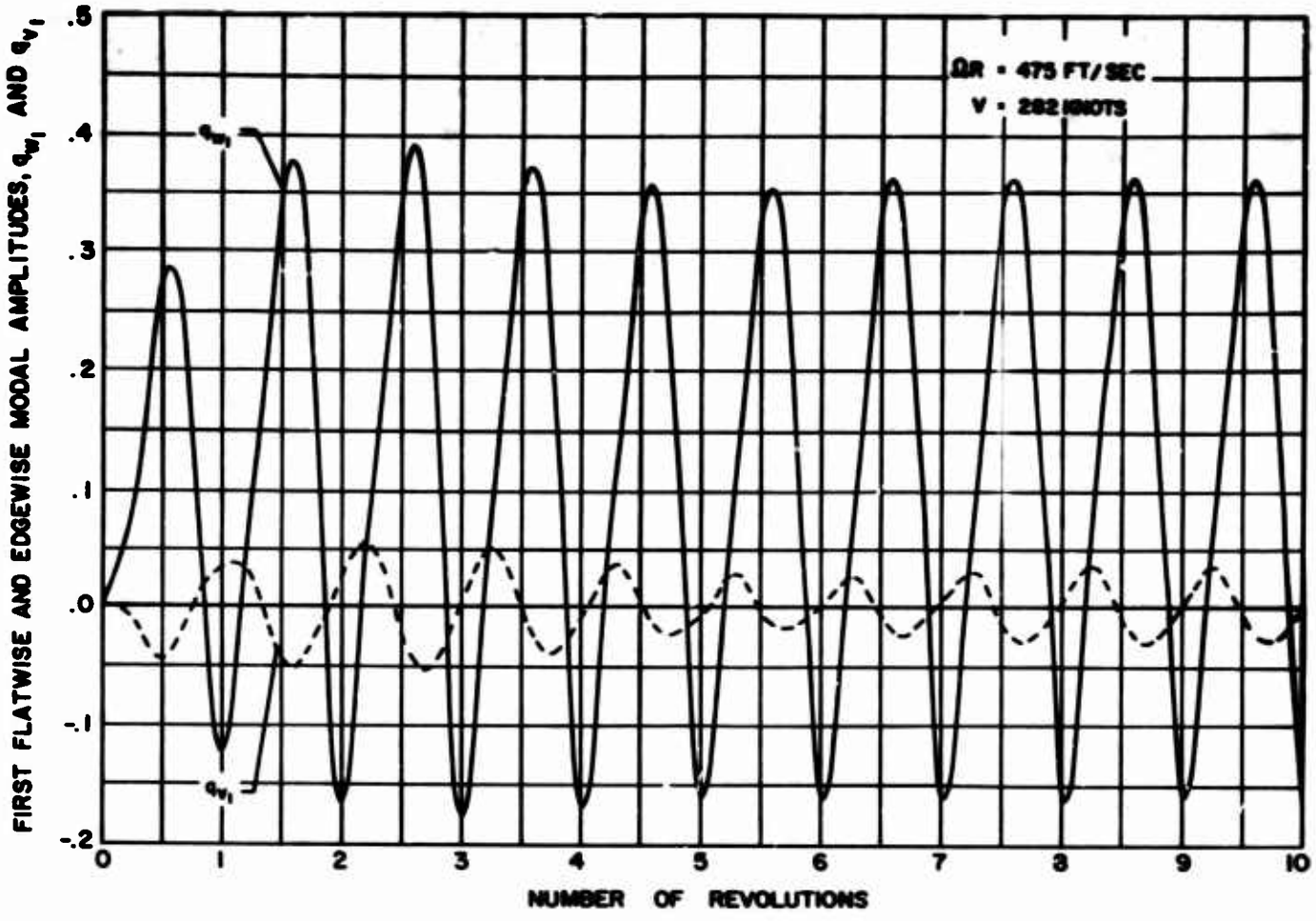

Figure 27. First Flatwise and Edgewise Modal Time History After an Instantaneous Gust for the Nonarticulated Blade with Center of Gravity 6% Aft of the 25% Chord; $\mu = 1.0, M_R = 1.99, \bar{\omega}_{w_1} = 1.12, M_{1,90} = .85, W_G = 30$ FT/SEC, $\bar{r}_{OA} = .12, \psi_0 = 0°$

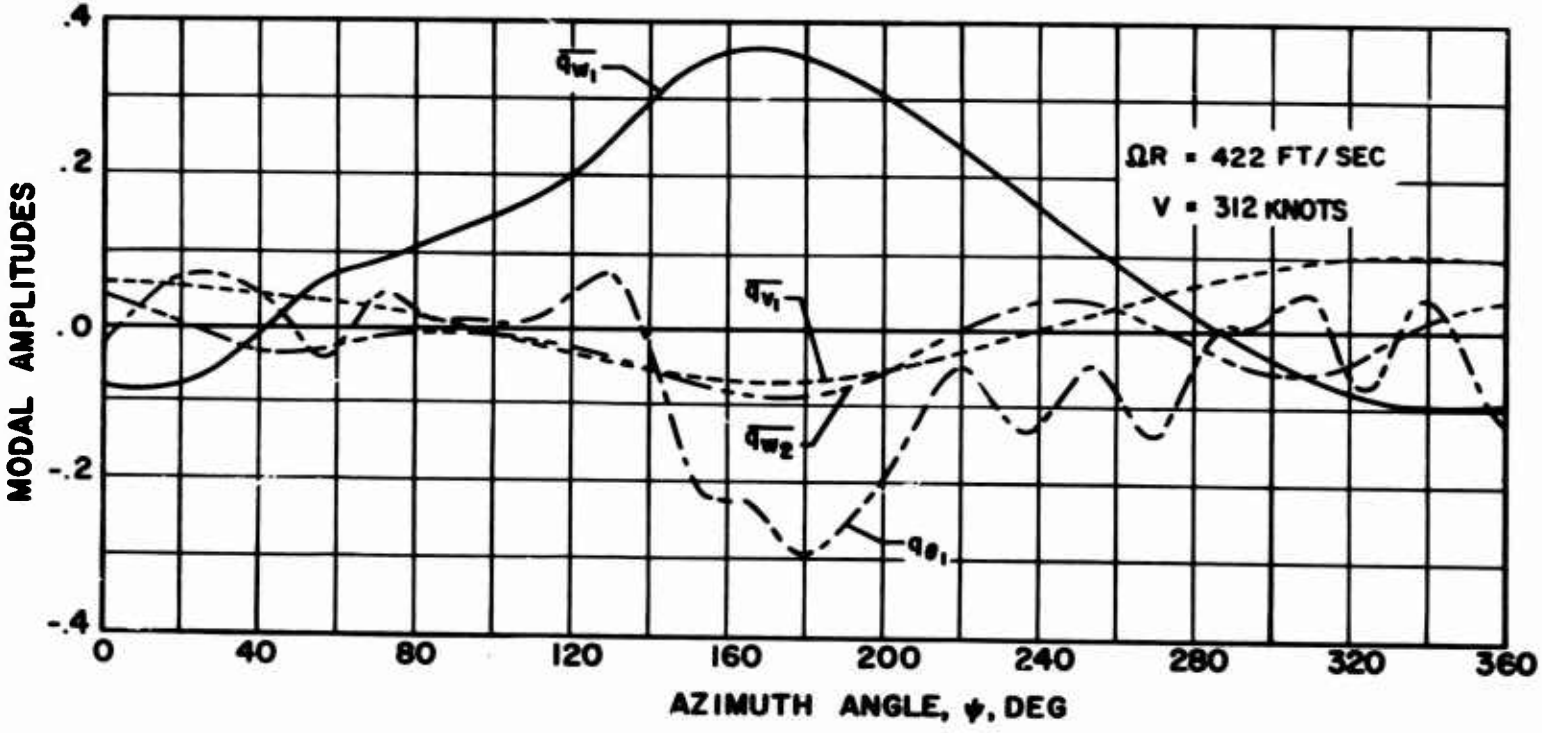

(a) 2nd Revolution

Figure 28. Flatwise, Edgewise and Torsional Modal Time History After an Instantaneous Gust for the Nonarticulated Blade with Center of Gravity 6% Aft of the 25% Chord; μ =1.25, M_R=1.99, ϖ_{w_1} =1.12, $M_{1,90}$=.85, W_G = 30 FT/SEC, $\bar{r}_{OA}$ =.12, ψ_0=0°.

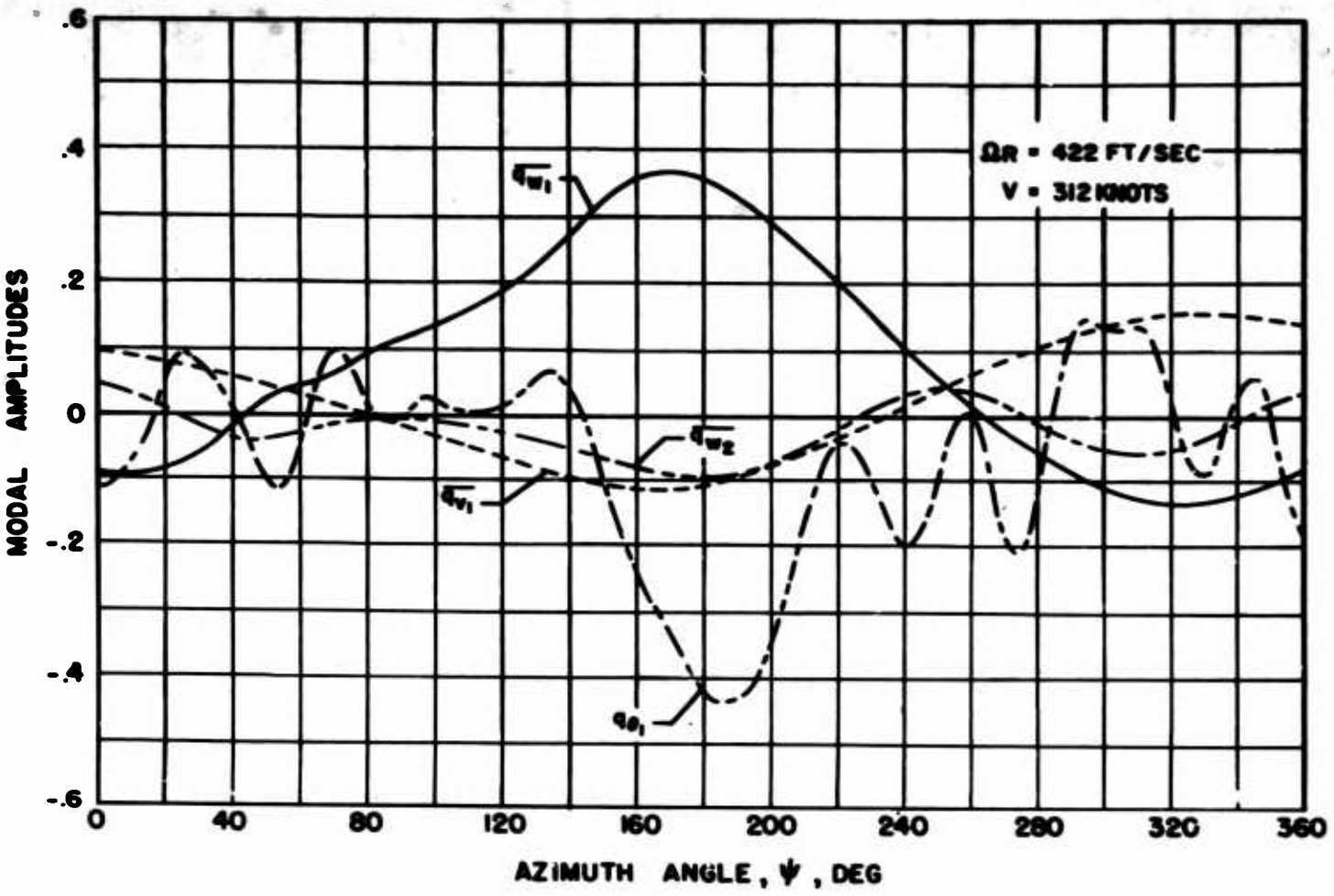

(b) 3rd Revolution

Figure 28. Continued.

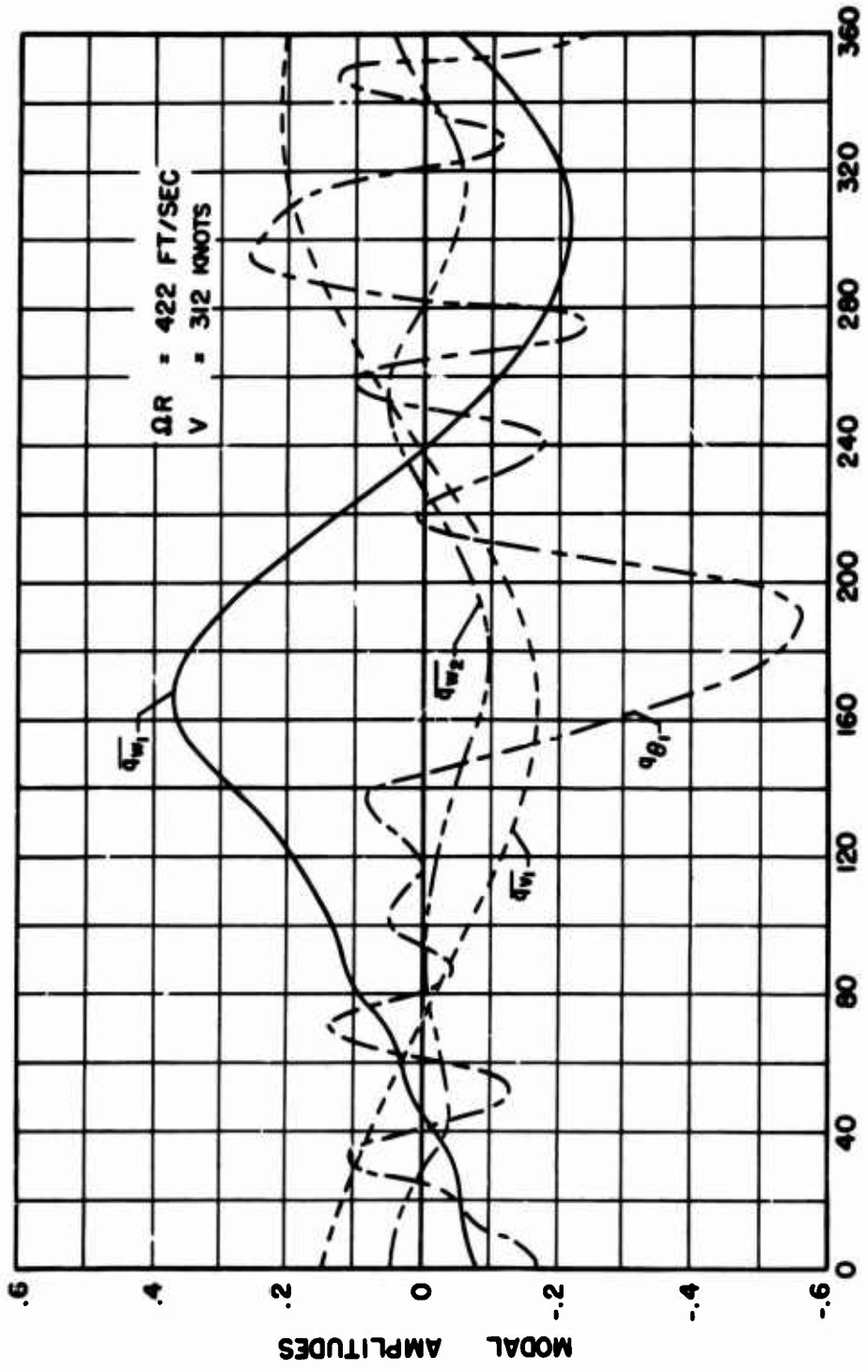

(c) 4th Revolution

Figure 28. Concluded.

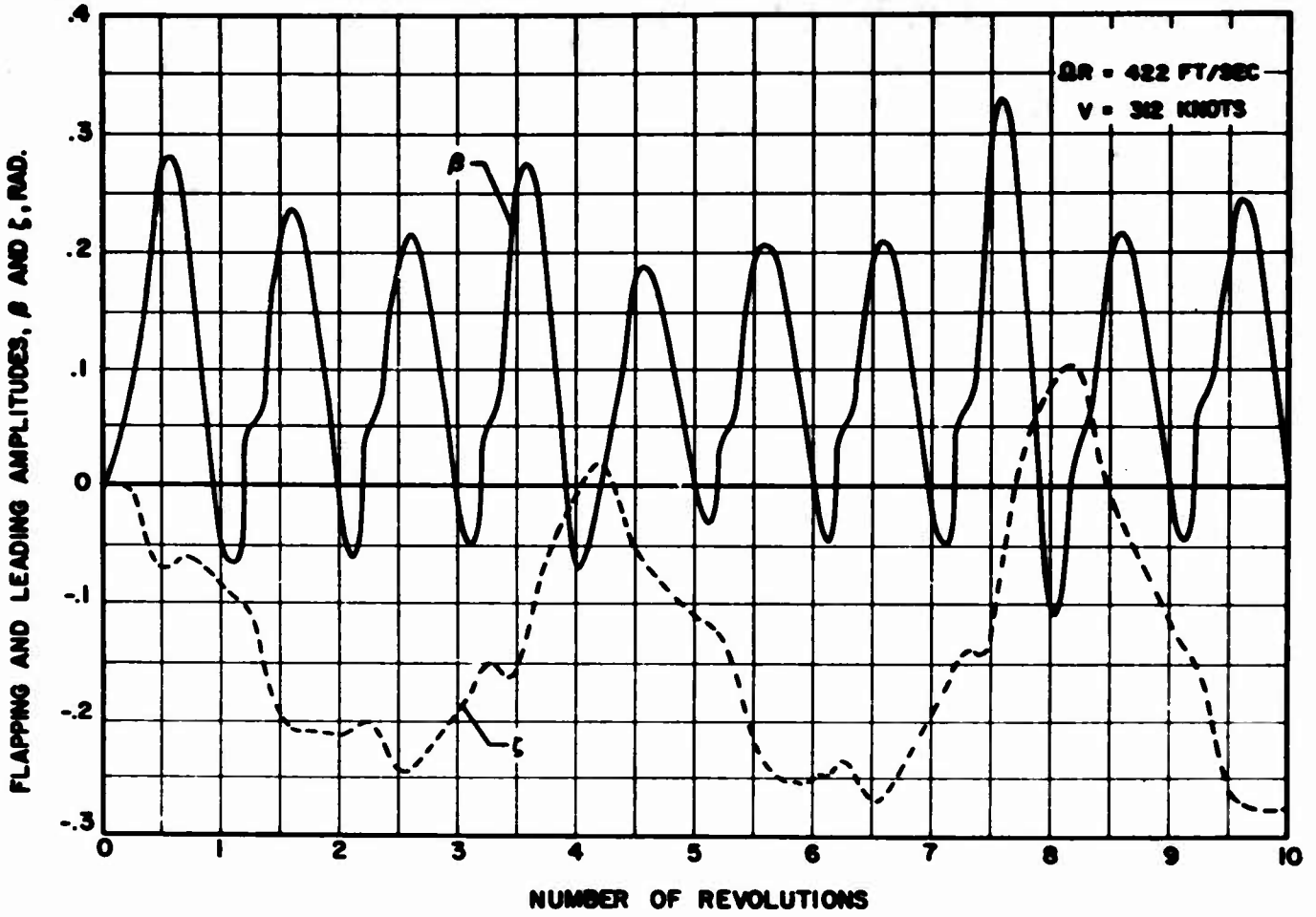

Figure 29. Flapping and Leading Time History After an Instantaneous Gust for the Articulated Blade With Center of Gravity 10% Aft of the 25% Chord; $\mu = 1.25, M_R = 1.85, \delta_3 = 0°, C_{FD} = 0, M_{1,90} = .85, W_G = 30$ FT/SEC, $\bar{r}_{OA} = .12, \psi_0 = 0°, \delta_4 = 0$.

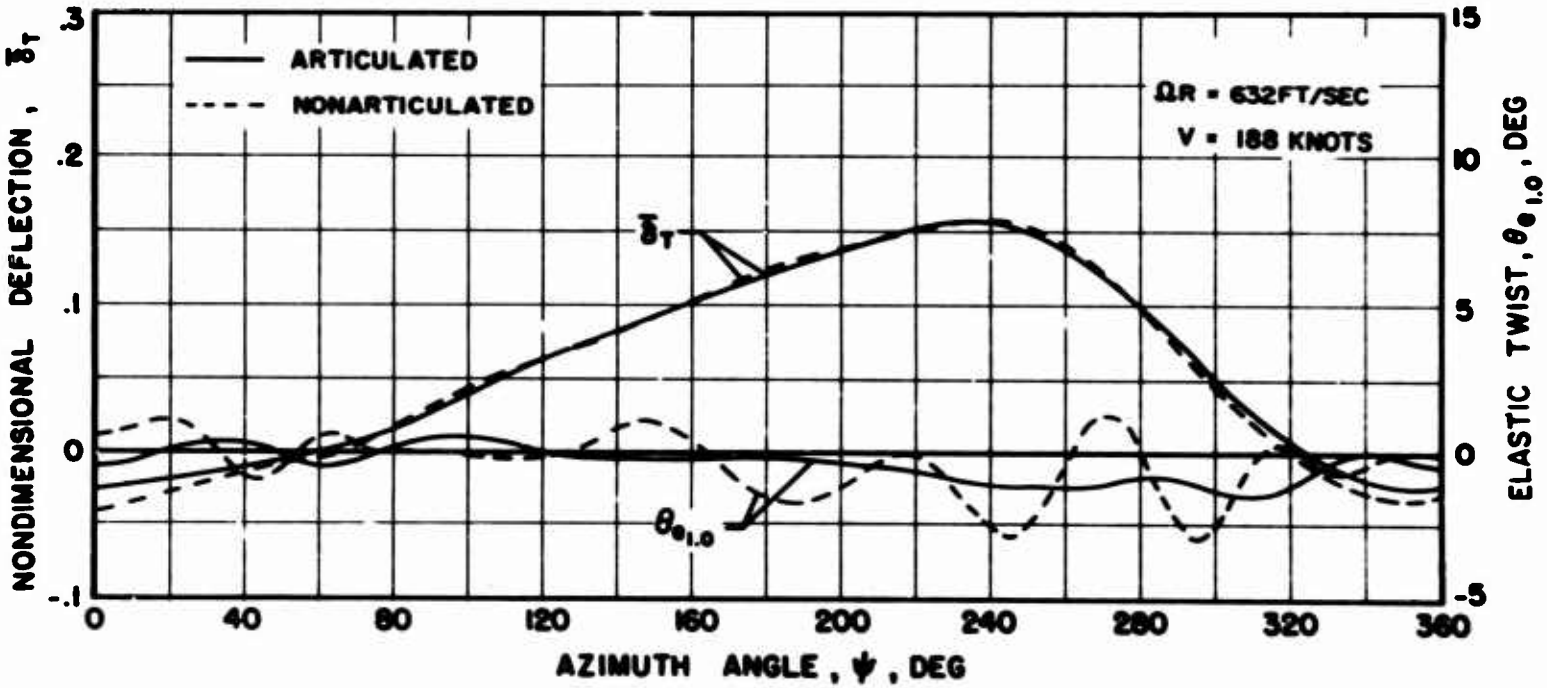

(a) $\mu = .5$

Figure 30. Articulated and Nonarticulated Blade Deflections During a Typical Revolution After an Instantaneous Gust; $M_{1,90} = .85$, $W_G = 30$ FT/SEC, $\bar{r}_{0A} = .12$, $\psi_0 = 0°$.

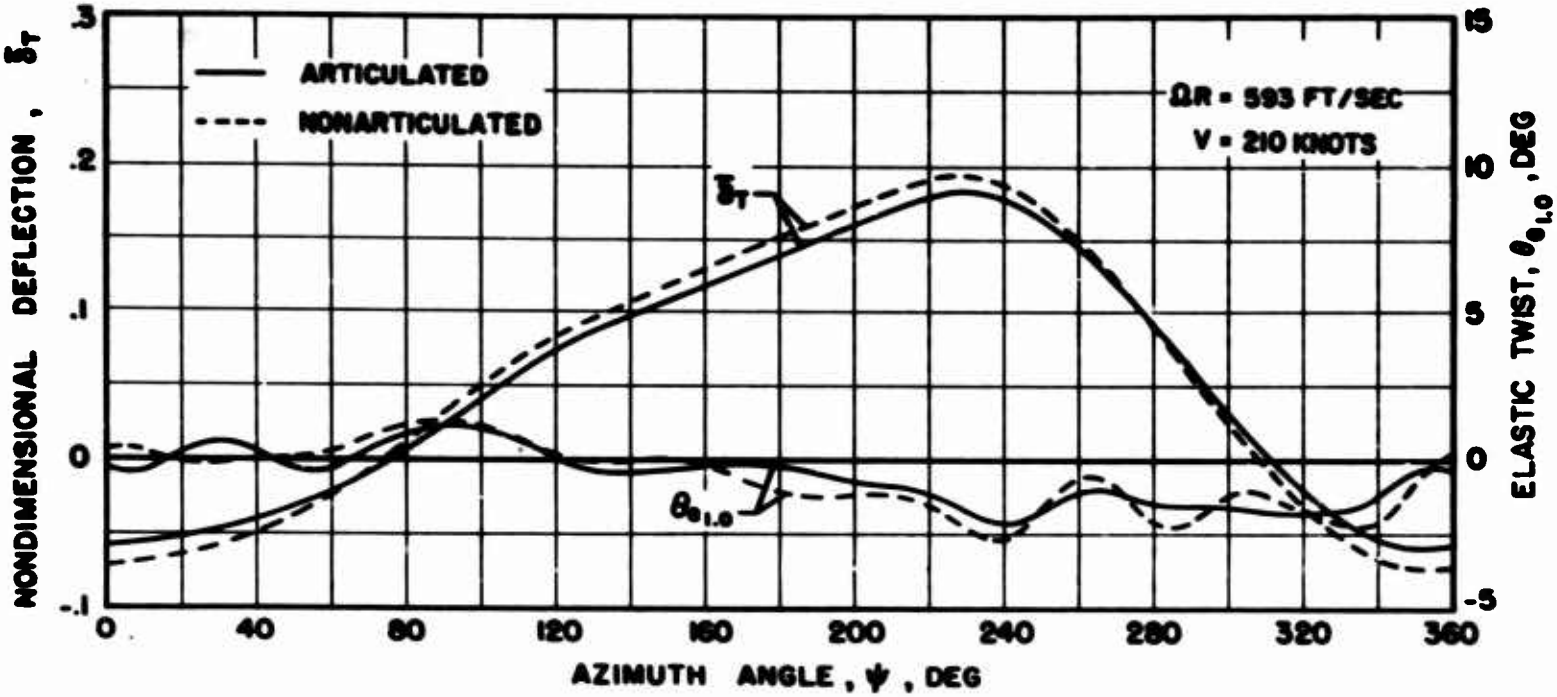

(b) $\mu = .6$

Figure 30. Continued.

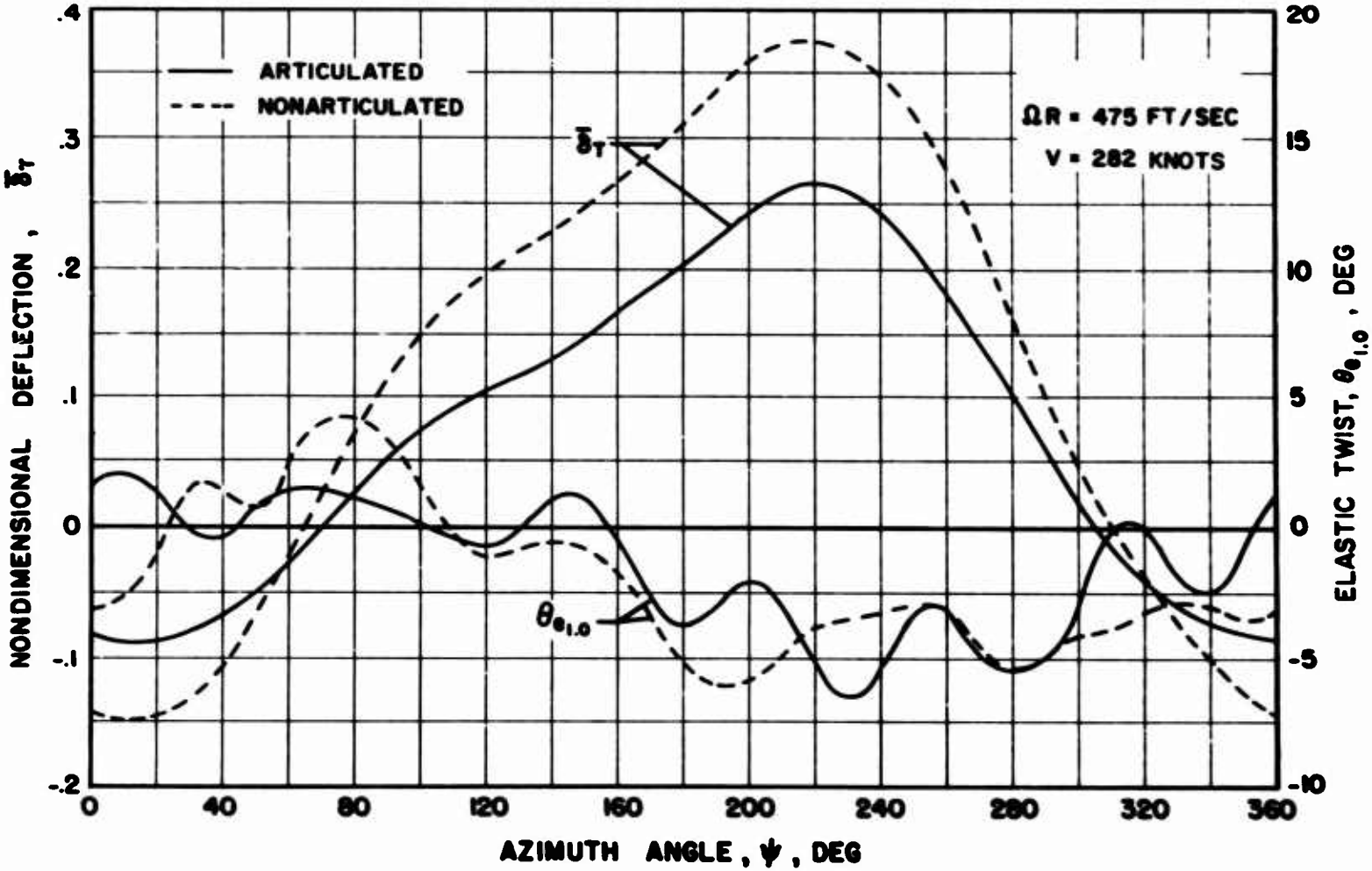

(c) $\mu = 1.0$

Figure 30. Concluded.

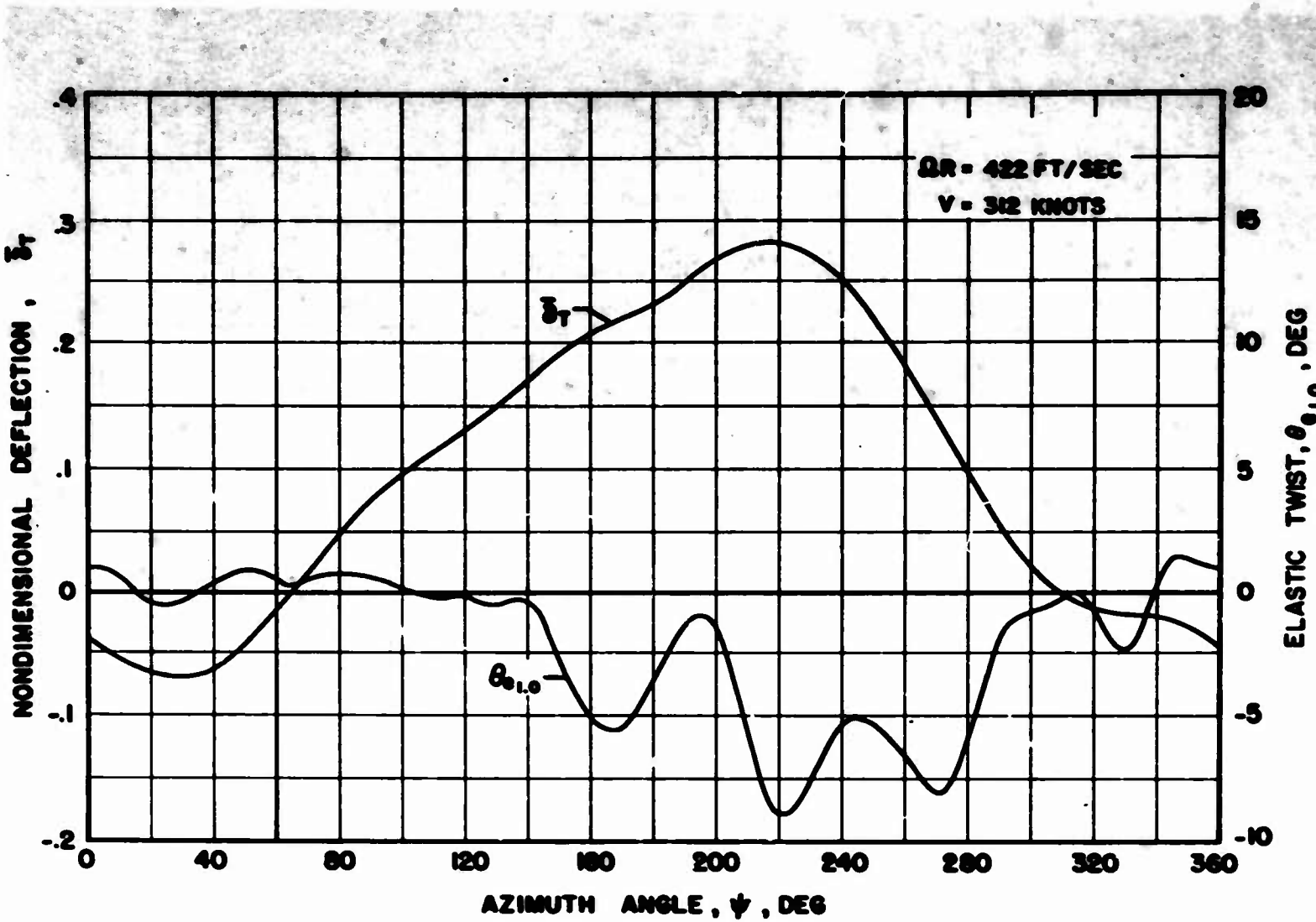

Figure 31. Articulated Blade Deflections During a Typical Revolution After an Instantaneous Gust; $\mu = 1.25, M_R = 1.85, \delta_3 = 0°, C_{FD} = 0, M_{1,90} = .85, W_G = 30$ FT/SEC, $\bar{r}_{OA} = .12, \psi_0 = 0°, \delta_4 = 0$.

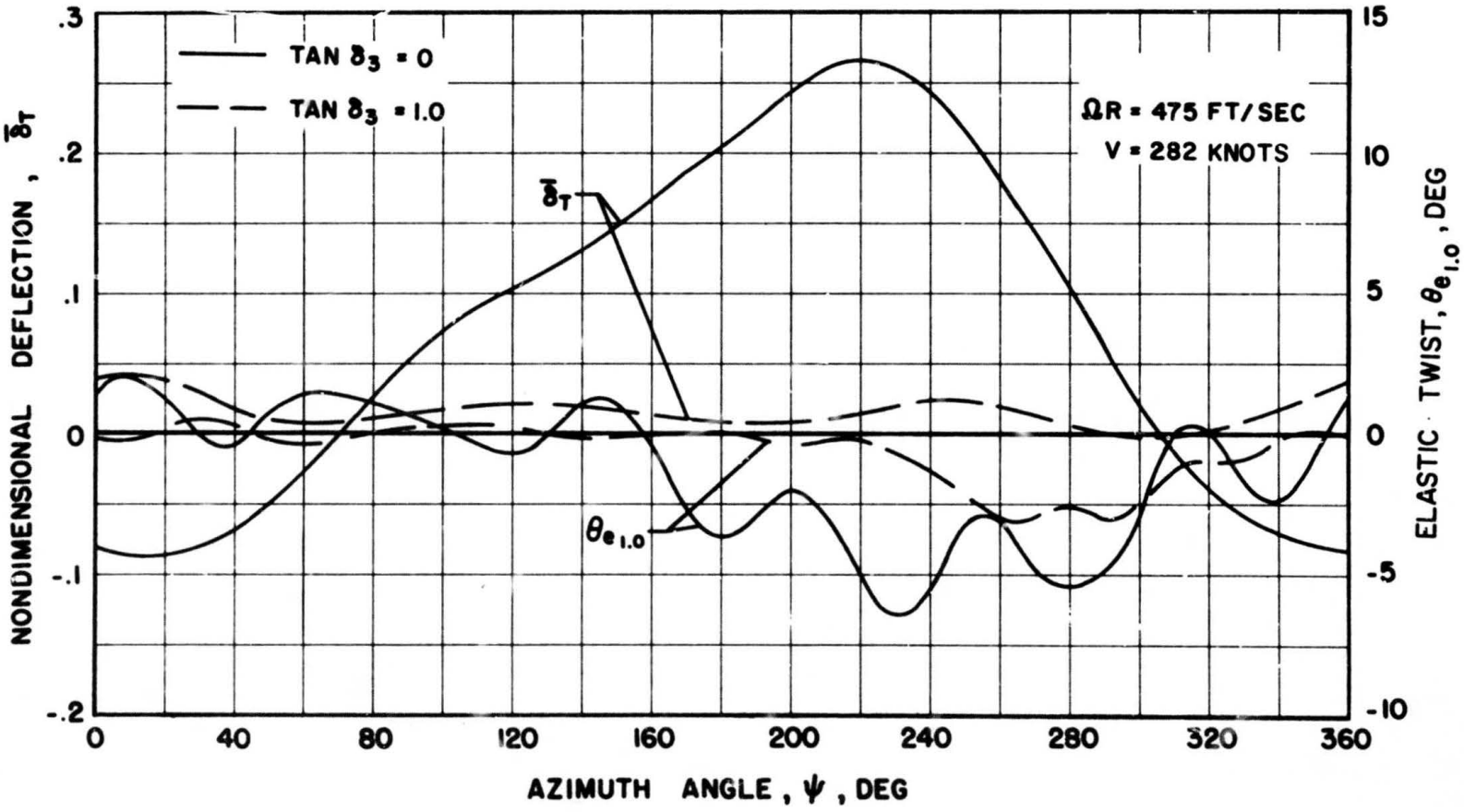

(a) $\mu = 1.0$

Figure 32. Effect of Pitch-Flap Coupling on Articulated Blade Deflections During a Typical Revolution After an Instantaneous Gust; $M_R = 1.85$, $C_{FD} = 0$, $M_{1,90} = .85$, $W_G = 30$ FT/SEC, $\bar{r}_{OA} = .12$, $\psi_0 = 0°$, $\delta_4 = 0$.

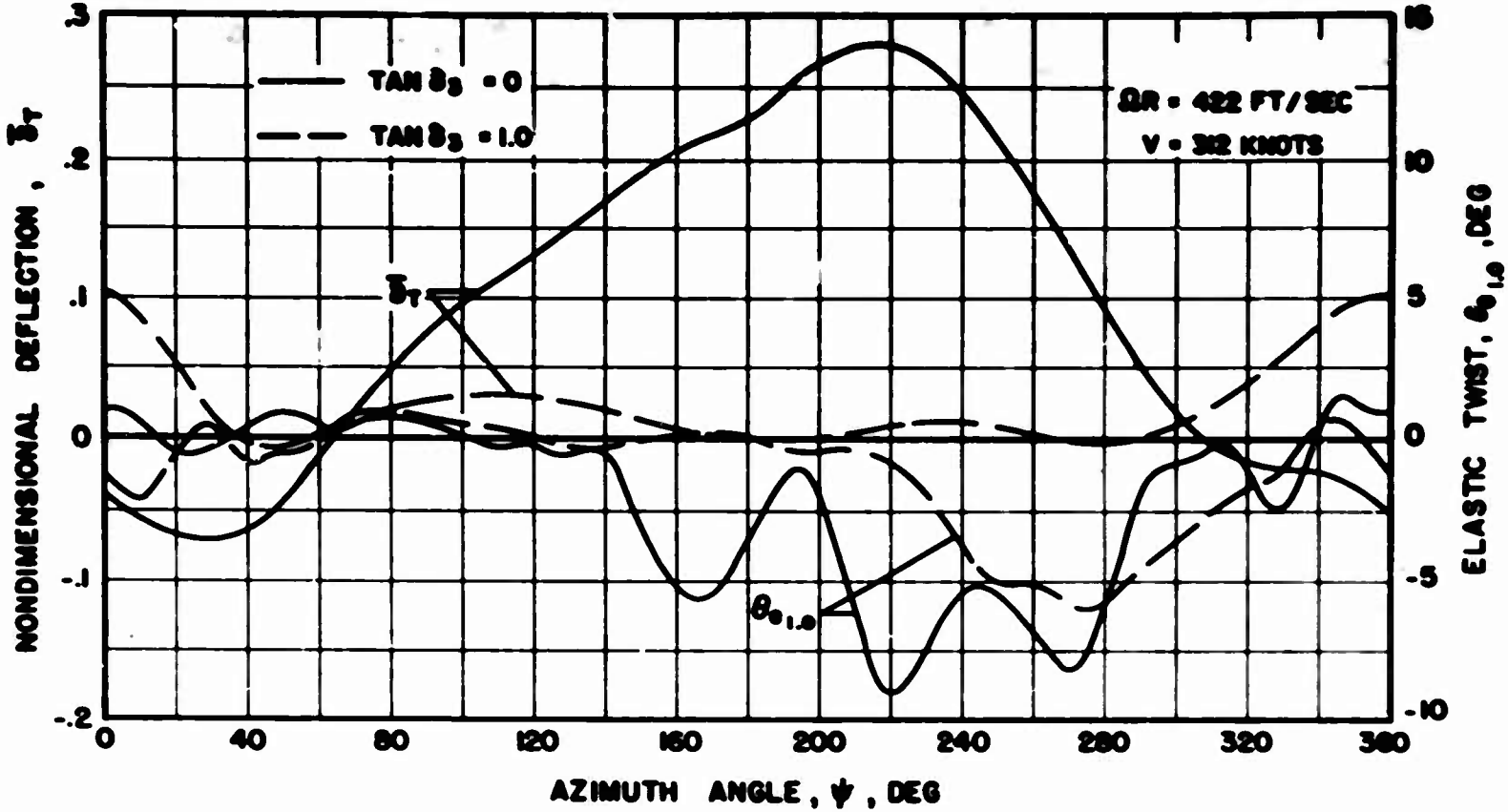

(b) $\mu = 1.25$

Figure 32. Continued.

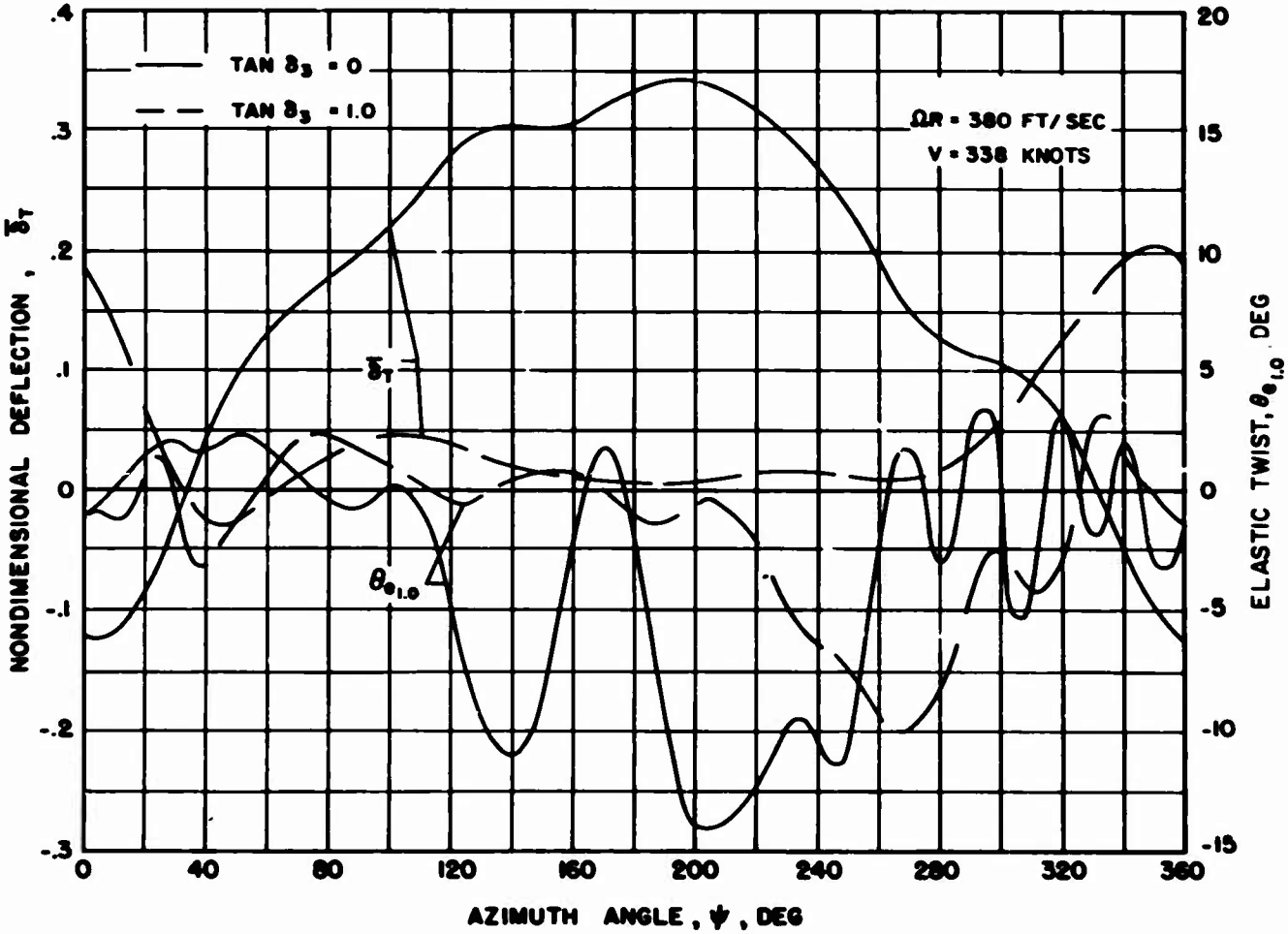

(c) $\mu = 1.5$

Figur. 32. Concluded.

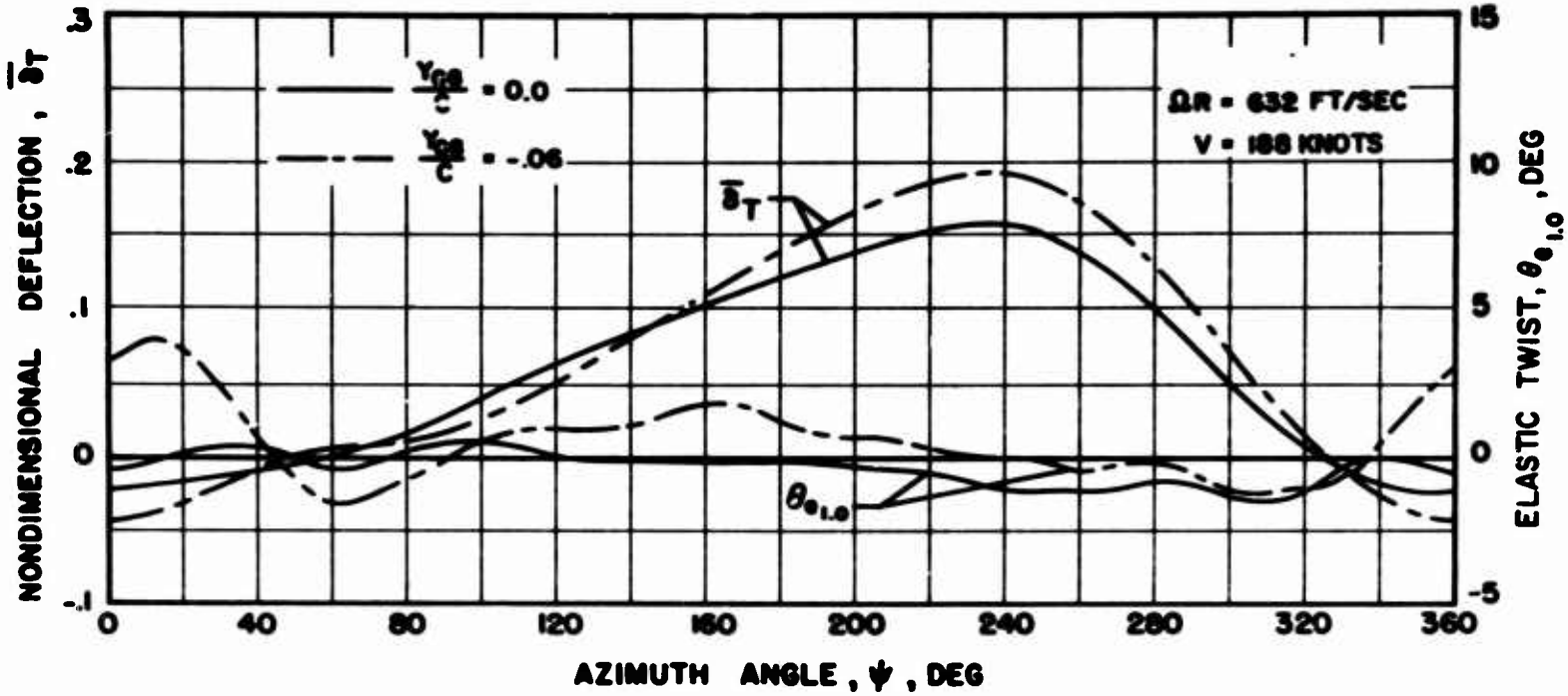

(a) μ = .5

Figure 33. Effect of Center-of-Gravity Offset on Articulated Blade Deflections During a Typical Revolution After an Instantaneous Gust; M_R = 1.85, $\delta_3 = 0°$, $C_{FD} = 0$, $M_{1,90} = .85$, $W_G = 30$ FT/SEC, $\bar{r}_{OA} = .12$, $\psi_0 = 0°$, $\delta_4 = 0$.

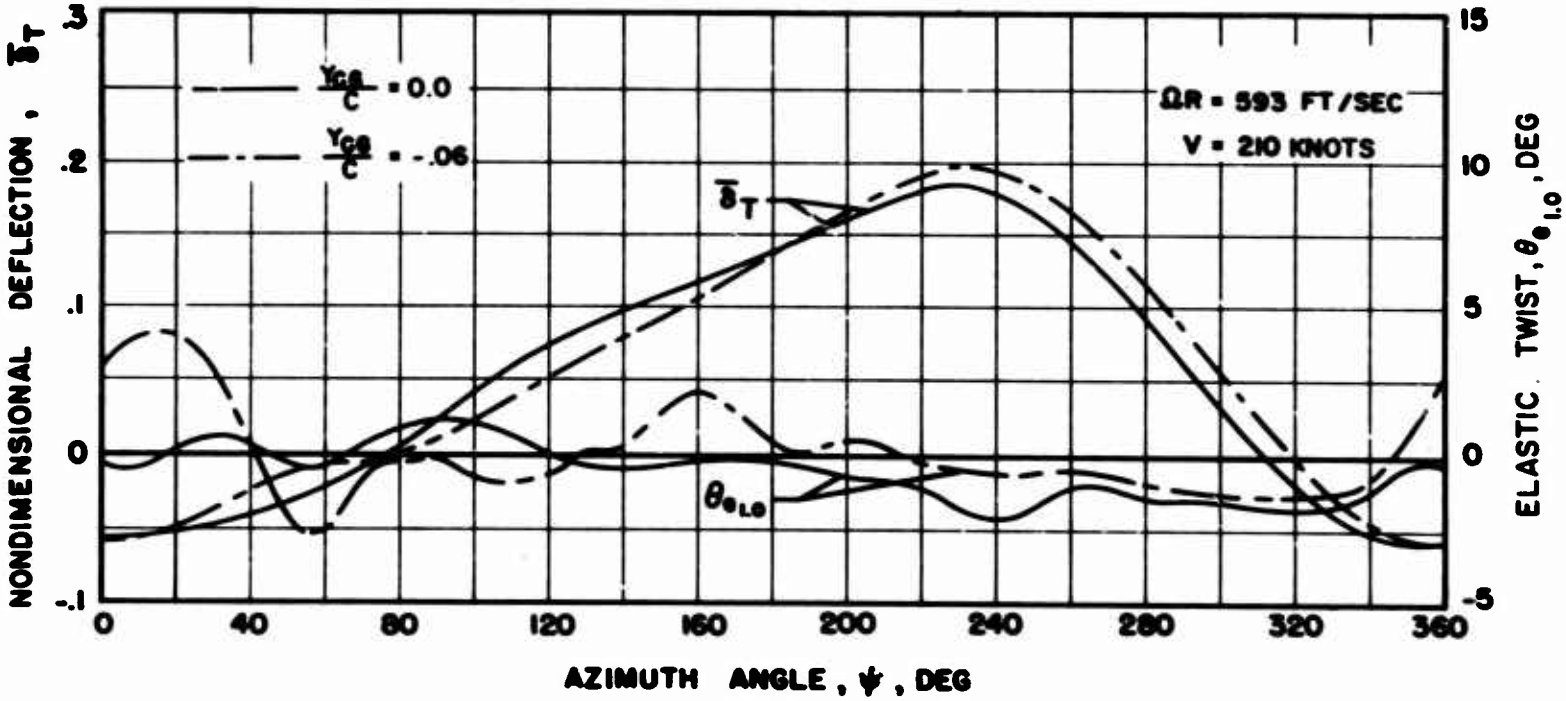

(b) $\mu = .6$

Figure 33. Continued.

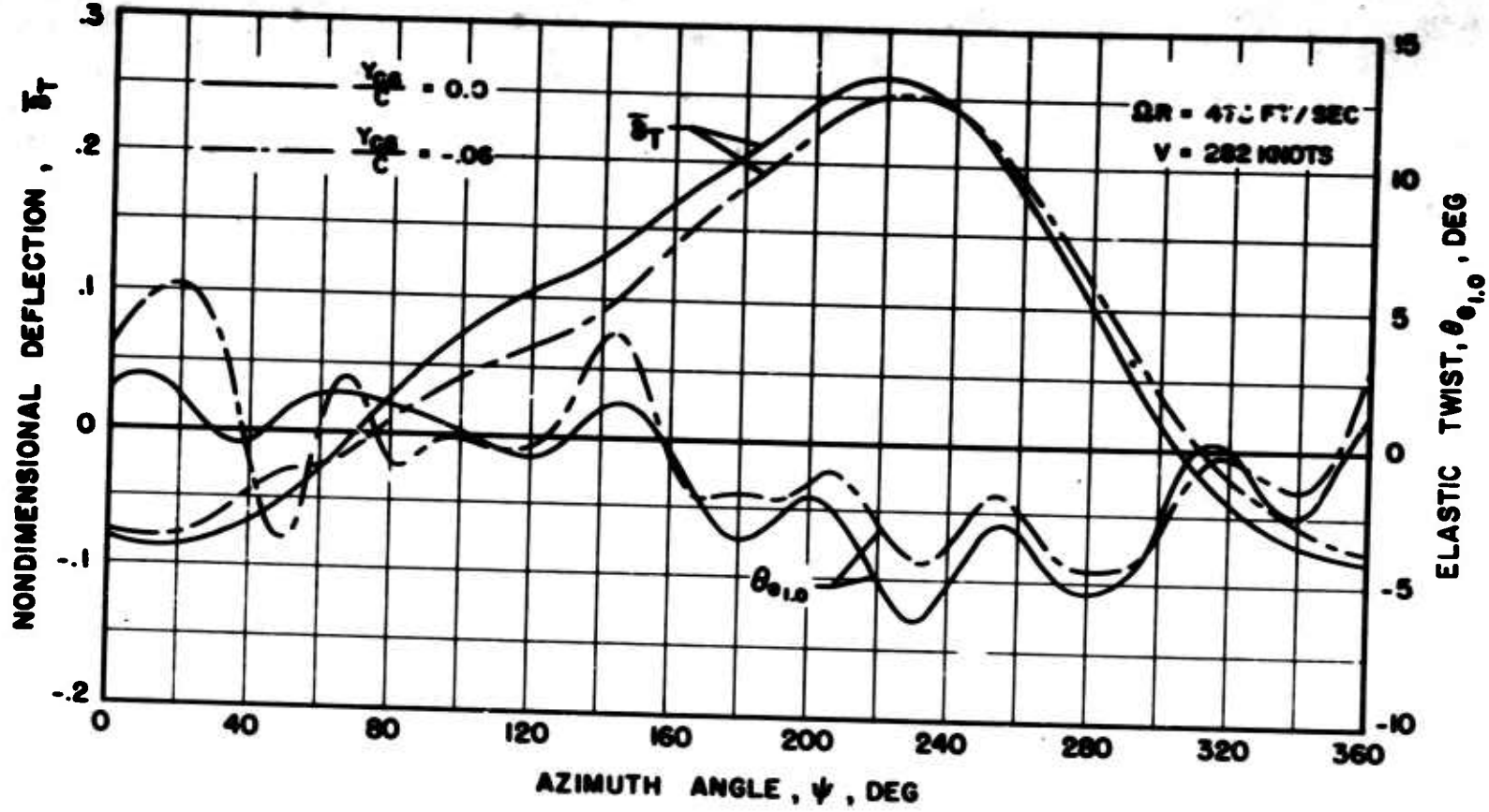

(c) $\mu = 1.0$

Figure 33. Continued.

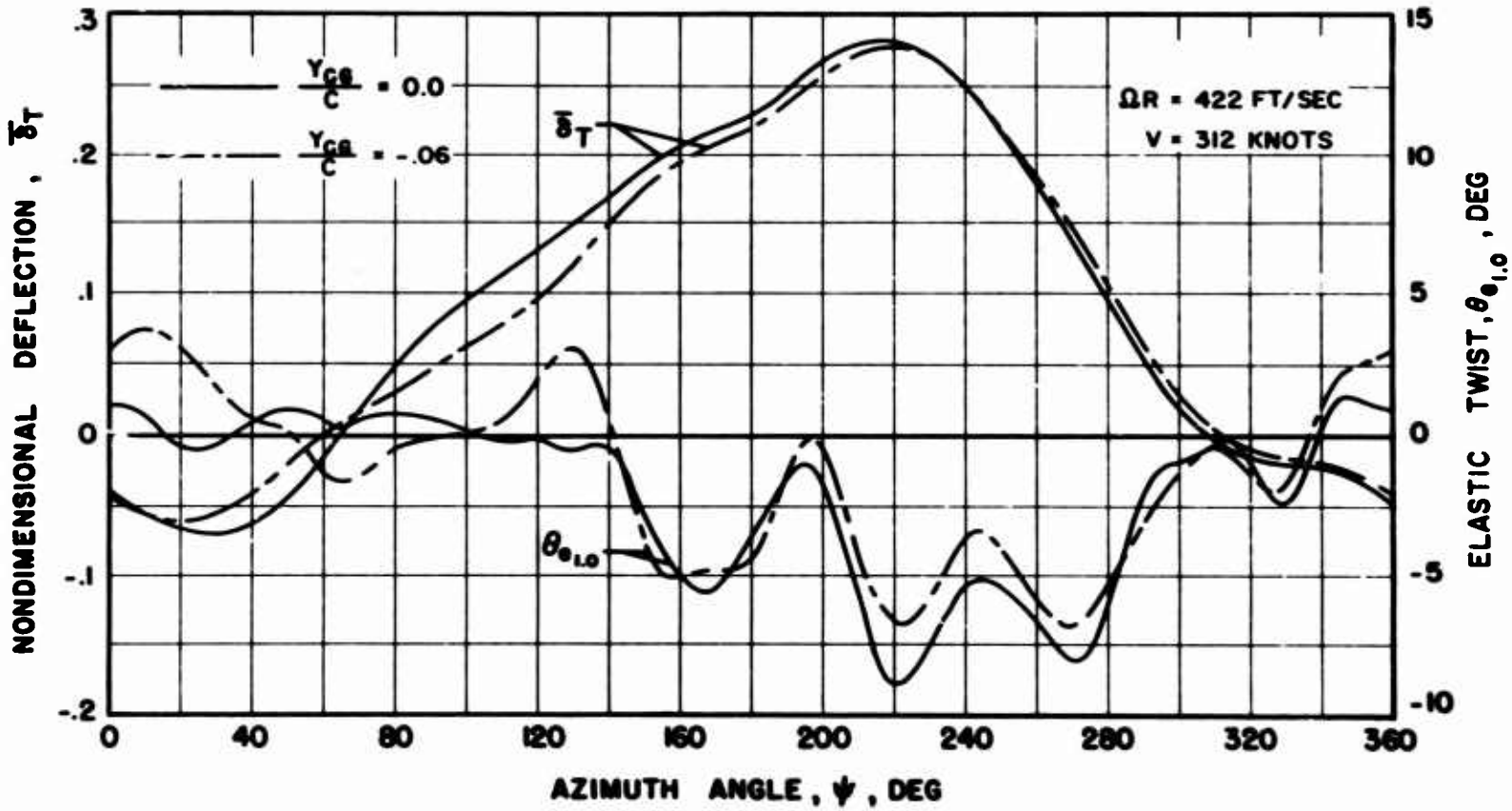

(d) μ = 1.25

Figure 33. Continued.

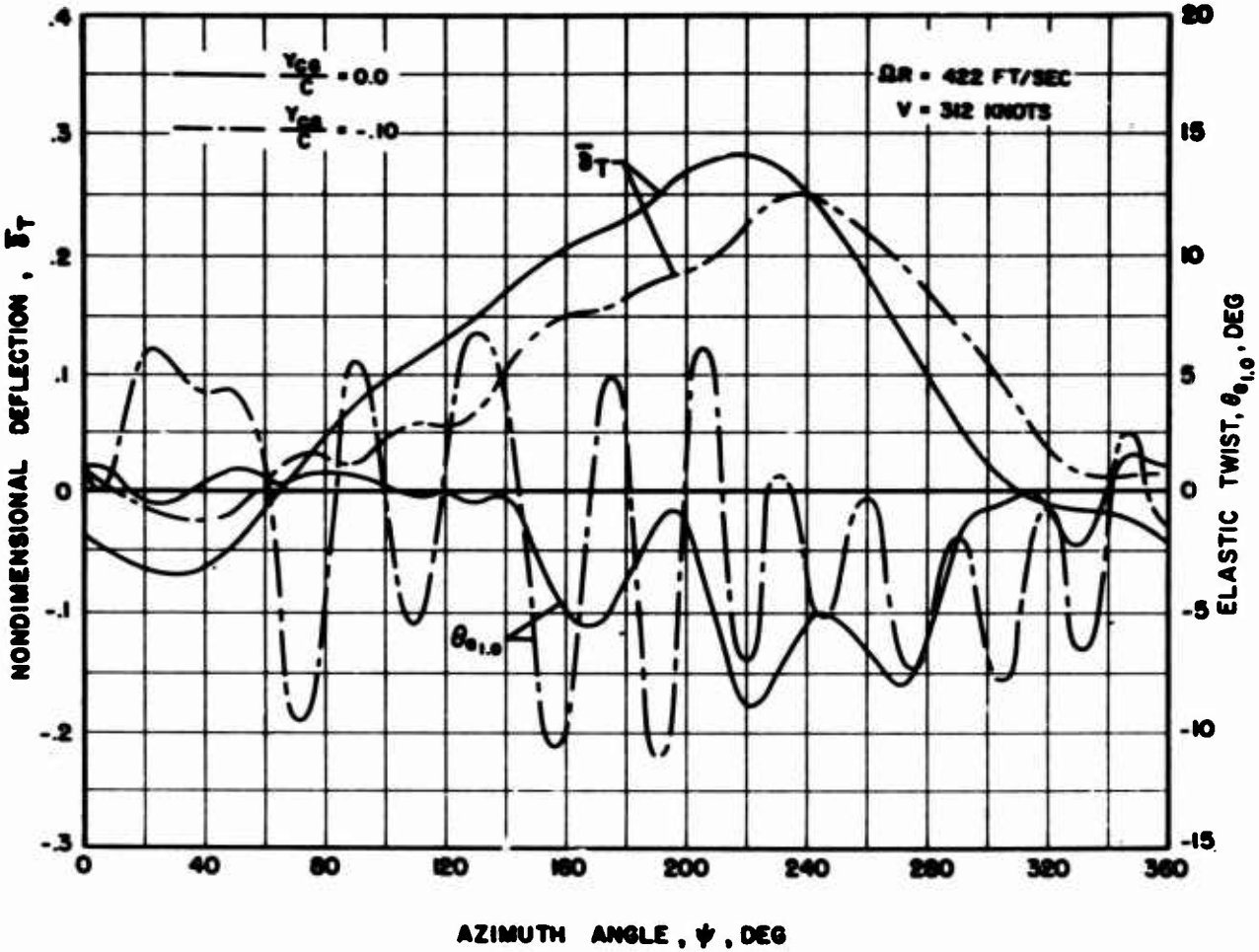

(e) μ = 1.25

Figure 33. Concluded.

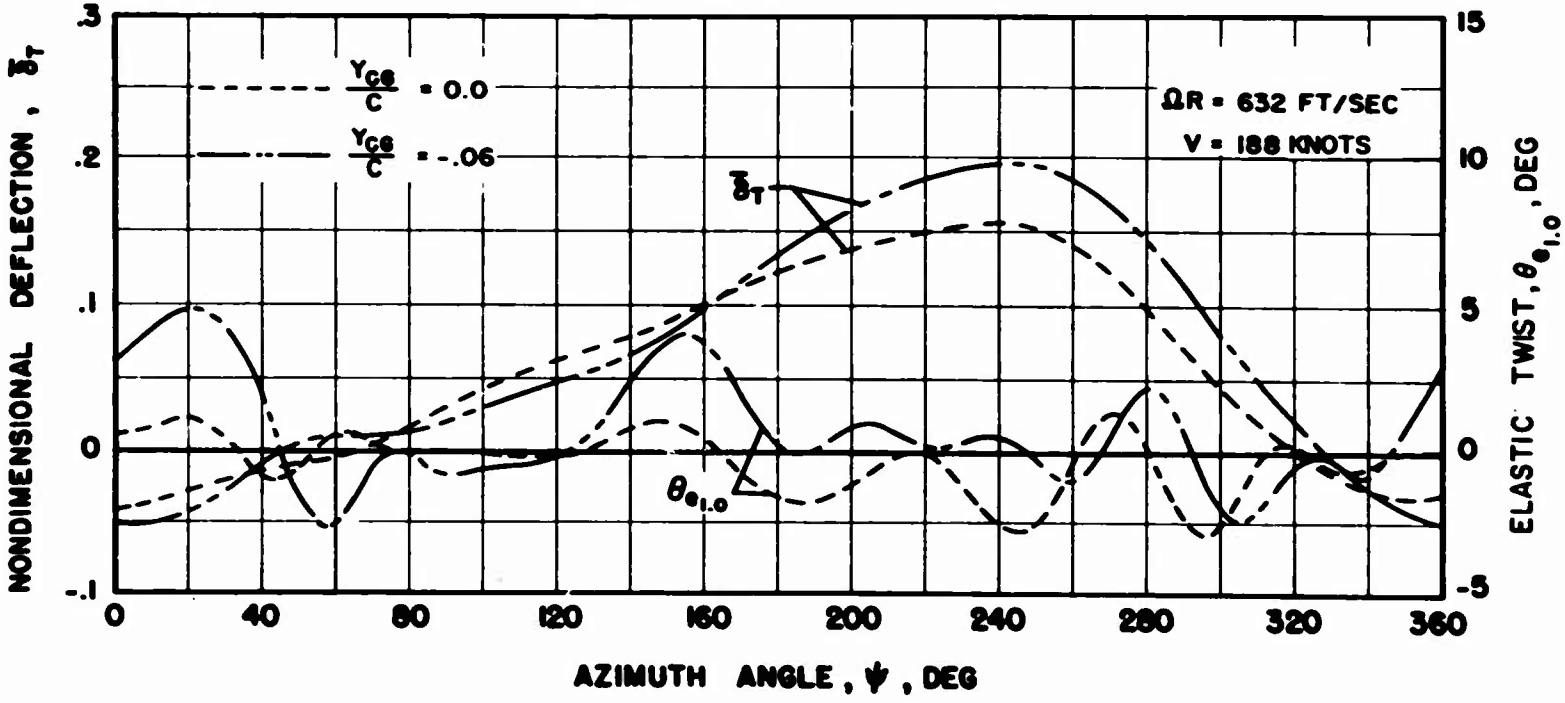

(a) μ = .5

Figure 34. Effect of Center-of-Gravity Offset on Nonarticulated Blade Deflections During a Typical Revolution After an Instantaneous Gust; M_R = 1.99, $\bar{\omega}_{w_1}$ = 1.12, $M_{1,90}$ = .85, W_G = 30 FT/SEC, $\bar{r}_{OA}$ = .12, ψ_0 = 0°.

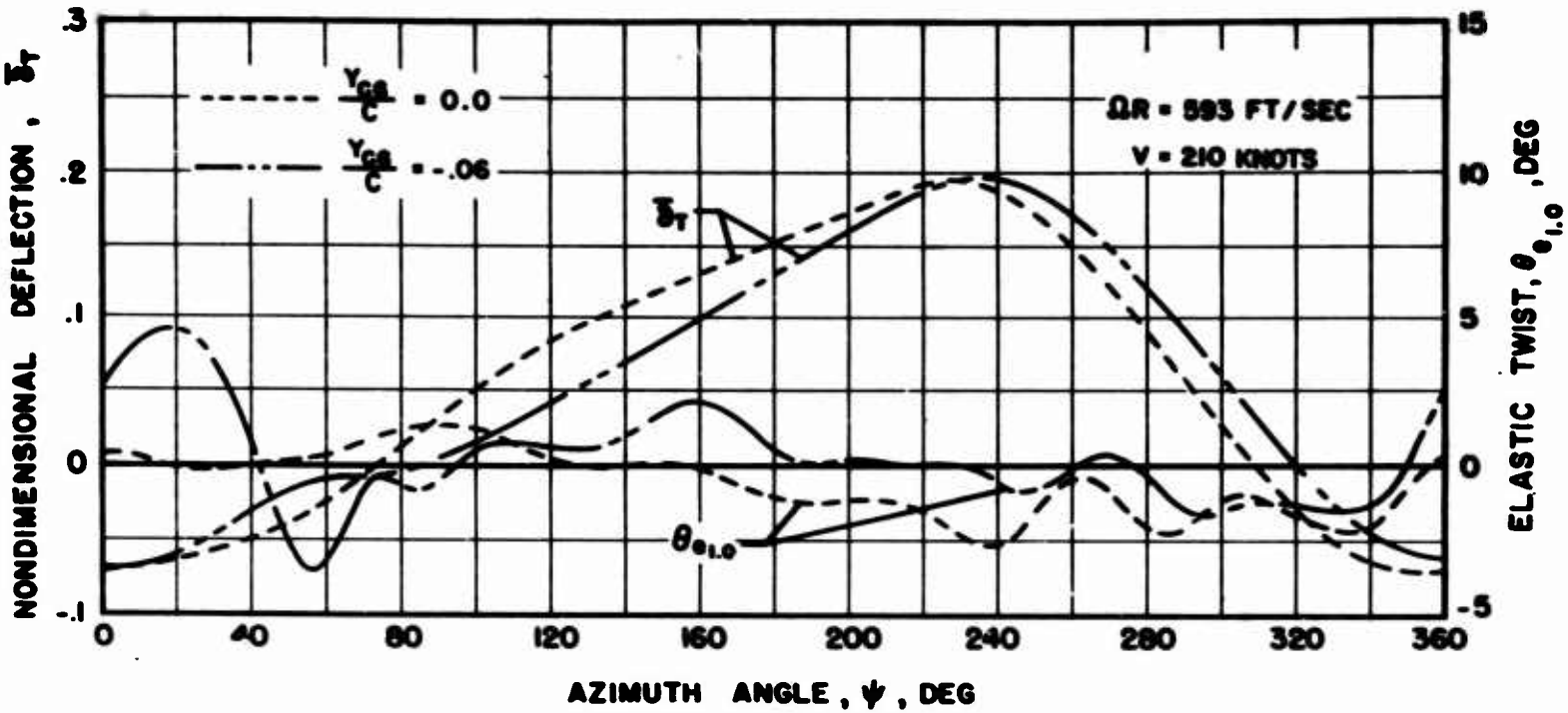

(b) $\mu = .6$

Figure 34. Continued.

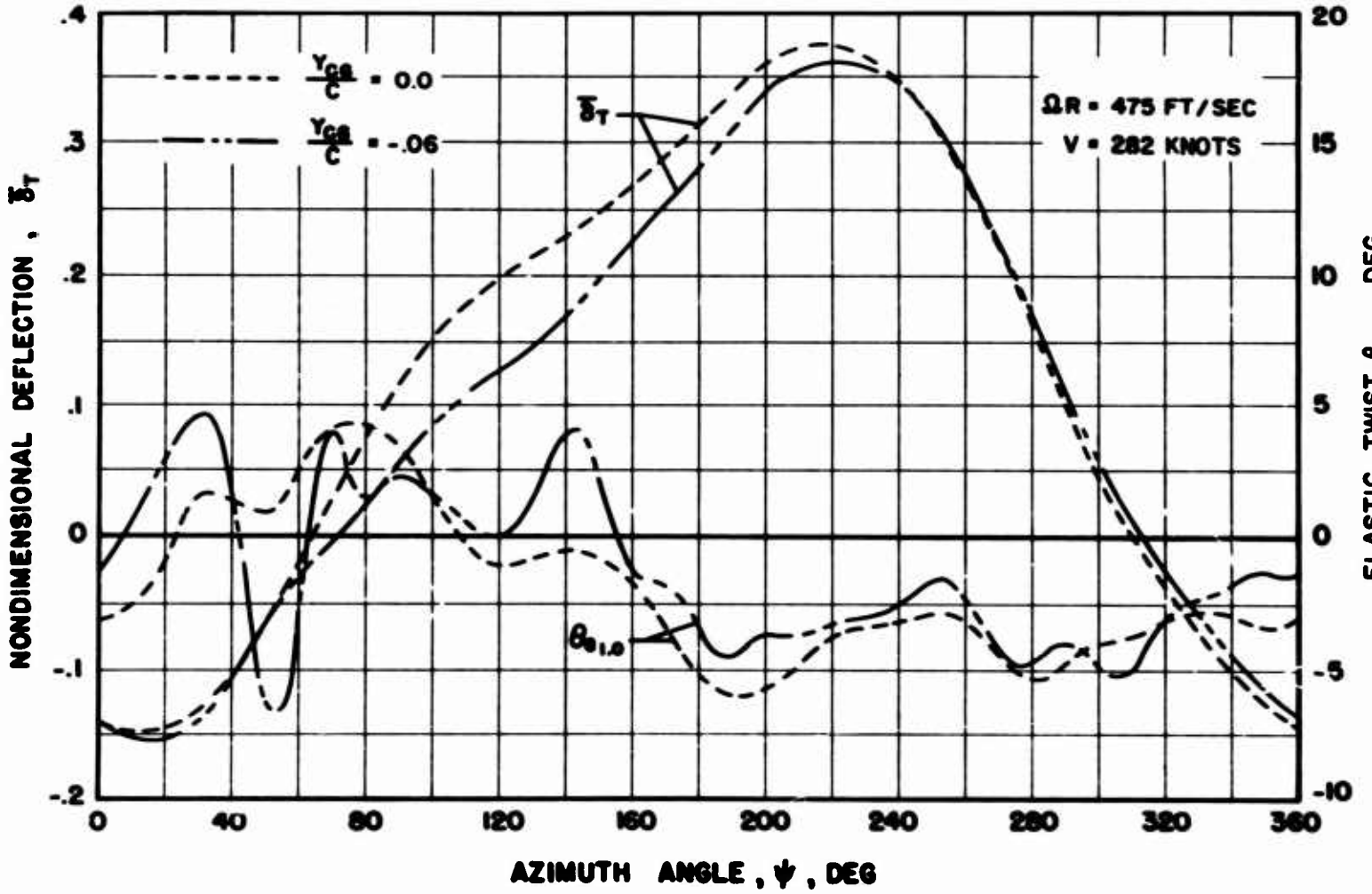

(c) μ = 1.0

Figure 34. Concluded.

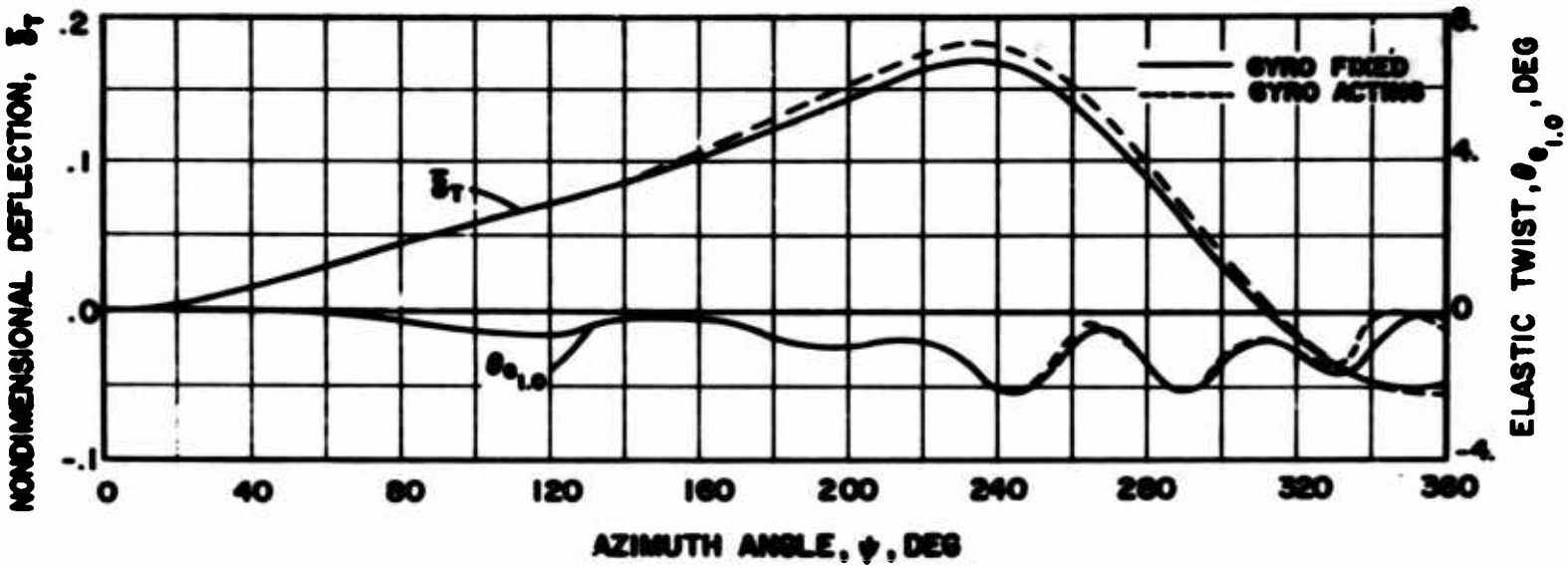

Figure 35. Effect of Gyro Feedback on Nonarticulated Blade Deflections During the First Revolution After an Instantaneous Gust; $\mu = .60, M_R = 1.99, \bar{\omega}_w = 1.12, M_{1,90^2} .85, W_G = 30$ FT/SEC, $T_{OA} = .12, \psi_0 = 0^\circ$.

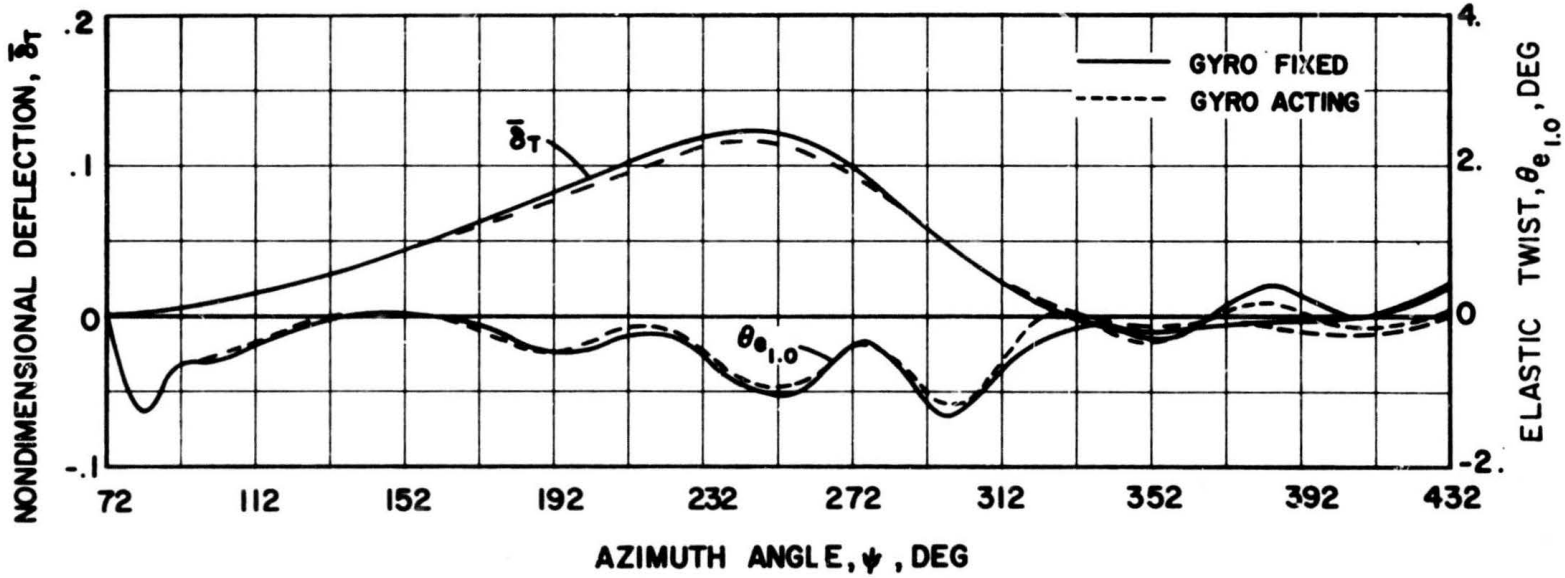

Figure 36. Effect of Gyro Feedback on Nonarticulated Blade Deflections During the First Revolution After an Instantaneous Gust; $\mu = .60, M_R = 1.99, \bar{\omega}_{W_1} = 1.12, M_{1,90} = .85, W_G = 30$ FT/SEC, $\bar{r}_{OA} = .12, \psi_O = 72°$.

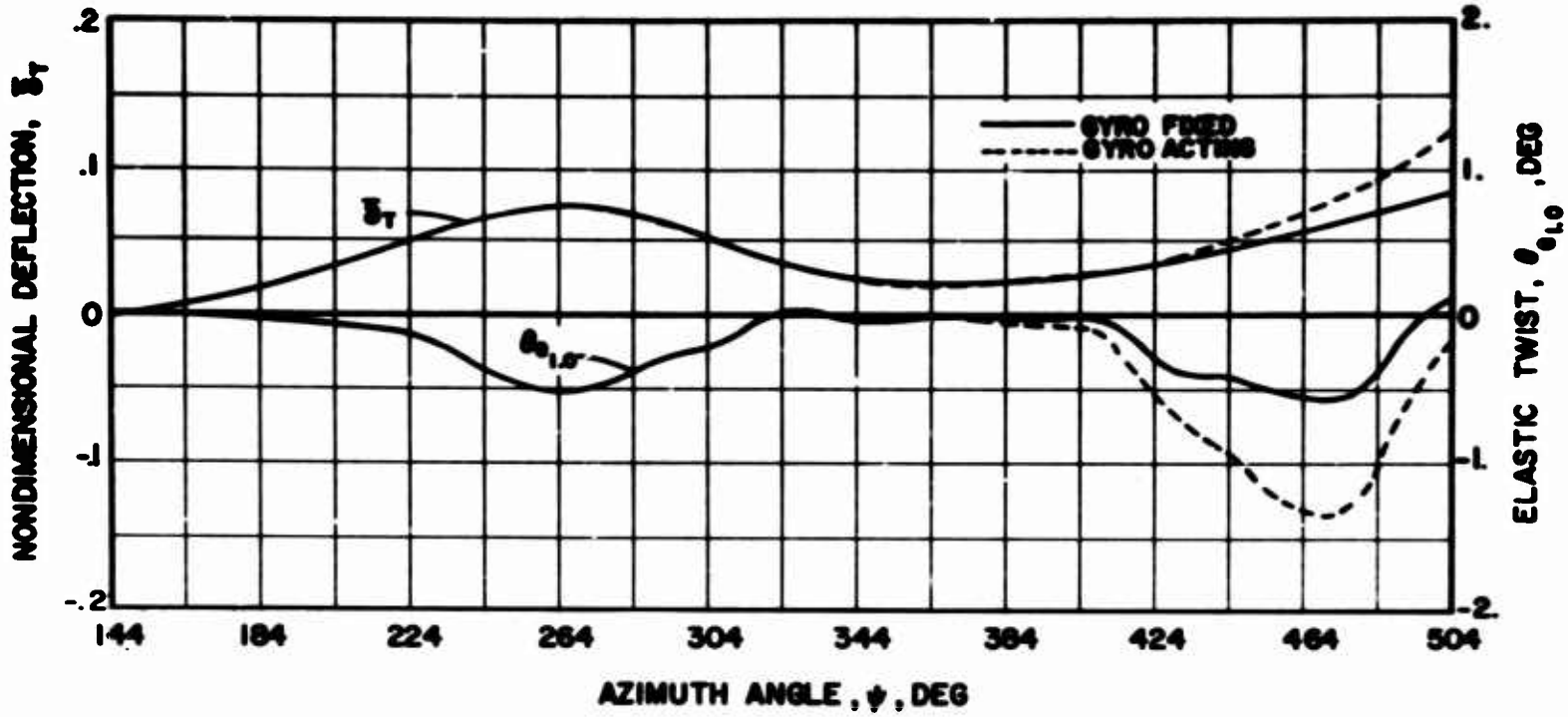

Figure 37. Effect of Gyro Feedback on Nonarticulated Blade Deflections During the First Revolution After an Instantaneous Gust; $\mu = .60$, $M_R = 1.99$, $\bar{\omega}_{w_1} = 1.12$, $M_{1,90} = .85$, $W_G = 30$ FT/SEC, $\bar{r}_{OA} = .12$, $\psi_0 = 144°$.

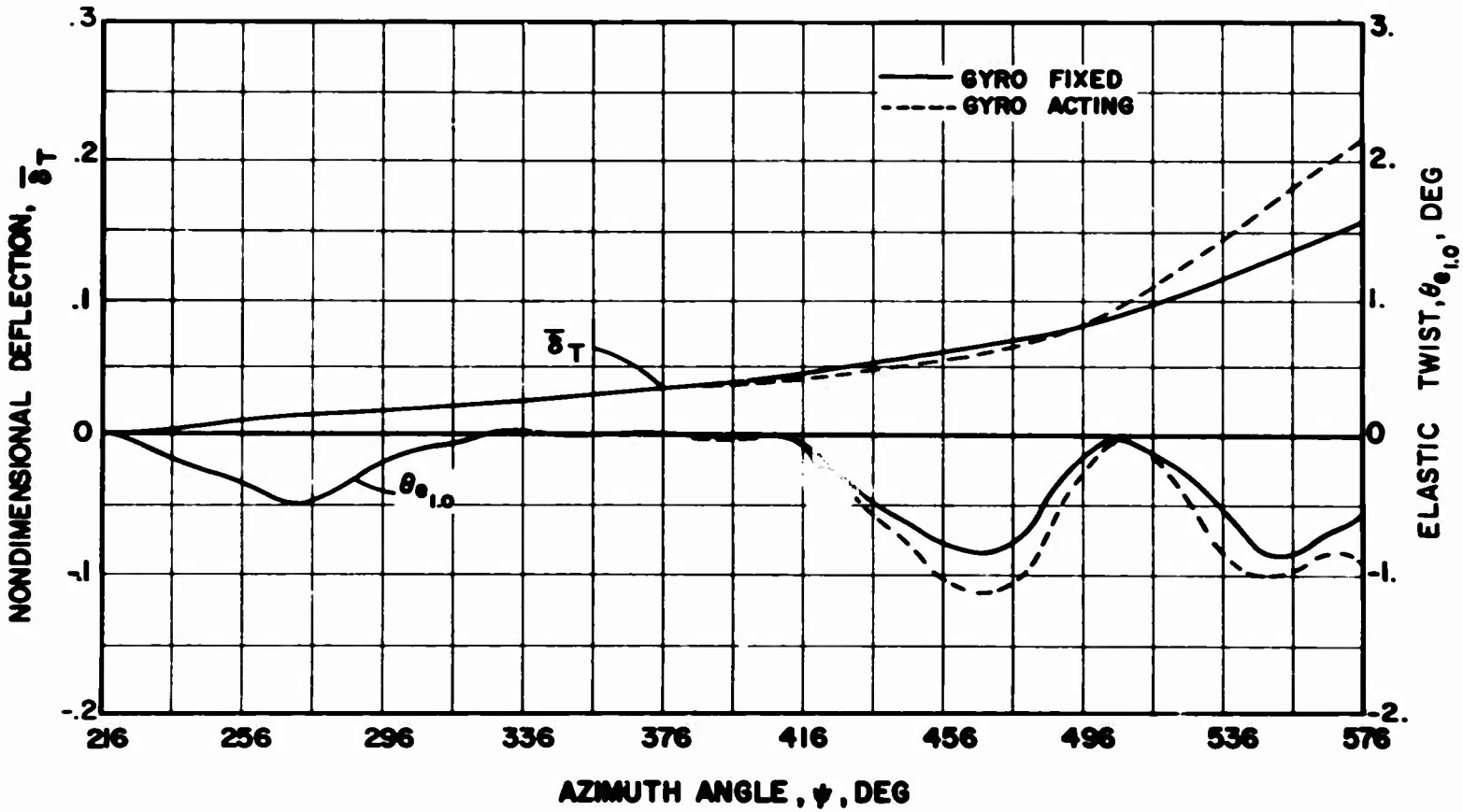

Figure 38. Effect of Gyro Feedback on Nonarticulated Blade Deflections During the First Revolution After an Instantaneous Gust; $\mu = .60$, $M_R = 1.99$, $\bar{\omega}_{w_1} = 1.12$, $M_{1,90} = .85$, $W_G = 30$ FT/SEC, $\bar{r}_{OA} = .12$, $\psi_O = 216°$.

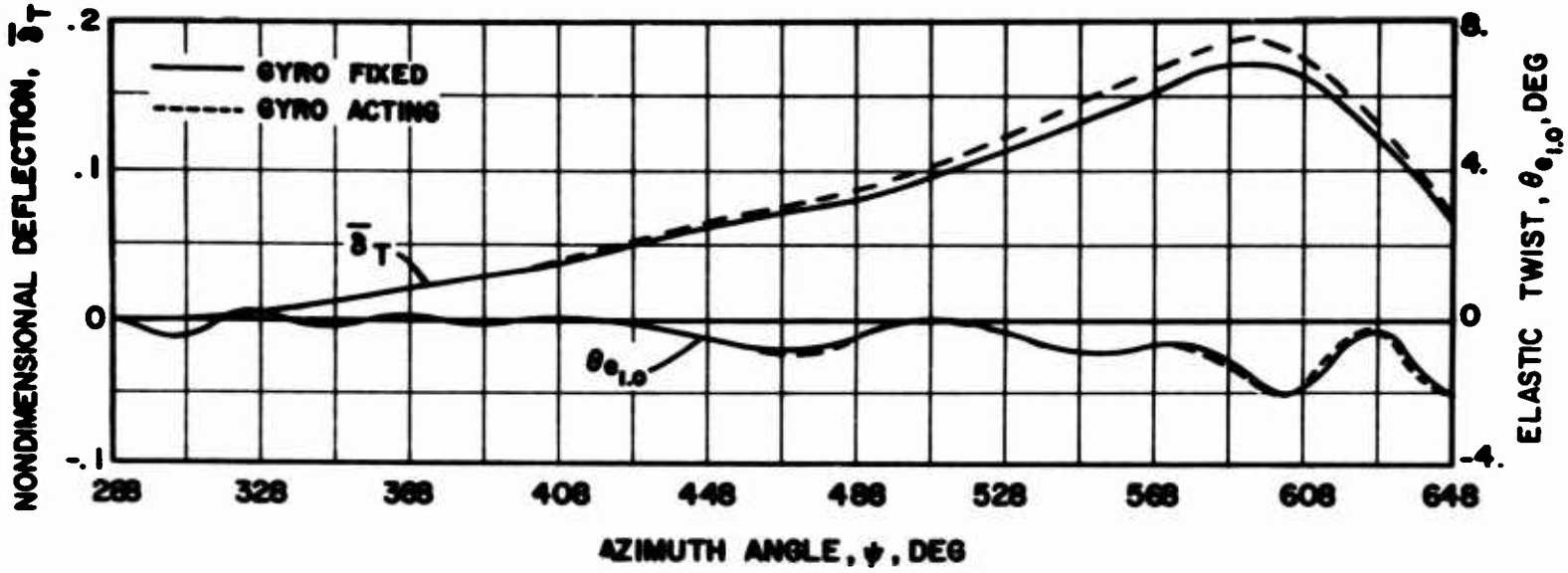

Figure 39. Effect of Gyro Feedback on Nonarticulated Blade Deflections During the First Revolution After an Instantaneous Gust; $\mu = .60, M_R = 1.99, \bar{\omega}_{w_1} = 1.12, M_{1,90} = .85, W_G = 30 FT/SEC, \bar{r}_{OA} = .12, \psi_0 = 288°$.

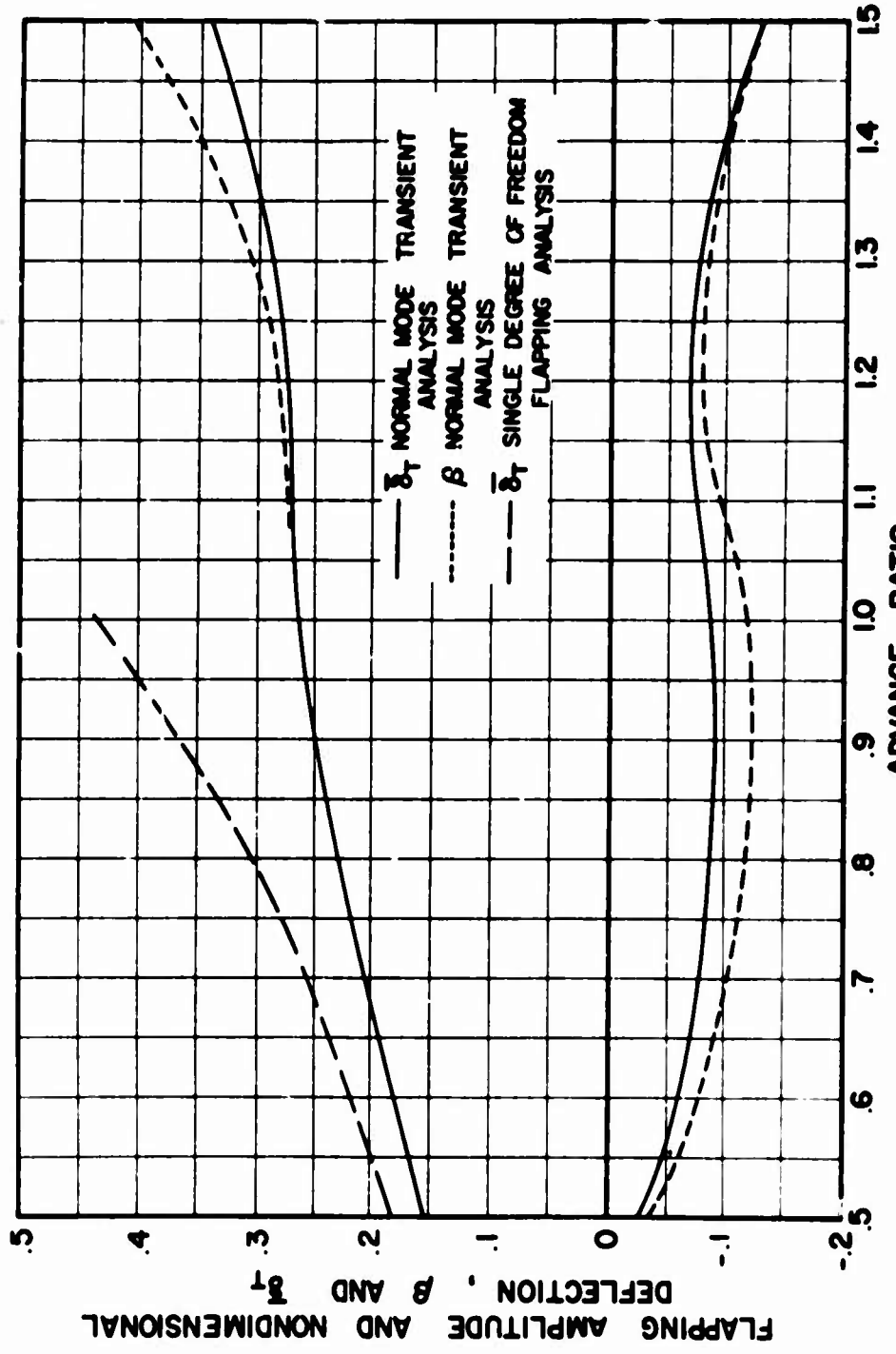

Figure 40. Effect of Higher Bending and Torsion Modes on Maximum and Minimum Articulated Blade Response During a Typical Revolution After an Instantaneous Gust; $M_R = 1.85, \delta_3 = 0°, C_{FD} = 0, M_{1,90} = .85,$ $W_G = 30$ FT/SEC, $\bar{r}_{OA} = .12, \psi_0 = 0°, \delta_4 = 0, Y_{cg}/C = 0.$

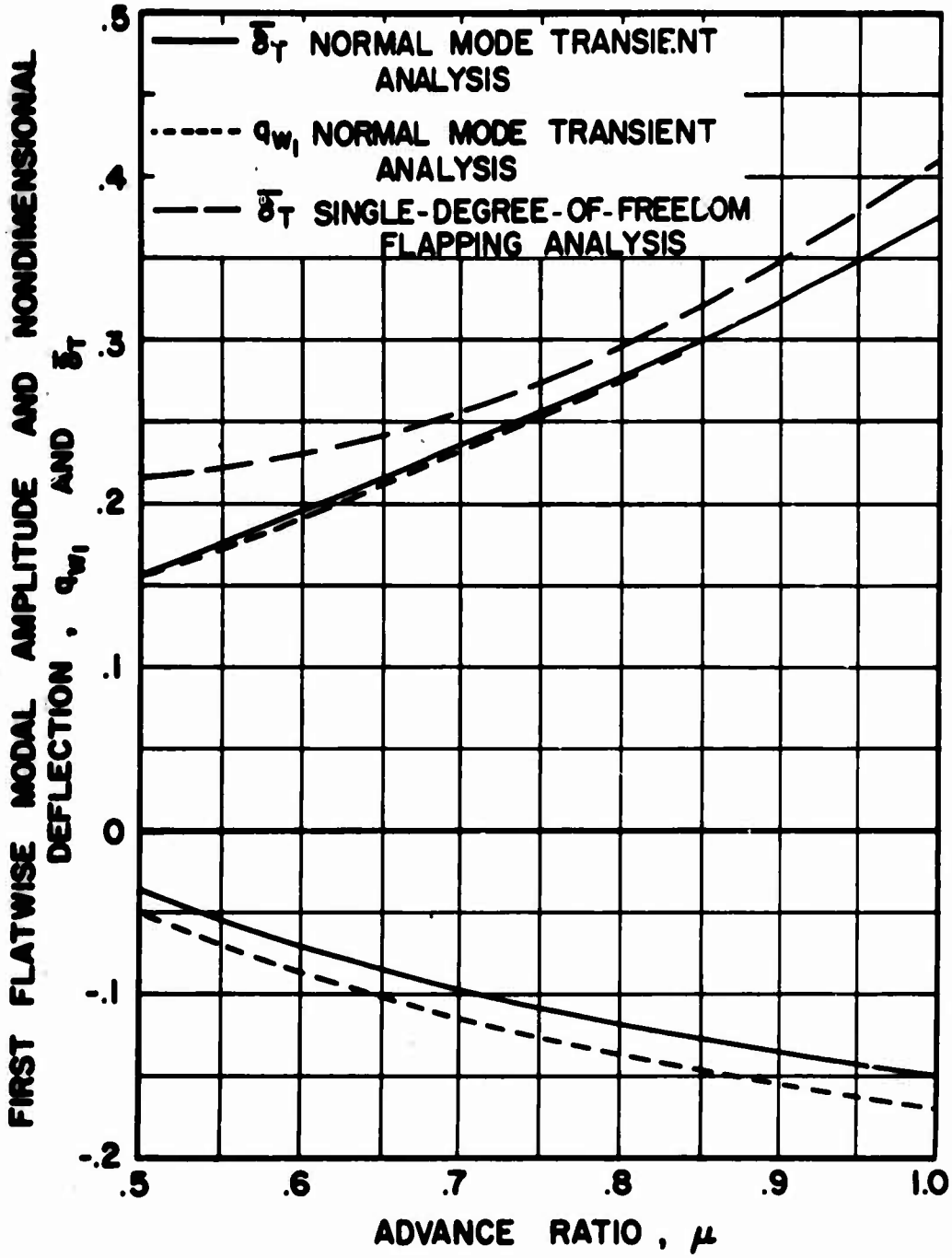

Figure 41. Effect of Higher Bending and Torsion Modes on Maximum and Minimum Non-articulated Blade Response During a Typical Revolution After an Instantaneous Gust; $M_R = 1.99, \bar{\omega}_{w_1} = 1.12, M_{1.90} = .85, W_G = 30$ FT/SEC, $T_{OA} = .12, \psi_0 = 0°$, $Y_{cg}/C = 0$, Control Gyro Fixed.

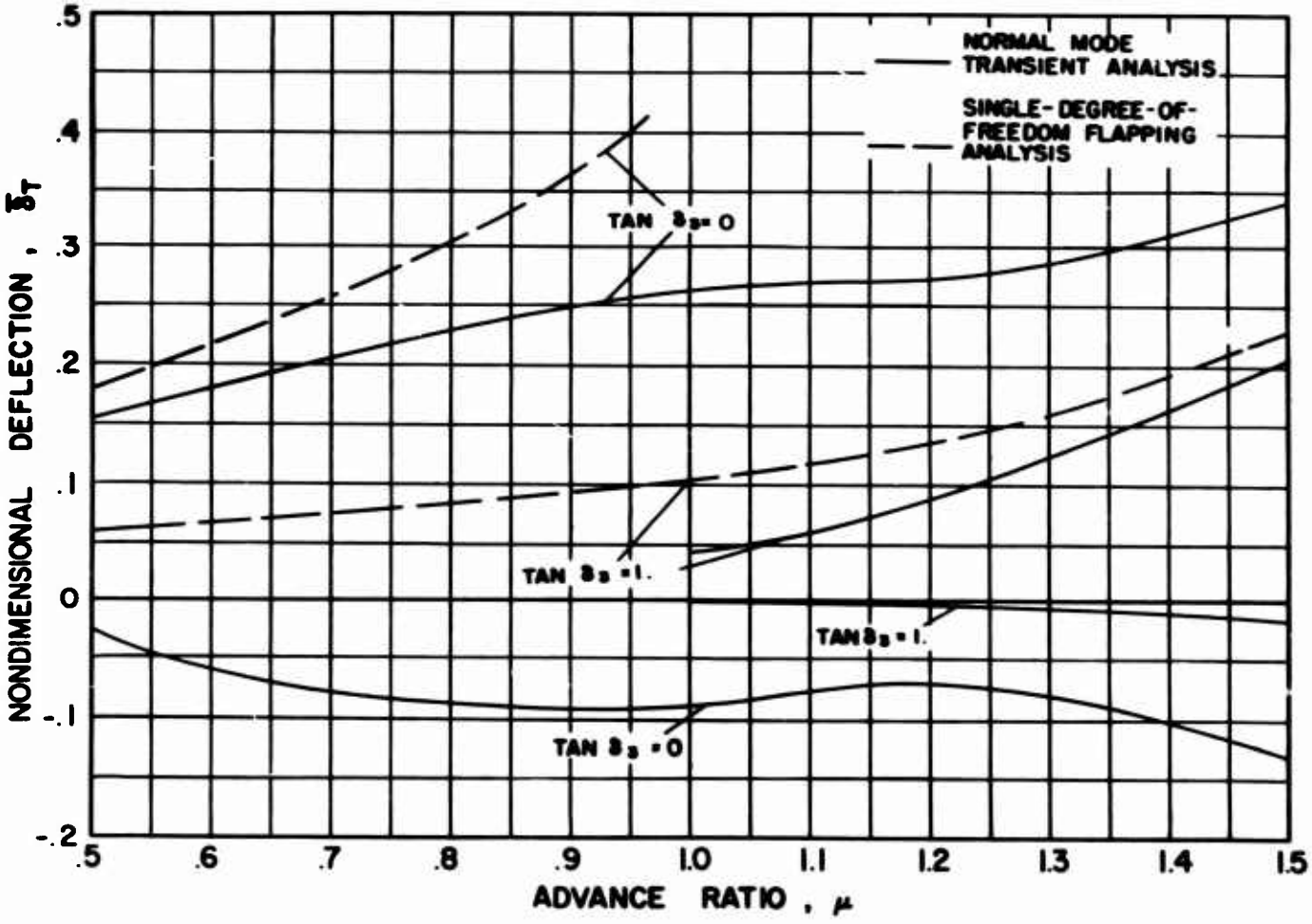

Figure 42. Effect of Pitch-Flap Coupling on Maximum and Minimum Articulated Blade Response During a Typical Revolution After an Instantaneous Gust; $M_R = 1.85$, $C_{FD} = 0$, $M_{1,90} = .85$, $W_G = 30$ FT/SEC, $\bar{r}_{OA} = .12$, $\psi_0 = 0°$, $\delta_4 = 0$, $Y_{cg}/C = 0$.

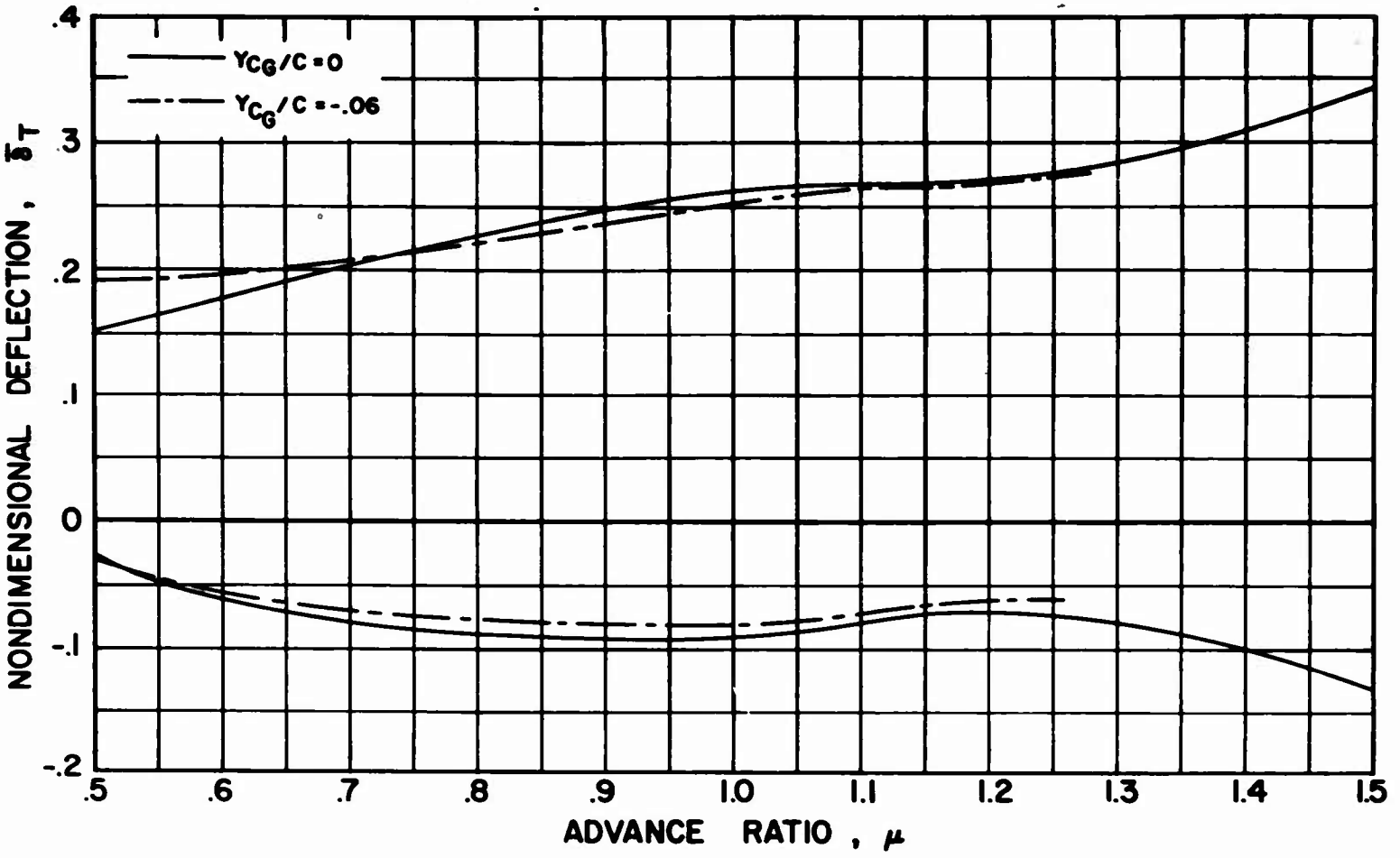

Figure 43. Effect of Center-of-Gravity Offset on Maximum and Minimum Articulated Blade Response During a Typical Revolution After an Instantaneous Gust; $M_R = 1.85$, $\delta_3 = 0°$, $C_{FD} = 0$, $M_{1,90} = .85$, $W_G = 30$ FT/SEC, $\bar{r}_{OA} = .12$, $\psi_0 = 0°$, $\delta_4 = 0$.

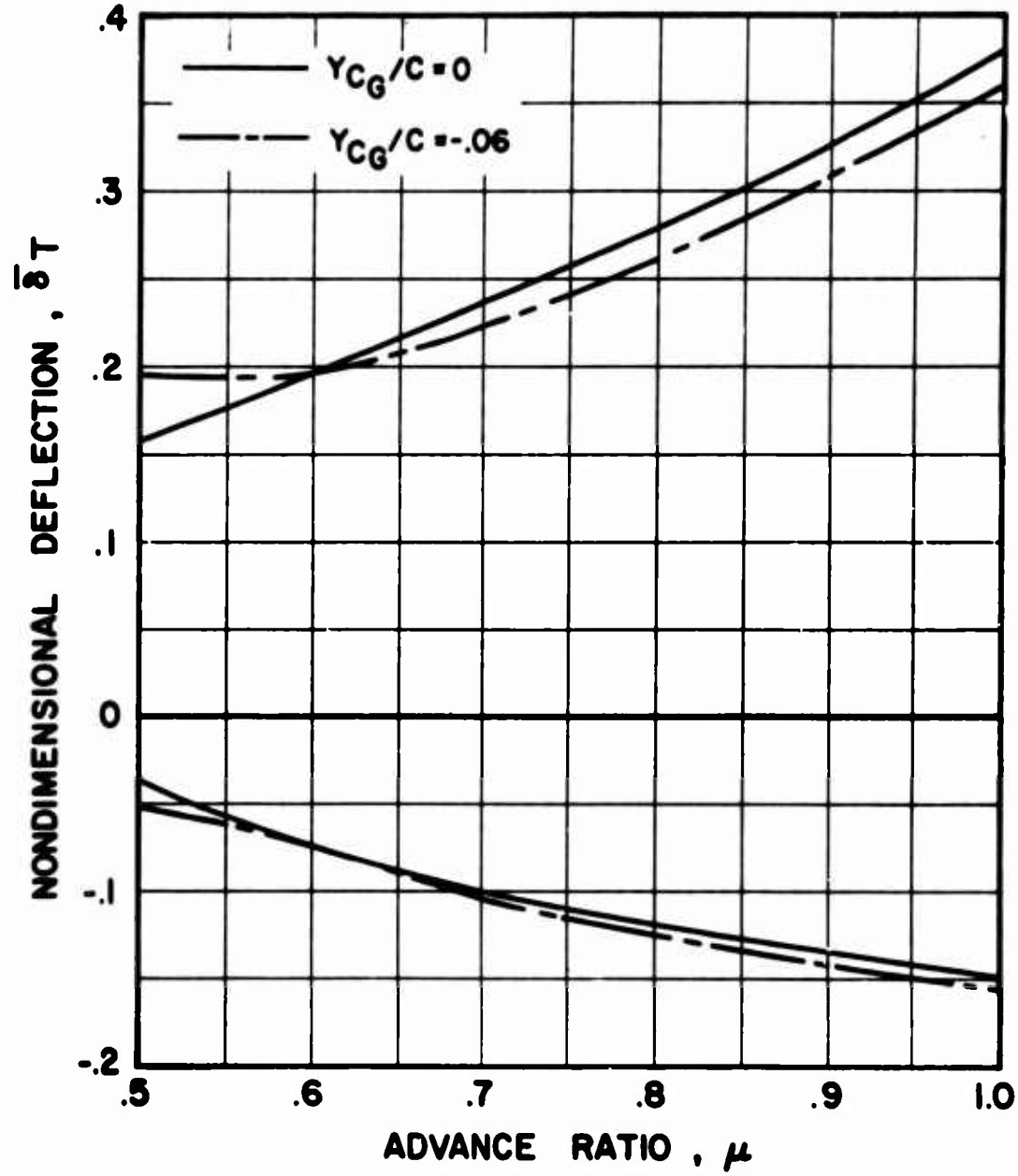

Figure 44. Effect of Center-of-Gravity Offset on Maximum and Minimum Nonarticulated Blade Response During a Typical Revolution After an Instantaneous Gust; $M_R = 1.99, \bar{\omega}_{W_1} = 1.12, M_{1,90} = .85, W_G = 30$ FT/SEC, $\bar{r}_{OA} = .12, \psi_0 = 0°$; Control Gyro Fixed.

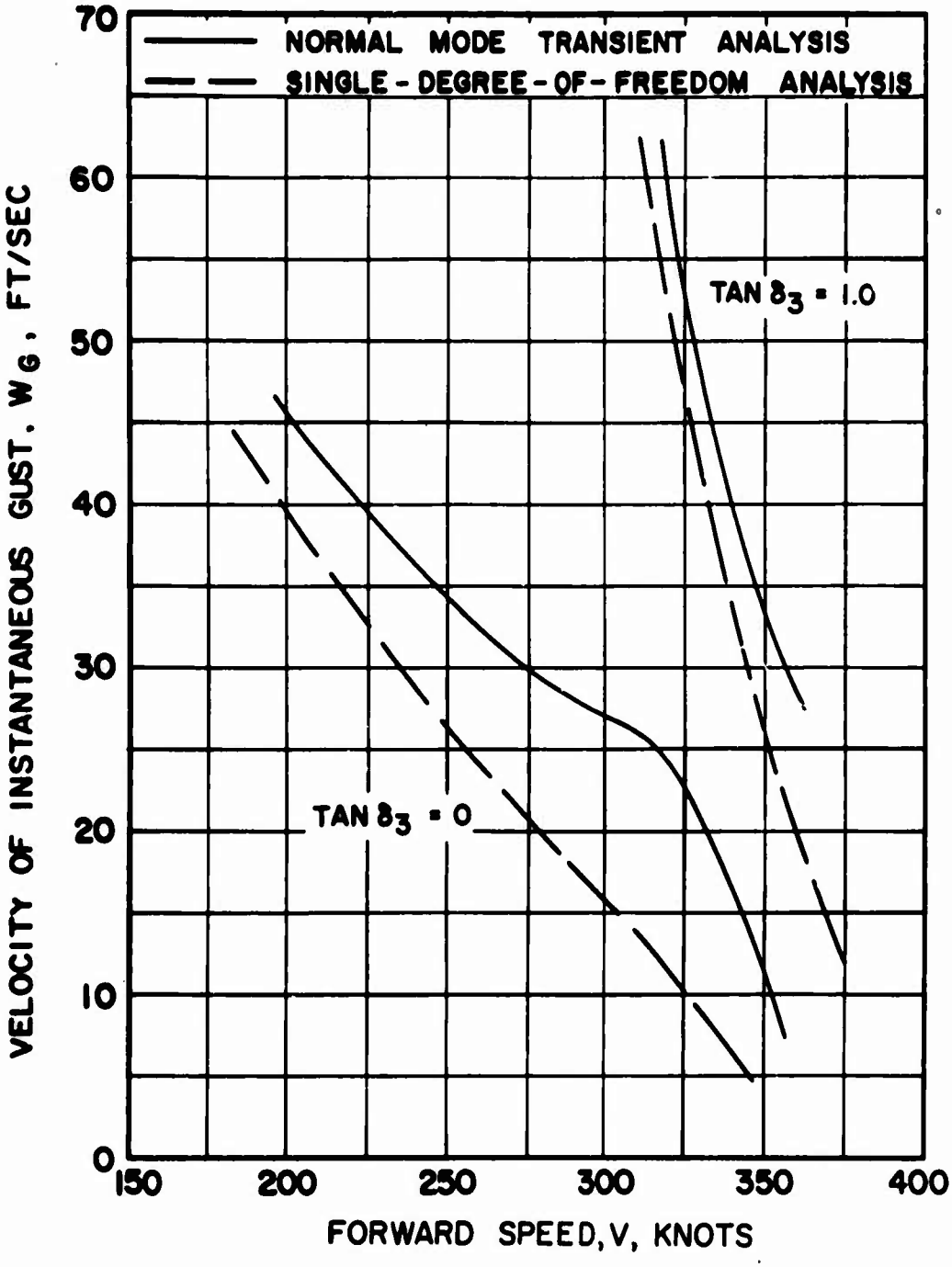

Figure 45. Effect of Sharp Edged Gust Velocity on Allowable Forward Speed for Articulated Blades; $M_R = 1.85$, $C_{FD} = 0$, $M_{1,90} = .85$, $\bar{r}_{OA} = .12$, $\psi_0 = 0°$, $\delta_4 = 0$, $\delta_T = .26$.

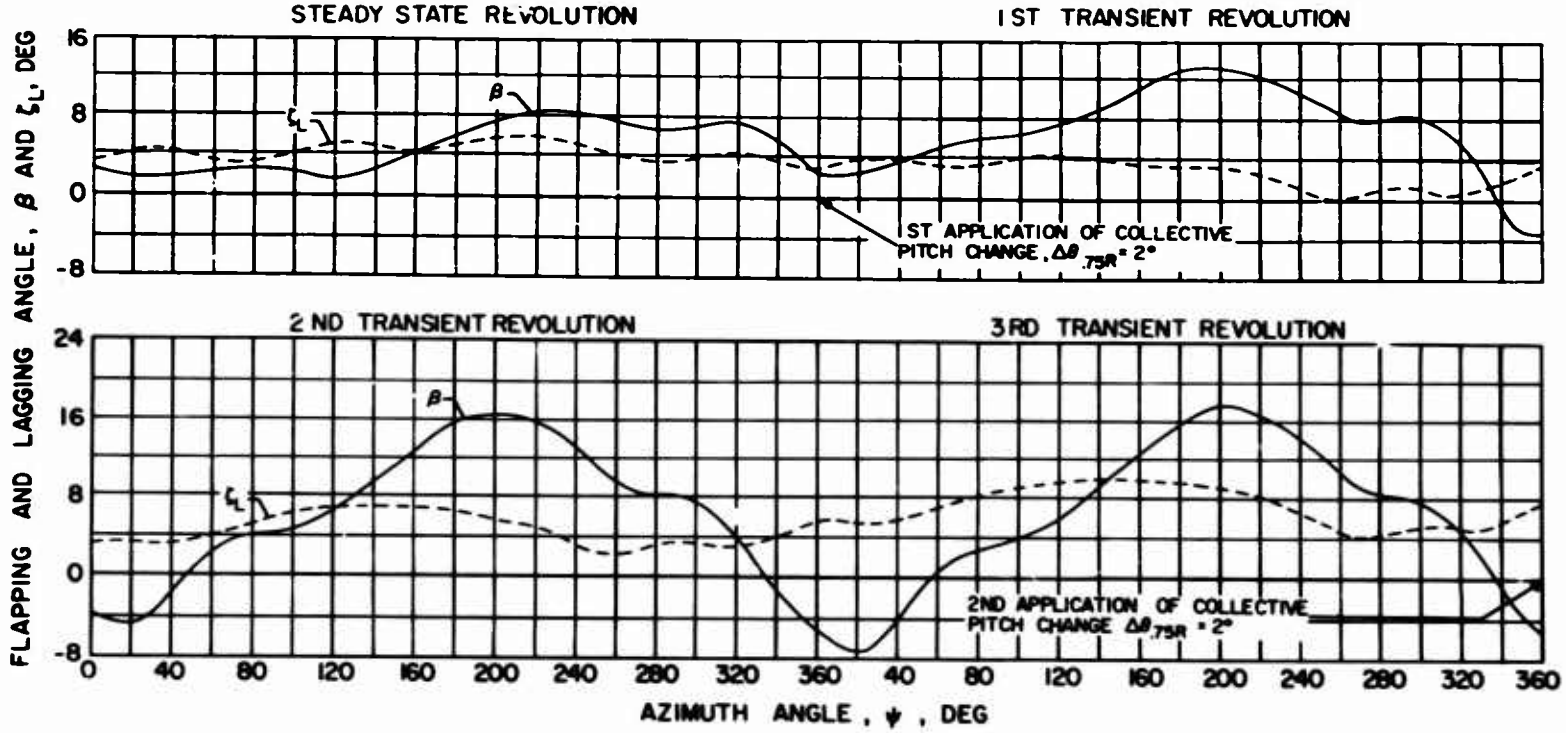

Figure 46. Transient Rotor Blade Response to Collective Pitch Change; Steady State $C_L/\sigma = .060, \Delta\theta_{.75R} = 2°, \mu = .5$; Lag Damping Present.

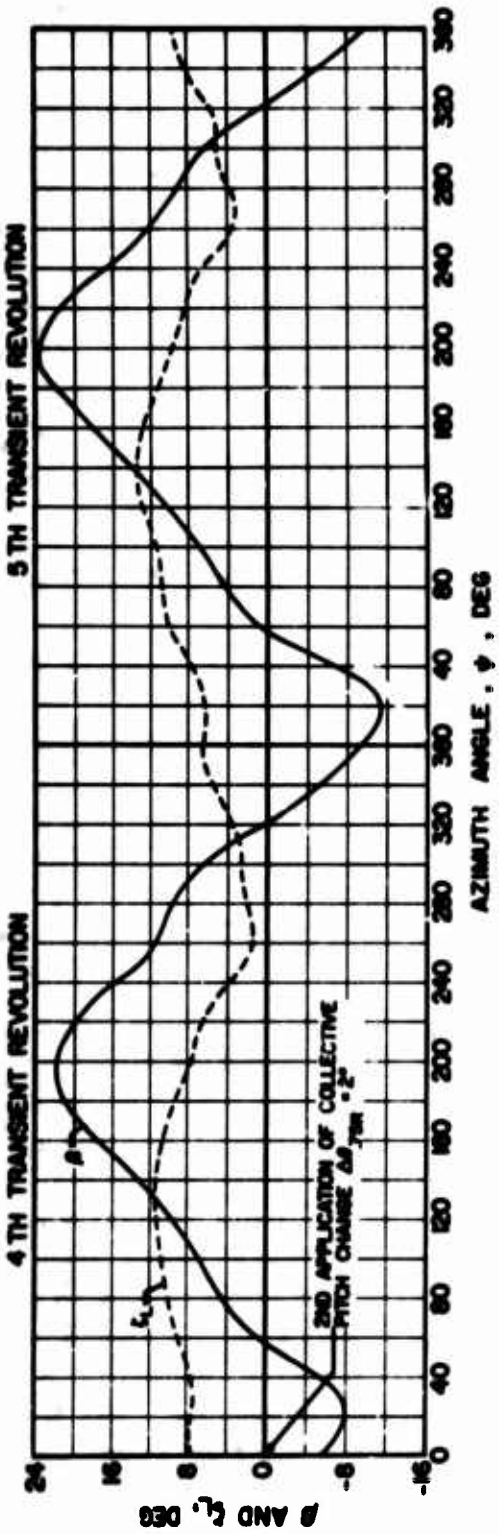

Figure 46. Concluded.

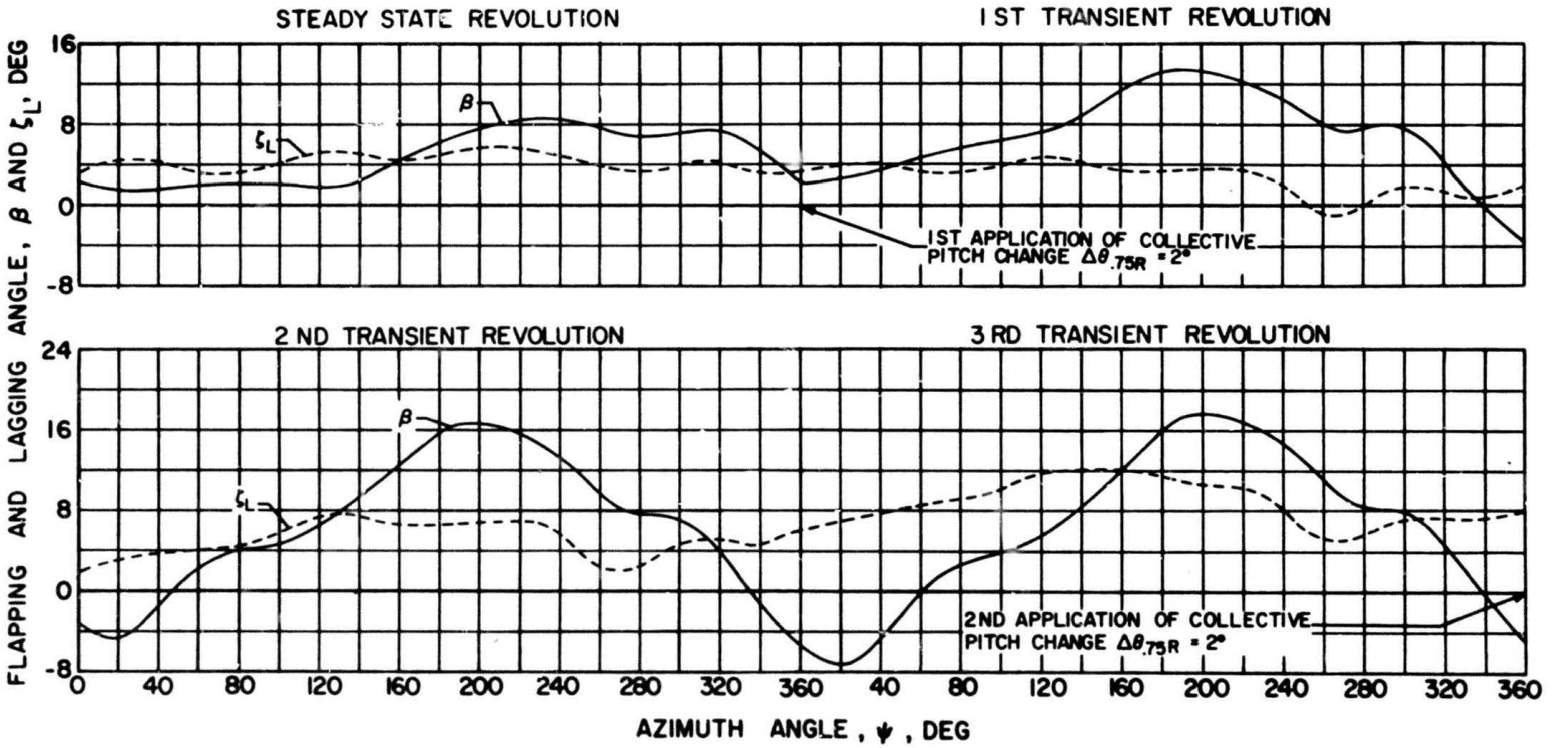

Figure 47. Transient Rotor Blade Response to Collective Pitch Change; Steady State $C_L/\sigma = .060, \Delta\theta_{.75R} = 2°, \mu = .5$; Lag Damping Not Present.

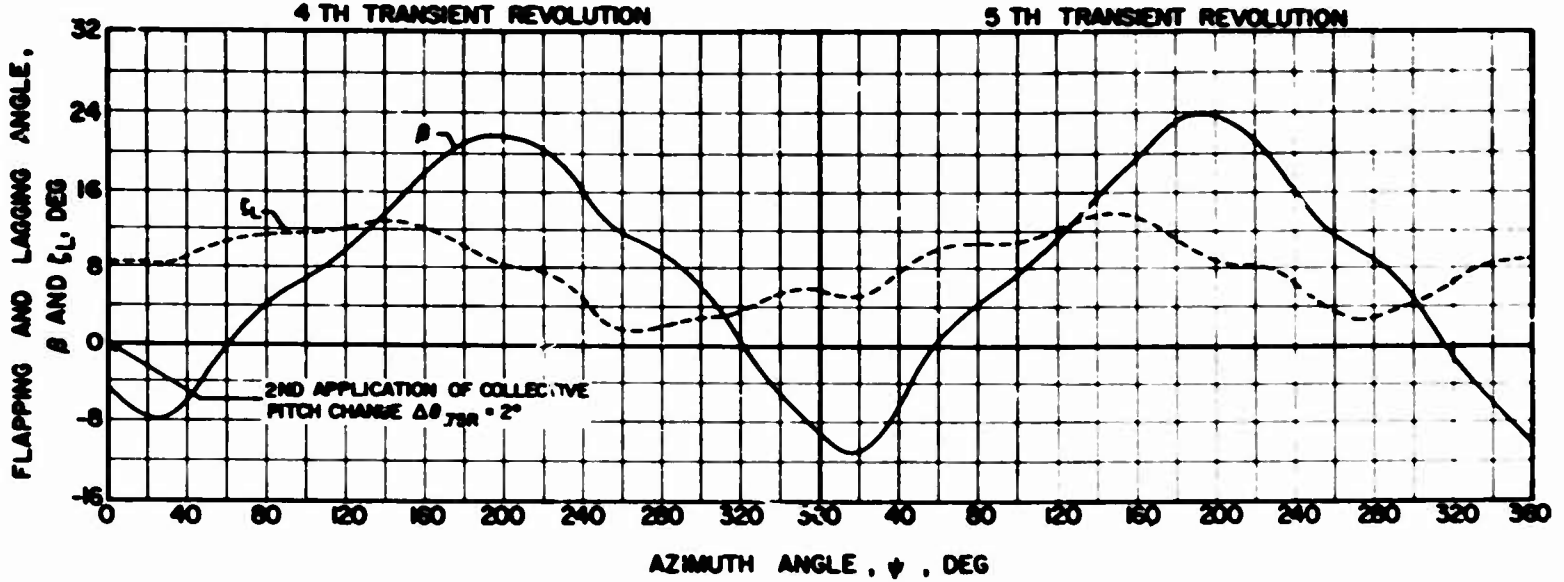

Figure 47. Concluded.

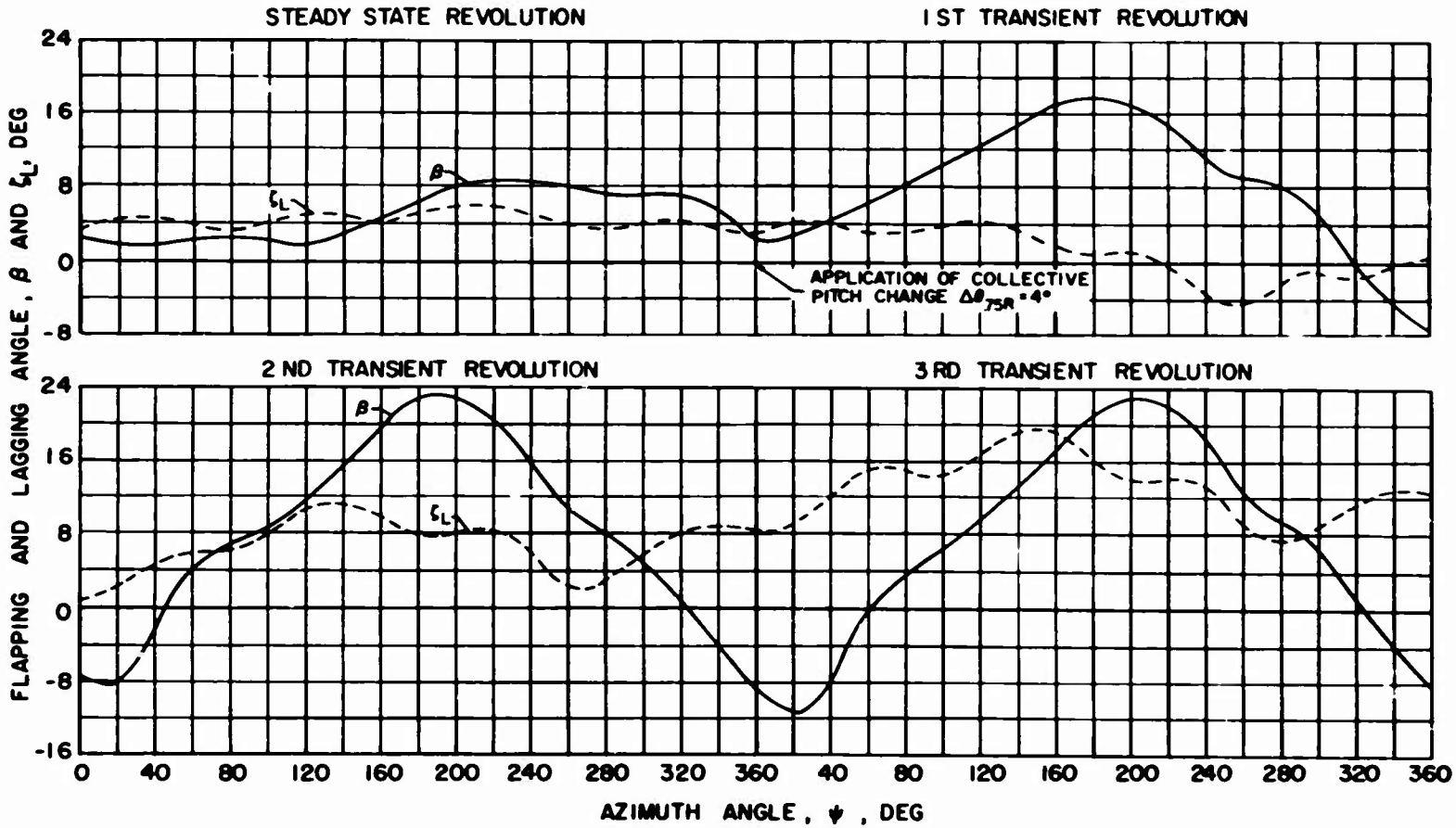

Figure 48. Transient Rotor Blade Response to Collective Pitch Change; Steady State $C_L/\sigma = .060, \Delta\theta_{.75R} = 4°$, $\mu = .5$; Lag Damping Not Present.

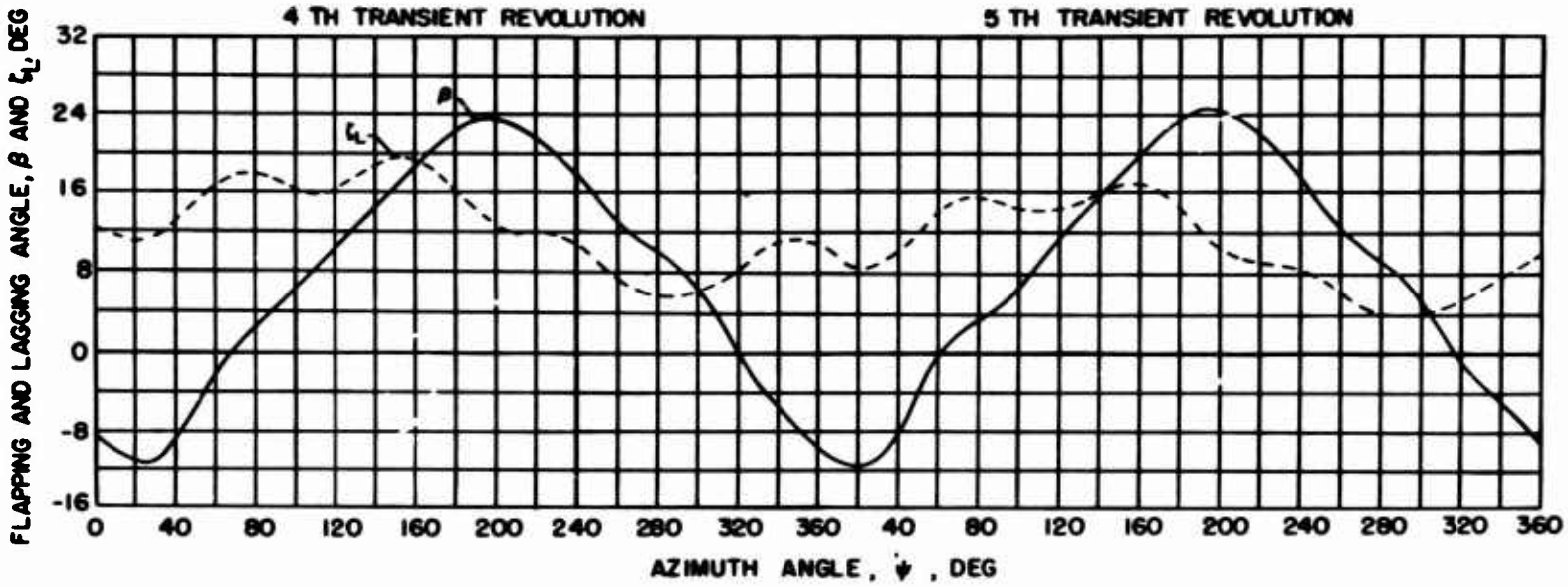

Figure 48. Concluded.

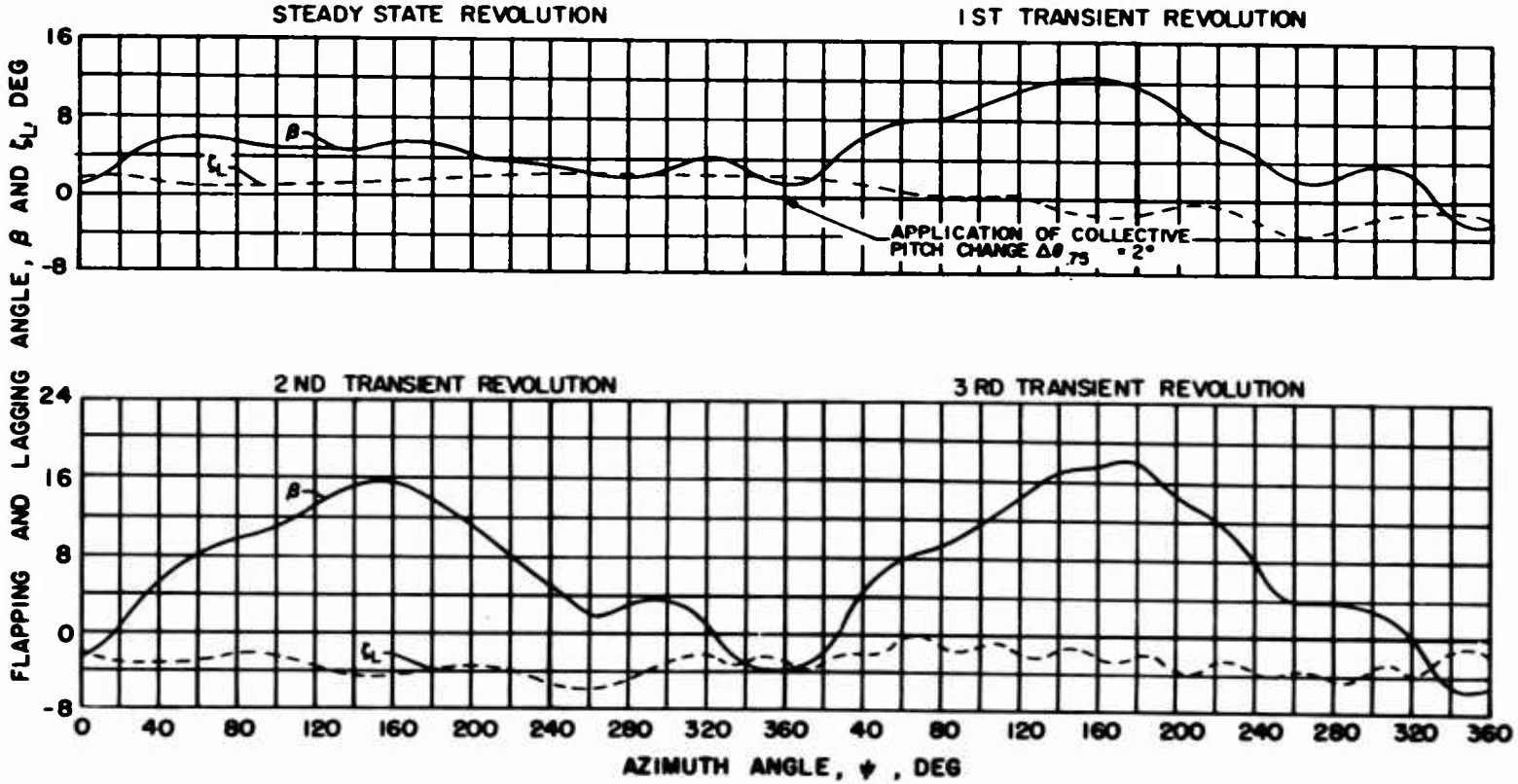

Figure 49. Transient Rotor Blade Response to Collective Pitch Change; Steady State $C_L/\sigma = .057, \Delta\theta_{.75R} = 2°, \mu = .7$; Lag Damping Not Present.

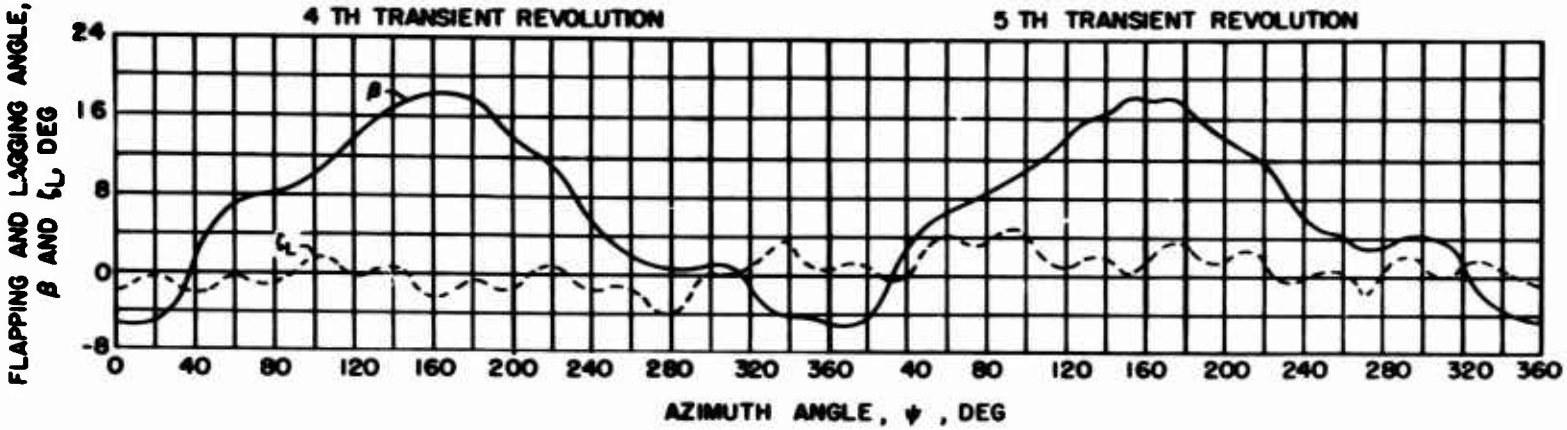

Figure 49. Concluded.

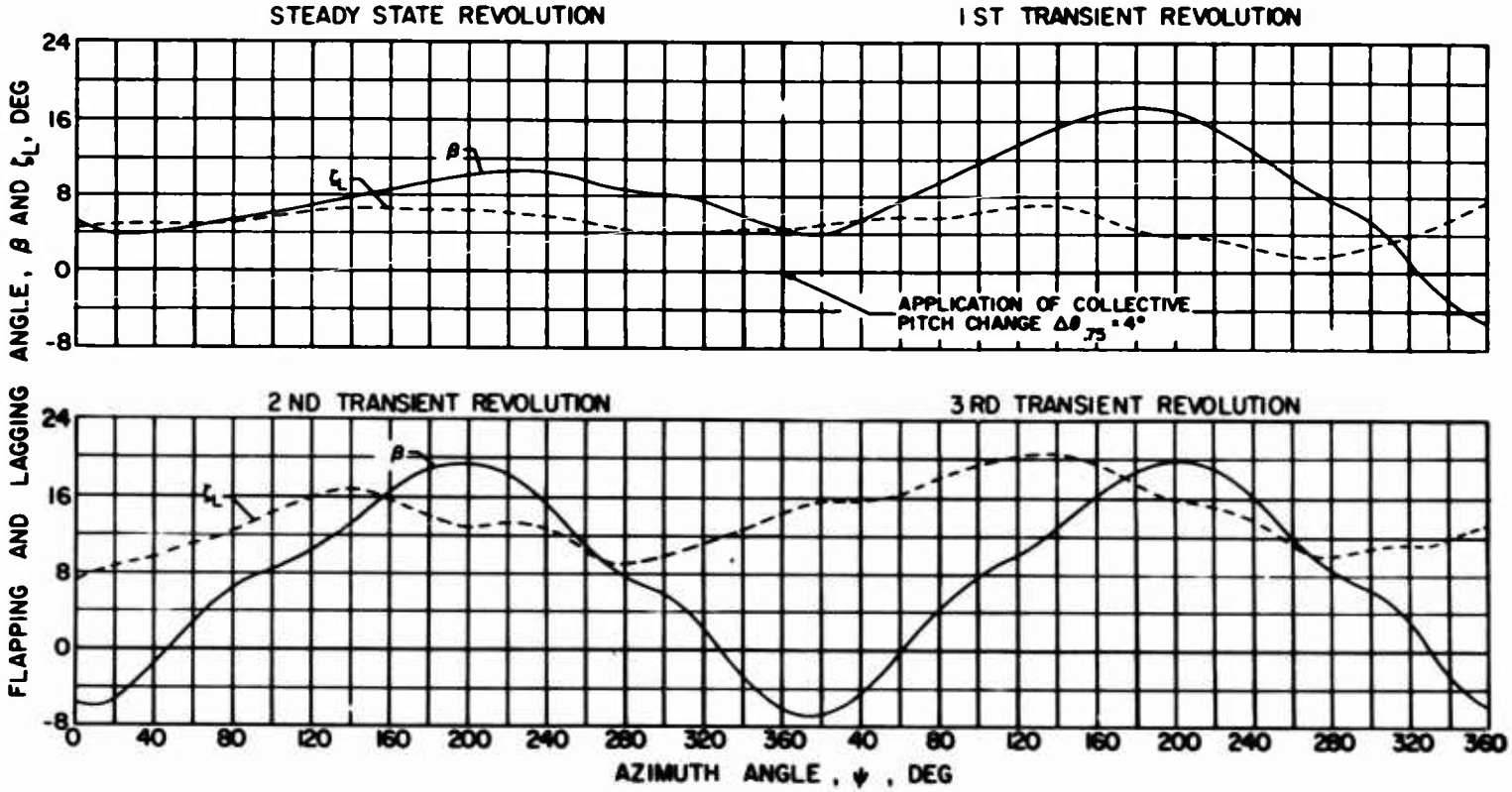

Figure 50. Transient Rotor Blade Response to Collective Pitch Change; Steady State $C_L/\sigma = .10, \Delta\theta_{.75R} = 4°, \mu = .3$; Lag Damping Not Present.

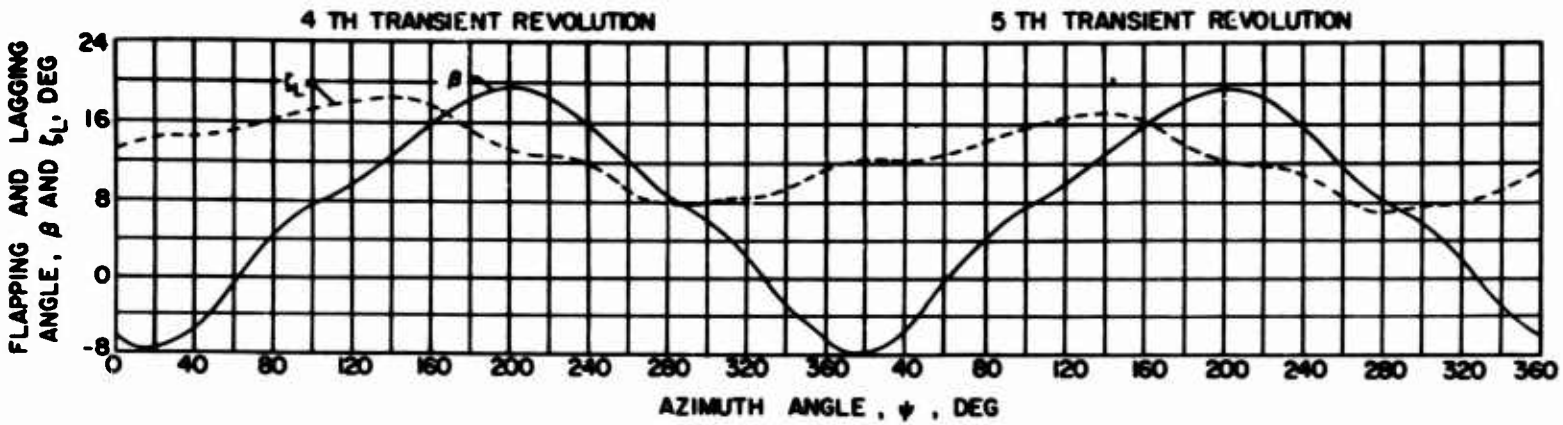

Figure 50. Concluded.

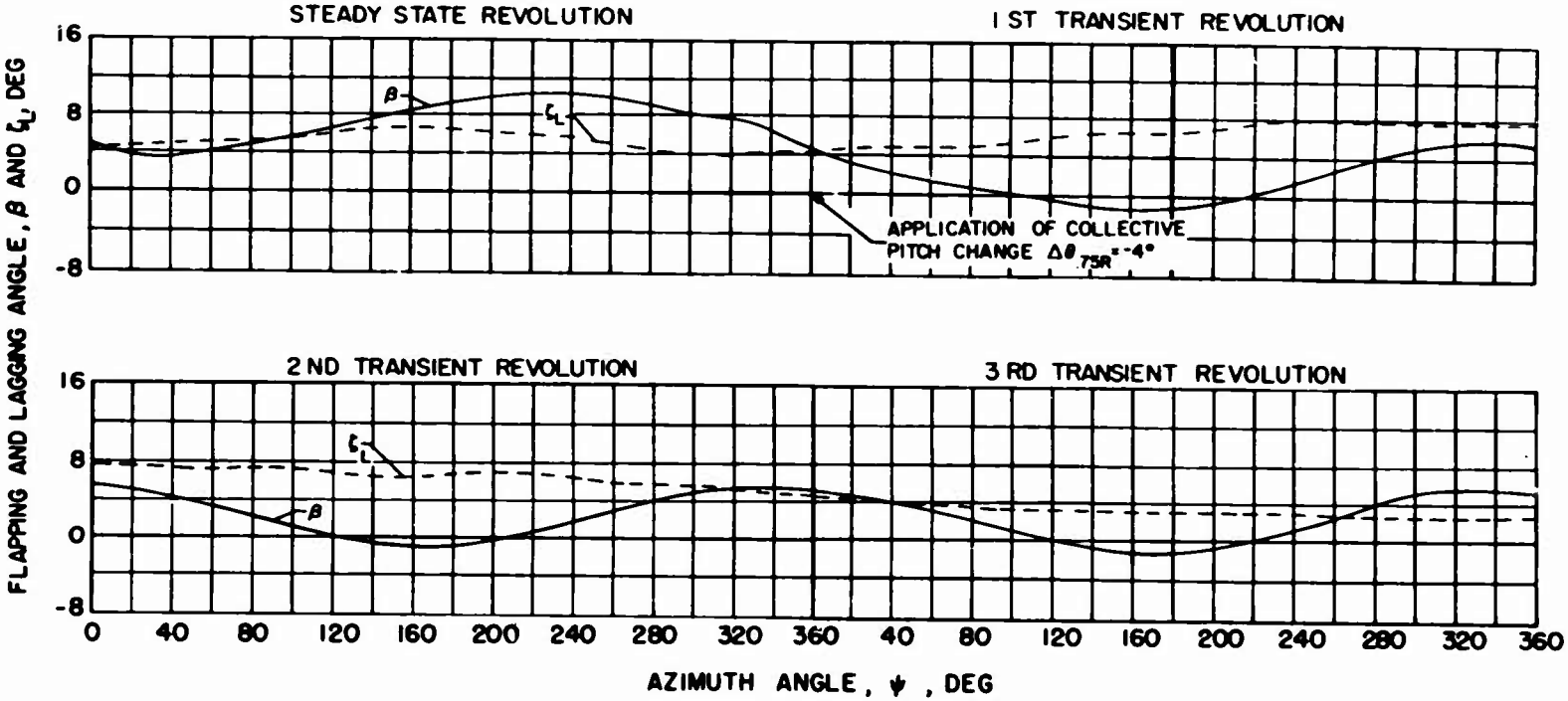

Figure 51. Transient Rotor Blade Response to Collective Pitch Change; Steady State $C_L/\sigma = .10, \Delta\theta_{.75R} = -4°, \mu = .3$; Lag Damping Not Present.

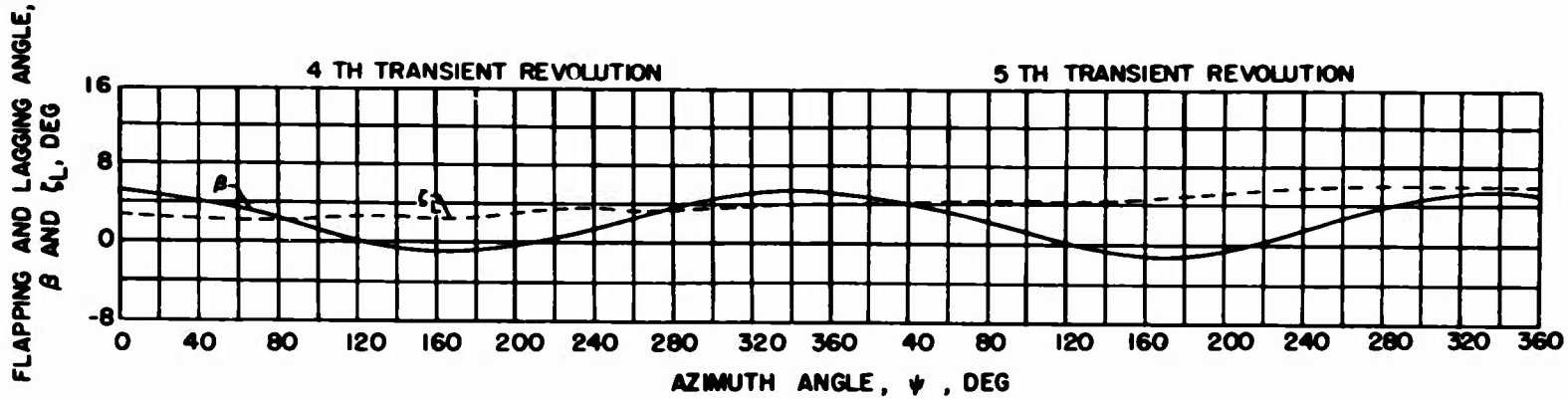

Figure 51. Concluded.

TABLE I. BLADE CONFIGURATIONS STUDIES WITH THE SIMPLIFIED FLAPPING OR BENDING STABILITY ANALYSIS

Configuration Number	Articulated or Nonarticulated	Number of Blades	M_R	$\bar{r}_{O_A}$	Ton δ_3	δ_4	D_F	$\bar{\omega}_{w_1}$	R	Control Gyro Condition
1	Articulated	5	1.85	.12	0.0	0.0	0.0	-	20.4	-
2	Articulated	5	.92	.12	0.0	0.0	0.0	-	20.4	-
3	Articulated	5	3.70	.12	0.0	0.0	0.0	-	20.4	-
4	Articulated	5	1.85	.12	.50	0.0	0.0	-	20.4	-
5	Articulated	5	1.85	.12	1.0	0.0	0.0	-	20.4	-
6	Articulated	5	1.85	.12	1.5	0.0	0.0	-	20.4	-
7	Articulated	5	1.85	.12	0.0	.25	0.0	-	20.4	-
8	Articulated	5	1.85	.12	0.0	.50	0.0	-	20.4	-
9	Articulated	5	1.85	.12	0.0	1.0	0.0	-	20.4	-
10	Articulated	5	1.85	.12	0.0	1.5	0.0	-	20.4	-
11	Articulated	5	1.85	.24	0.0	0.0	0.0	-	20.4	-
12	Articulated	5	1.85	.54	0.0	0.0	0.0	-	20.4	-
13	Articulated	5	1.85	.77	0.0	0.0	0.0	-	20.4	-
14	Articulated	5	1.85	.12	0.0	0.0	.50	-	20.4	-
15	Articulated	5	1.85	.12	0.0	0.0	1.00	-	20.4	-

TABLE I - CONCLUDED

Configuration Number	Articulated or Nonarticulated	Number of Blades	M_R	$\bar{r}_{O_A}$	Tan δ_3	δ_4	D_F	$\bar{w}_{w_1}$	AR	Control Gyro Condition
16	Nonarticulated	5	1.99	.12	-	-	-	1.12	20.4	Fixed
17	Nonarticulated	5	.99	.12	-	-	-	1.12	20.4	Fixed
18	Nonarticulated	5	3.98	.12	-	-	-	1.12	20.4	Fixed
19	Nonarticulated	5	1.99	.12	-	-	-	1.22	20.4	Fixed
20	Nonarticulated	5	1.99	.12	-	-	-	1.44	20.4	Fixed
21	Nonarticulated	5	1.99	.12	-	-	-	1.70	20.4	Fixed
22	Nonarticulated	5	1.99	.12	-	-	-	2.12	20.4	Fixed
23	Nonarticulated	5	1.99	.12	-	-	-	3.74	20.4	Fixed
24	Nonarticulated	7	2.78	.12	-	-	-	1.18	28.6	Fixed
25	Nonarticulated	6	2.39	.12	-	-	-	1.11	24.4	Fixed
26	Nonarticulated	4	1.59	.12	-	-	-	1.14	16.3	Fixed
27	Nonarticulated	3	1.19	.12	-	-	-	1.16	12.3	Fixed
28	Nonarticulated	2	.795	.12	-	-	-	1.23	8.15	Fixed
29	Nonarticulated	5	1.99	.12	-	-	-	1.12	20.4	Acting

TABLE II. BASIC PROPERTIES OF ROTOR SYSTEM FOR FLAPPING OR BENDING STABILITY STUDIES WITH THE EXTENDED NORMAL MODE TRANSIENT ANALYSIS

Item	Symbol	Value	Units
Radius	R	31.0	ft
Number of Blades	b	5	-
Chord	c	1.52	ft
Flatwise Bending Stiffness	EI_F	1.56×10^6	$lb\text{-}ft^2$
Edgewise Bending Stiffness	EI_E	1.53×10^6	$lb\text{-}ft^2$
Torsional Stiffness	JG	2.43×10^6	$lb\text{-}ft^2$
Mass per Unit Length	m	.205	slugs/ft
Flap-Lag Hinge Offset	$\overline{e}$	.0339	-
Tip Loss Factor	B	.98	-
Aerodynamic Root Cutout	$\overline{r}_{OA}$	.12	-
Structural Root Cutout	$\overline{r}_{OS}$	.056	-
Mass Radius of Gyration in Torsion Divided by Rotor Radius	k_z	.0112	-

TABLE III. ROTOR CONFIGURATIONS FOR FLAPPING OR BENDING STABILITY STUDIES WITH THE EXTENDED NORMAL MODE TRANSIENT ANALYSIS

Configuration Number	Articulated or Nonarticulated	Tan δ_3	$\frac{Y_{C_\theta}}{C}$	Control Gyro Condition
1	Articulated	0.0	0.0	-
2	Nonarticulated	-	0.0	Fixed
3	Articulated	1.0	0.0	-
4	Nonarticulated	-	0.0	Acting
5	Articulated	0.0	-.06	-
6	Nonarticulated	-	-.06	Fixed
7	Articulated	0.0	-.10	-

TABLE IV. FLIGHT CONDITIONS FOR FLAPPING OR BENDING STABILITY STUDIES WITH THE EXTENDED NORMAL MODE TRANSIENT ANALYSIS

Condition Number	μ	ΩR ft/sec	λ_G	V Knots	w_G ft/sec
1	.50	632	.0475	188.	30.0
2	.60	593	.0507	210.	30.0
3	1.00	475	.0633	282.	30.0
4	1.25	422	.0712	312.	30.0
5	1.50	380	.0788	338.	30.0
6	1.80	339	.0885	361.	30.0
7	1.00	475	.0729	282.	34.5

TABLE V. ARTICULATED BLADE ELASTIC MODAL FREQUENCIES

ΩR ft/sec	Frequencies-Cycles/Revolution							
	ω_{w_0}	ω_{w_1}	ω_{w_2}	ω_{w_3}	ω_{v_0}	ω_{v_1}	ω_{v_2}	ω_{θ_1}
632	1.026	2.65	4.88	7.96	.226	3.35	8.84	8.59
593	1.026	2.66	4.97	8.18	.226	3.45	9.27	9.14
475	1.026	2.74	5.34	9.11	.225	3.92	11.11	11.39
422	1.026	2.79	5.59	9.75	.225	4.23	12.30	12.81
380	1.026	2.84	5.86	10.40	.225	4.56	13.49	14.21
339	1.026	2.91	6.20	11.22	.225	4.98	14.96	15.91

TABLE VI. NONARTICULATED BLADE ELASTIC MODAL FREQUENCIES

ΩR ft/sec	Frequencies-Cycles/Revolutions						
	ω_{w_1}	ω_{w_2}	ω_{w_3}	ω_{w_4}	ω_{v_1}	ω_{v_2}	ω_{θ_1}
632	1.05	2.73	5.03	8.11	.686	4.06	8.59
593	1.06	2.76	5.14	8.36	.715	4.24	9.14
475	1.08	2.89	5.63	9.44	.836	4.98	11.39
422	1.09	2.98	5.97	10.17	.913	5.46	12.81

TABLE VII. BASIC FLAPPING OR BENDING INSTABILITY RESULTS FROM NORMAL MODE TRANSIENT ANALYSIS CALCULATIONS

Configuration (Table III)	Flight Condition (Table IV)	μ	λ_G	β_{MAX} OR $q_{w_{MAX}}$	β_{MIN} OR $q_{w_{MIN}}$	$\frac{\beta_{MAX}}{\lambda_G}$ OR $\frac{q_{w_{MAX}}}{\lambda_G}$	$\frac{\beta_{MIN}}{\lambda_G}$ OR $\frac{q_{w_{MIN}}}{\lambda_G}$
1	1	.50	.0475	.155	-.036	3.26	-.758
1	2	.60	.0507	.182	-.077	3.59	-1.52
1	3	1.00	.0633	.268	-.123	4.23	-.194
1	4	1.25	.0712	.305	-.102	4.28	-1.43
1	5	1.50	.0788	.448	-.141	5.69	-1.79
1	7	1.00	.0729	.296	-.123	4.06	-1.69
2	1	.50	.0475	.163	-.054	3.43	-1.14
2	2	.60	.0507	.192	-.088	3.78	-1.74
2	3	1.00	.0633	.388	-.176	6.12	-2.78
2	4	1.25	.0712	.400	-.275	5.61	-3.86
3	3	1.00	.0633	.031	0	.489	0.0
3	4	1.25	.0712	.092	0	1.29	0.0
3	5	1.50	.0788	.186	-.060	2.36	-0.76
3	6	1.80	.0885	.286	-.330	3.23	-3.76

TABLE VII - CONCLUDED

Configuration (Table III)	Flight Condition (Table IV)	μ	λ_G	β_{MAX} OR $q_{w_{MAX}}$	β_{MIN} OR $q_{w_{MIN}}$	$\frac{\beta_{MAX}}{\lambda_G}$ OR $\frac{q_{w_{MAX}}}{\lambda_G}$	$\frac{\beta_{MIN}}{\lambda_G}$ OR $\frac{q_{w_{MIN}}}{\lambda_G}$
4	2	.60	.0507	.174	-.069	3.43	-1.36
5	1	.50	.0475	.223	-.083	4.69	-1.75
5	2	.60	.0507	.243	-.115	4.80	-2.27
5	3	1.00	.0633	.309	-.143	4.88	-2.26
5	4	1.25	.0712	.312	-.105	4.38	-1.47
6	1	.50	.0475	.226	-.081	4.75	-1.70
6	2	.60	.0507	.245	-.109	4.83	-2.15
6	3	1.00	.0633	.392	-.177	6.20	-2.80
6	4	1.25	.0712	*	*	*	*
7	4	1.25	.0712	.330	-.109	4.63	-1.53
7	5	1.50	.0788	.538	-.139	6.83	-1.76

* Indefinitely large due to instability, see Figure 28 and page 14.

CONCLUSIONS

1. The response of the rotor blade in flapping or flatwise bending is essentially proportional to the size of a gust disturbance, provided the rotor response does not exceed the conventional fuselage clearance requirements.

2. The single-degree-of-freedom flapping analysis used in this part of the investigation generally provides approximate results suitable for preliminary design studies, as verified by comparison with more elaborate analyses. For advance ratios beyond unity and for center-of-gravity offsets beyond 6% chord, participation of other modal displacements, principally lead-lag or edgewise and torsion, may make the single-degree-of-freedom analysis inaccurate.

3. Blade mass parameter and pitch-flap coupling are the most important parameters affecting flapping or flatwise bending stability.

4. Nonarticulated and articulated conventional blades behave in the same qualitative fashion with respect to flapping response below advance ratios of unity. The articulated blade response is somewhat smaller than the nonarticulated blade response for the same stiffness.

5. Normal Mode Transient Analysis calculations showed that sufficiently large control increments under heavy rotor loads at high speed could produce impractically large flapping and lead-lag excursions, but no catastrophic instability. This same result was obtained for a number of different flight conditions of a typical rotor both with and without mechanical lag damping.

RECOMMENDATIONS

1. The single-degree-of-freedom flapping analysis appears to be quite adequate through advance ratios of unity and chordwise aft center-of-gravity offsets up to 6% with respect to the 25% chord and elastic axis. In order to extend this range of usefulness, a three-degree-of-freedom analysis incorporating flapping or flatwise bending, lead-lag or edgewise motion, and torsion is suggested.

2. The flapping or flatwise bending response to control inputs should be investigated; a procedure similar to that used in this report for gust response could be used. Then, a corresponding set of practical operating boundaries should be generated and compared with the gust boundaries.

3. The effects of fuselage motions and control corrections on flapping or flatwise bending response should be investigated.

4. The flapping or flatwise bending response of typical rotors to more realistic isolated and statistical gust representations should be investigated.

5. The existence of a coupled flapping and lagging catastrophic instability was not detected with the Normal Mode Transient Analysis for the cases considered. In order to determine if a range of parameters exists for which this instability can be predicted, further analysis is suggested. The flapping and lagging response to various control or gust excitations should be calculated. The effect of excluding nonlinear aerodynamic and dynamic terms as well as various rotor blade degrees of freedom should be systematically determined.

REFERENCES CITED

1. Horvay, C., "Rotor Blade Flapping Motion," Quarterly of Applied Mathematics, Vol. V, No. 2, July 1947.

2. Gessow, A., and Crim, A. D., A Method for Studying the Transient Blade-Flapping Behavior of Lifting Rotors at Extreme Operating Conditions, NACA TN 3366, National Advisory Committee for Aeronautics, Langley Field, Virginia, November 1954.

3. Hohenemser, K. H., Some Aerodynamic and Dynamic Problems of the Compound Rotary-Fixed Wing Aircraft, American Helicopter Society, Proceedings of the Eighth Annual Forum, May 1952.

4. Jenkins, J. L., Calculated Blade Response at High Tip-Speed Ratios, NASA SP-116, National Aeronautics and Space Administration Langley Field, Virginia, April 1966.

5. Perisho, C. H., "Analysis of the Stability of a Flexible Helicopter Rotor Blade at High Advance Ratio," Journal of the American Helicopter Society, Vol. 4, No. 2, April 1952.

6. Smith, A. F., Jenney, D. S., and Arcidiacono, P. J., A Linearized Theory for the Estimation of Helicopter Rotor Characteristics at Advance Ratios Above 1.0, American Helicopter Society, Proceedings of the Nineteenth Annual Forum, May 1963.

7. Young, M. I., "A Theory of Rotor Blade Motion Stability in Powered Flight," Journal of the American Helicopter Society, Vol. 9, No. 3, July 1964.

8. Tanner, W. H. , Charts for Estimating Rotary Wing Performance in Hover and High Forward Speeds, Sikorsky Aircraft Division of United Aircraft Corporation; NASA CR-114, National Aeronautics and Space Administration, Washington D. C., November 1964.

9. Cooper, D., Hansen, K. C., and Kaplita, T. T., Single Rotor Helicopter Dynamics Following Power Failure at High Speeds, Sikorsky Aircraft Division of United Aircraft Corporation; USAAVLABS Technical Report 66-30, U. S. Army Aviation Materiel Laboratories, Fort Eustis, Virginia, June 1966.

10. Hohenemser, K. H. and Heaton, P. W., "Aeroelastic Instability of Torsionally Rigid Helicopter Blades," Journal of the American Helicopter Society, Vol. 12, No. 2, April 1967.

Unclassified

Security Classification

DOCUMENT CONTROL DATA - R & D

(Security classification of title, body of abstract and indexing annotation must be entered when the overall report is classified)

1. ORIGINATING ACTIVITY (Corporate author)	2a. REPORT SECURITY CLASSIFICATION
Sikorsky Aircraft Division of United Aircraft Corporation Stratford, Connecticut	Unclassified 2b. GROUP

3. REPORT TITLE

PREDICTION OF ROTOR INSTABILITY AT HIGH FORWARD SPEEDS
Volume V - Flapping and Flap-Lag Instability

4. DESCRIPTIVE NOTES (Type of report and inclusive dates)
Final Report

5. AUTHOR(S) (First name, middle initial, last name)
H. L. Elman
Charles F. Niebanck
Lawrence J. Bain

6. REPORT DATE	7a. TOTAL NO. OF PAGES	7b. NO. OF REFS
February 1969	122	10

8a. CONTRACT OR GRANT NO.	9a. ORIGINATOR'S REPORT NUMBER(S)
DA 44-177-AMC-332(T) b. PROJECT NO. 1F125901A13904 c. d.	USAAVLABS Technical Report 68-18E 9b. OTHER REPORT NO(S) (Any other numbers that may be assigned this report) SER-50469

10. DISTRIBUTION STATEMENT
This document has been approved for public release and sale; its distribution is unlimited.

11. SUPPLEMENTARY NOTES	12. SPONSORING MILITARY ACTIVITY
Volume V of a 5-volume report	US Army Aviation Materiel Laboratories Fort Eustis, Virginia

13. ABSTRACT

This volume deals with an investigation of the unstable flapping or flatwise bending tendency which arises during operation at high forward speeds and reduced rotational speeds. The principal parameters influencing flapping or flatwise bending are enumerated and discussed. The simplified analysis used a single degree of freedom, rigid flapping for an articulated blade or the first flatwise bending mode for a nonarticulated blade. This analysis was used to calculate response to an instantaneous gust, and practical operating boundaries were defined in terms of maximum allowable flapping or bending excursions. The simple analysis was used to investigate a range of various parameters. The simple analysis was supplemented with similar calculations with the extended Normal Mode Transient Analysis. These results showed that the simpler analysis predicted all trends correctly and provided results which were somewhat conservative with respect to those of the Normal Mode Transient Analysis.

The existence of a flap-lag instability was investigated with the Normal Mode Transient Analysis, which included blade stall, compressibility, and reverse-flow effects. Three advance ratio conditions were chosen, with the rotor operating in high-speed flight under stalled conditions. While large control pulses were found to produce blade excursions which were unacceptably large from a practical standpoint, no tendency of the rotor to become catastrophically unstable was noted.

DD FORM 1 NOV 68 1473 REPLACES DD FORM 1473, 1 JAN 64, WHICH IS OBSOLETE FOR ARMY USE.

Unclassified

Security Classification